

Propulsion system design

15.1 Introduction

In this chapter we will summarize the fundamentals for ACV and SES propulsor selection. We will also discuss issues which need to be considered when selecting supporting components to achieve the designer's overall objective – an efficient and readily manœuvrable craft.

ACV propulsion

ACVs are generally propelled by free or ducted air propellers, or by ducted fans. Air propulsor types are illustrated in Fig. 15.1. Available thrust is strongly affected by wind speed, so a designer has to consider carefully the requirements for thrust at hump speed as well as at design operating speed. It is normal to aim at minimum 20% thrust margin when transiting hump, to provide reasonable acceleration against the wind and sea. This is not usually an issue for craft with design speeds of greater than 55 knots, while it may become the controlling factor for utility craft with operating speeds in the 30–50 knots range.

The main design issue for air propulsion is to minimize the propulsor diameter (and so the system weight), while obtaining the desired efficiency for minimized power and an acceptably low emitted noise level. Propeller or fan blade tip speeds tend to be high. At speeds above 200 m/s the induced pressure field at blade tips creates significant noise. Open propellers adapted from aircraft often have tip speeds higher than this and so craft designed in the 1960s became known for their high noise signature. Since the mid 1970s craft have been developed with ducted propulsors, which are able to use lower tip speed to develop the same thrust, as the blade loading can be kept much higher in the outer 25% of the radius rather than tapering off to zero at the tip. Reduction of the tip vortices due to the presence of a duct also results in lower external noise.

Ducted propellers or fans are optimized as a system. Air flow around the duct, typically an aerofoil section, can provide additional thrust. If a fan is used, then flow straightener vanes are usually installed to maximize the developed thrust and remove the asymmetrical response to rudders which is otherwise present from the rotating slipstream. The duct also acts as a fin, providing directional stability for the craft.

SES propulsion

SES use water screws (open propellers) or water jets for propulsion, see Fig. 15.2. A subcavitating fixed pitch propeller is the simplest installation, relatively light and inexpensive. This has limitations though. Subcavitating propellers are very efficient at low speeds. Installation under the sidehulls of an SES often requires considerable shaft angles and possibly a vee gearbox to the engine.



(a)



(b)

Fig. 15.1 Air propulsion types. (a) Pylon mounted open propellers on Hoverlloyd SRN-4 at Calais. The two integrated ducted fan craft in the foreground had just crossed the channel on the 25th anniversary of the first crossing by SRN-1. (b) Twin ducted propellers in the Griffon 2500TD.

The loading on a propeller blade is controlled by the suction pressure on the upper surface. As blade loading is increased this drops to water vapour pressure, causing cavities to form containing water vapour and air from solution. Cavitation starts at the blade tips and spreads inwards to eventually cover the whole blade forward surface.

In the speed range up to 35 knots it is possible to use subcavitating propeller blades which are designed to avoid suction pressures which may cause cavitation. Some cavitation at the blade tips is unavoidable due to vortices from the circulation, though this is usually over less than 2% of the blade area. Significant cavitation is unavoidable for



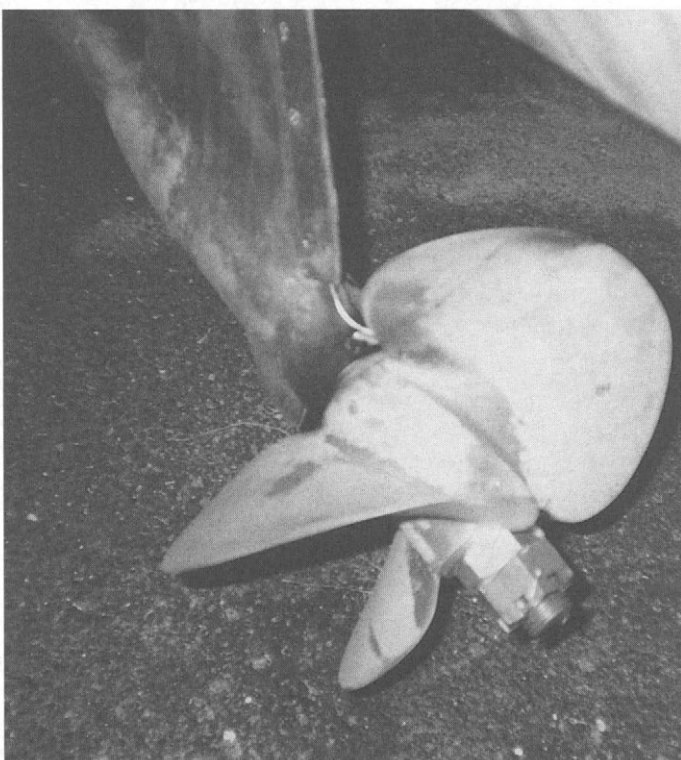
Fig. 15.1 (c) Integrated lift/thrust from single axial fan on the Griffon 375TD. (d) Air jet propulsion an an 'amateur' hovercraft racing in 1967.

propellers installed on craft designed for service speeds higher than about 35 knots. To stabilize the cavitation, fully cavitating or ventilated blade sections need to be used.

Several ‘series’ of cavitating blade sections have been developed, for example the Newton–Rader [109] and DTMB [82,85] series designs. Propellers using these sections have been successfully developed for SES with speeds up to 90 knots. Efficiency in the region 0.6–0.7 is typical for these propellers, compared with 0.65–0.75 for subcavitating propellers.



(a)



(b)

Fig. 15.2 (a) Model of Hovermarine HM.5 showing subcavitating propeller and rudder arrangement. (b) Close-up view of Hovermarine HM.2 subcavitating propeller.

Water jets have developed greatly since the early 1970s when units typically had efficiencies in the range 0.45–0.6. This has recently been driven by demands from catamaran ferry builders, though the initial impetus was for hydrofoils and SES due to potential simplification of the machinery and transmission arrangements. Units with system efficiency in the range 0.65–0.8 are now available, see Fig. 15.3, which plots achieved efficiency for KaMeWa installations. They offer lower vibration than a water screw, but require careful design of the inlet system.

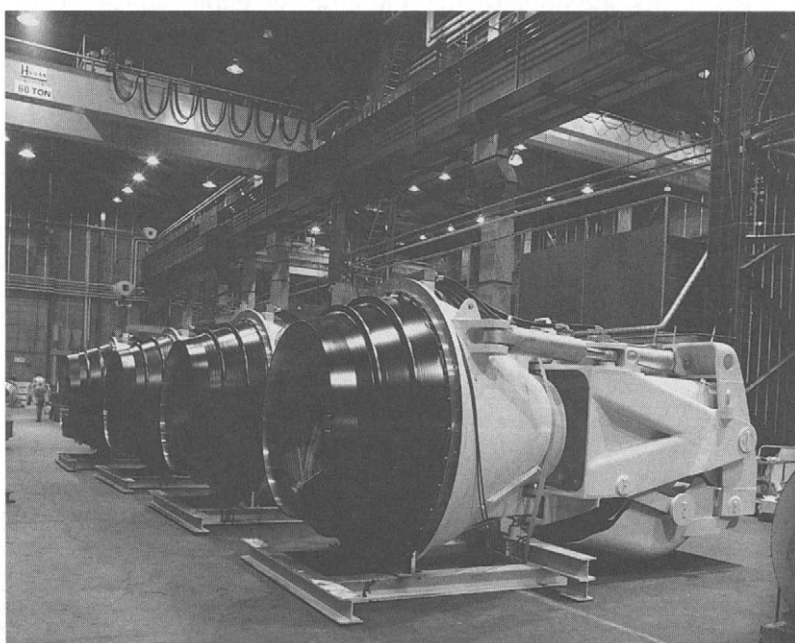
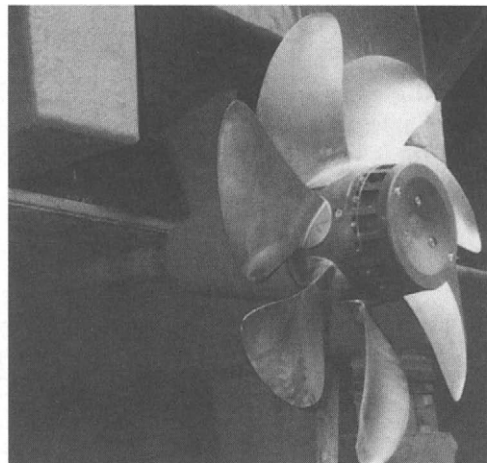


Fig. 15.2 (c) The Mekat supercavitating/superventilating propeller. (d) A group of large KaMeWa waterjet units type 125 prior to installation.

Efficient water jets for service speeds of up to 60 knots have been developed so far. While demand in the fast ferry market continues to press for increasing service speeds, it may be expected that units with similar efficiency for the speed range towards 100 knots will appear in the near future.

Other propulsion systems

Various other propulsion systems have been experimented with, mainly surface contact devices for propulsion of load-carrying platforms, see Fig. 15.4. Examples are hydraulic powered wheel units, winching systems and tracked propulsion. Platforms have also been towed by tractors, tugs and helicopters. The main challenge for design of these systems has been reliable traction over the usually difficult terrain and control of vehicle track when it is on a slope. Brief guidelines for these devices are given later in this chapter.

Basic theories

Before looking at selection for a particular craft, it is useful to review the physical phenomena which apply to both air and water propellers. Our purpose is to give an insight into the efficiency with which power (torque) is translated into thrust at various speeds and to discuss the basis on which blade geometry and number are best selected. This information should allow initial sizing of propulsors without reference to design of the units themselves, allowing realistic enquiries to suppliers prior to selection of candidates and optimization. Propulsor selection and design aspects are then discussed in more detail in following sections of this chapter.

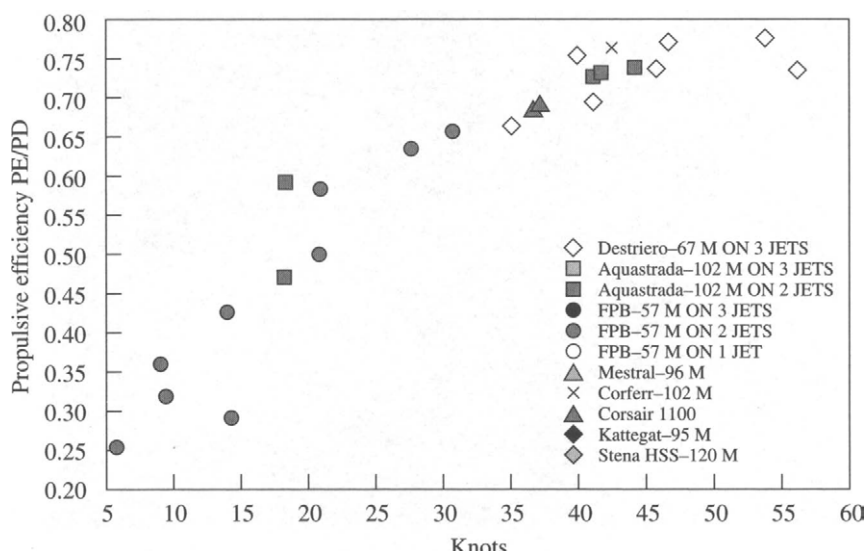


Fig. 15.3 Water-jet efficiency in practice, KaMeWa recent experience.

Momentum theory

Air propellers, ducted fans, water screws and water jets all deliver their propulsion as a reactive force to the momentum in the mass of air or water which is accelerated – they are momentum exchange devices. The fluid is accelerated by the action of the rotating blades. The lift and drag forces generated by air or water flow over the blades may be resolved into a thrust in the direction of craft motion and a torque which is the force required to rotate the impeller, see Fig. 15.5(a).

Without considering the air or water interaction with individual blades, momentum theory treats the propeller as a disc providing acceleration to the fluid in the direction of its movement. The principle is illustrated in Fig. 15.5(b). Incoming fluid at V_0 (the forward speed of the impeller, which is the craft speed plus/minus the wind speed or water current speed) is accelerated at the impeller disc to V_d . The streamlines continue to contract until flow has reached V_j . The velocity is assumed uniform over the disc area, implying a discontinuity at the outer diameter.

$$V_0 = V_c +/ - V_w$$

$$V_d = V_0 (1 + a)$$

$$V_j = V_0 (1 + b) \quad (15.1)$$

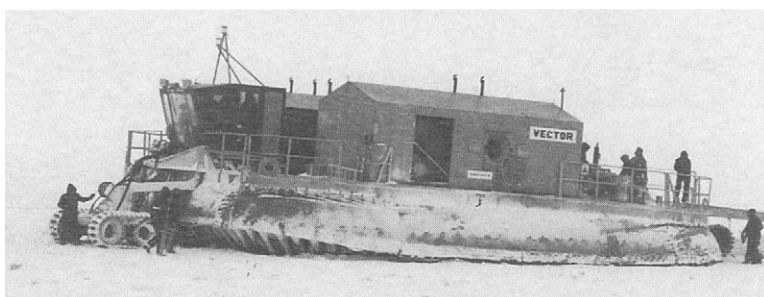
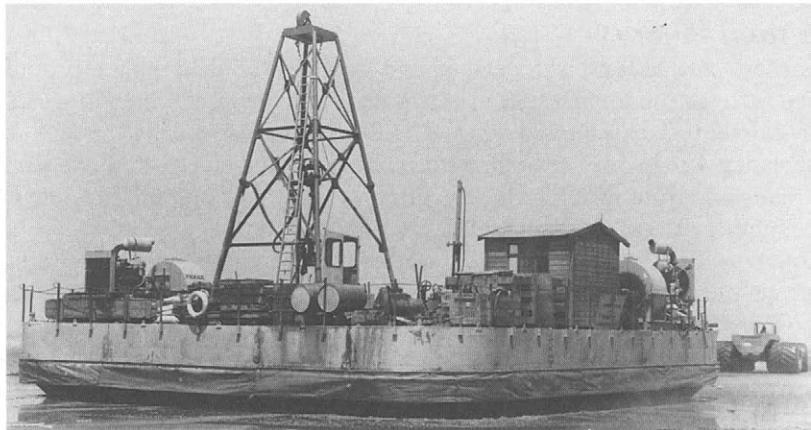


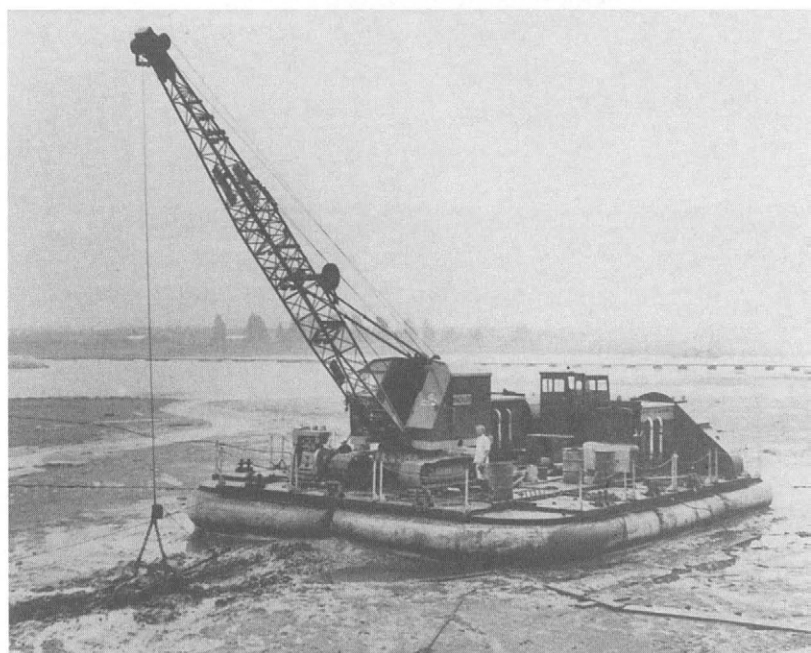
Fig. 15.4 Air cushion platform propulsion. (a) Direct propulsion by hydraulic powered wheels/tracks on the Wartsila Vector. (b) Winch propulsion along wires across the Peace river in Alaska during pipeline construction.



(c)

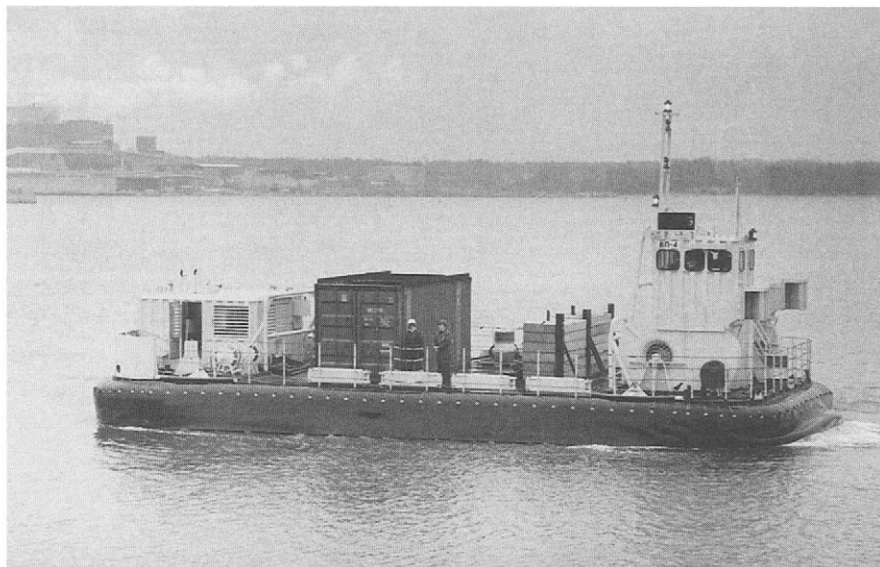


(d)(i)



(d)(ii)

Fig. 15.4 (c) Overland towing of a soil sampling rig. (d)(i) Overwater tow of an outfall pipe dredging rig at high tide. (d)(ii) The rig at work.



(e)

Fig. 15.4 (e) Wartsilla TAV.40 arctic resupply hoverbarge with air jet vents for slow speed propulsion/control.

The mass flow through the impeller is

$$\dot{m} = \rho_a/g A_d V_d \quad (15.2)$$

where $\rho_a = 1.293 \text{ kg m}^{-3}$ and $g = 9.81 \text{ m/s}^2$, and the thrust developed is

$$T = \rho_a/g A_d V_d [V_j - V_0] \quad (15.3)$$

The thrust at the impeller disc is equal to the static pressure increment across it:

$$T = A_d (p_2 - p_1) \quad (15.4)$$

where p_2 is the static pressure just downstream of the impeller disc and p_1 the static pressure just upstream of it. Using Bernoulli's equation we can show by considering flow either side of the disc, that for a free propeller $b = 2a$ in equation (15.1), as follows. Upstream:

$$p_0 + 0.5\rho_a/g V_0^2 = p_1 + 0.5\rho_a/g V_d^2 \quad (15.5)$$

downstream:

$$p_2 + 0.5\rho_a/g V_d^2 = p_0 + 0.5\rho_a/g V_j^2 \quad (15.6)$$

thus

$$p_2 - p_1 = 0.5 \rho_a/g [V_j^2 - V_0^2] \quad (15.7)$$

so

$$T = A_d 0.5 \rho_a/g [V_j^2 - V_0^2] \quad (15.8)$$

Equating to (15.3) we obtain

$$V_d [V_j - V_0] = 0.5 [V_j^2 - V_0^2]$$

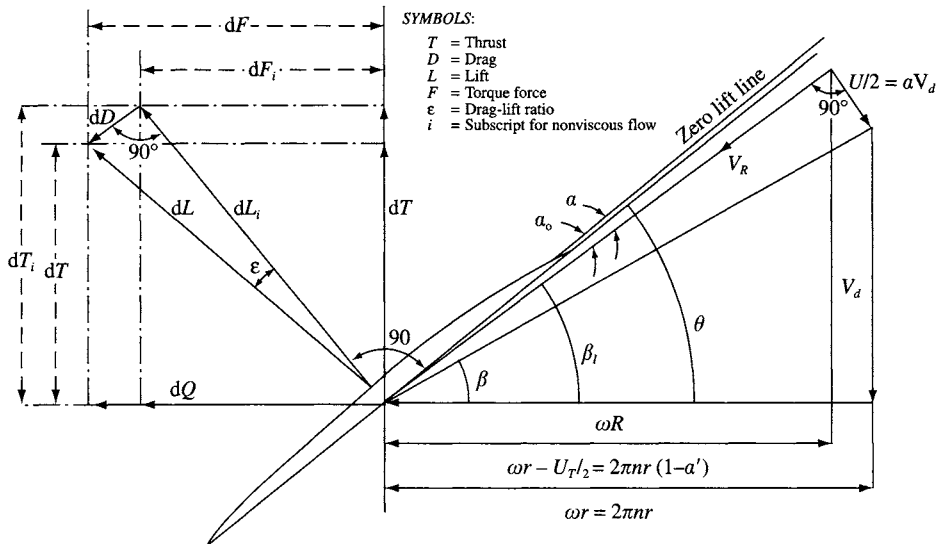


Fig. 15.5(a) Blade velocity vector diagram.

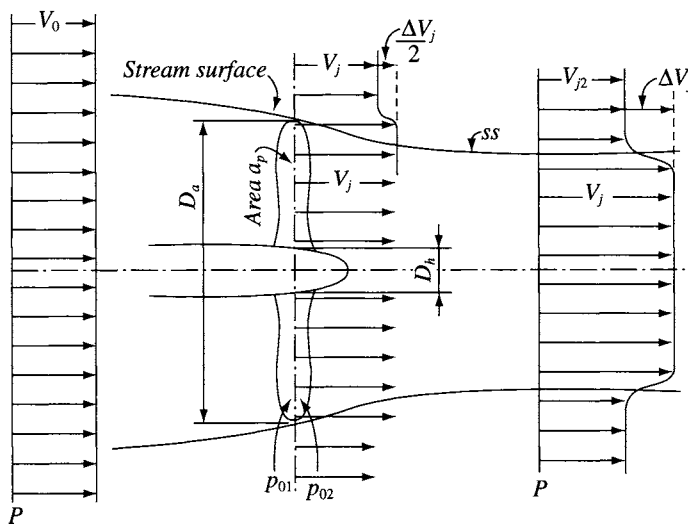


Fig. 15.5(b) Momentum exchange principle diagram.

Using the relations in (15.1)

$$[1 + a] b = 0.5 [(1 + b)^2 - 1] = 0.5 [b^2 + 2b]$$

on reduction this becomes

$$a = 0.5 b$$

The useful work done by the impeller moving at V_0 is

$$T V_0 = \rho_a/g A_d V_d [V_j - V_0] V_0 \quad (15.9)$$

The kinetic energy applied to accelerate the flow to V_j across the disc is

$$E = 0.5 \rho_a/g A_d V_d [V_j^2 - V_0^2] \quad (15.10)$$

The ideal efficiency is the ratio of useful work to the applied kinetic energy, thus

$$\begin{aligned} \eta_i &= T V_0/E \\ &= 2 [V_j - V_0] V_0 / [V_j^2 - V_0^2] \\ &= 2 V_0 / [V_j + V_0] \end{aligned} \quad (15.11a)$$

since $V_j = V_0(1 + 2a)$, the ideal efficiency is

$$\eta_i = 1/(1 + a) \quad (15.11b)$$

Now the power absorbed by the impeller is

$$N = T V_0 / \eta_i \quad (15.12)$$

$$N = N g / 550 \quad \text{shp (where } T \text{ is lbf} = \text{lb. ft/s)}$$

$$N = N g / 1000 \quad \text{kW (where } T \text{ is kgf} = \text{kg. m/s)}$$

so the unit thrust developed is

$$T/N = 746 / [(1 + a) V_0] \text{ kgf/kW} \quad (15.13)$$

the disc loading varies with craft forward speed and a , which is a measure of the kinetic energy or velocity increment generated by the propeller. This may be expressed as

$$\begin{aligned} T/A_d &= p_2 - p_1 = 0.5 \rho_a/g [V_j^2 - V_0^2] \quad (\text{from 15.7}) \\ &= 0.5 \rho_a/g V_0^2 [(1 + 2a)^2 - 1] \end{aligned} \quad (15.14)$$

If we take as an example an ACV at $V = 50$ kt (84.4 ft/s, 25.75 m/s) in still air; as V_j is increased this gives trends tabulated in Table 15.1 and shown in Fig. 15.6 for ideal thrust/power against disc loading for an air propeller. A water screw has a similar relationship between ideal efficiency and disc loading, theoretically displaced by the increase in water density, a factor of 835. Cavitation prevents water screw efficiency

Table 15.1 Variation of ideal efficiency with slipstream jet velocity

V_j	V_j/V_0	a	η_i	T/N (kgf/kW)	T/A_d (kgf/m ²)	η_i Ducted	T/N Ducted
36.05	1.4	0.2	0.833	24.14	41.95	0.909	26.34
41.20	1.6	0.3	0.769	22.28	68.17	0.870	25.19
46.35	1.8	0.4	0.714	20.69	97.88	0.833	24.14
51.50	2.0	0.5	0.667	19.31	131.09	0.800	23.17
64.38	2.5	0.75	0.571	16.09	251.69	0.727	21.07
77.25	3.0	1	0.500	14.48	349.58	0.667	19.31
128.75	5.0	2	0.333	9.65	1048.73	0.500	14.48

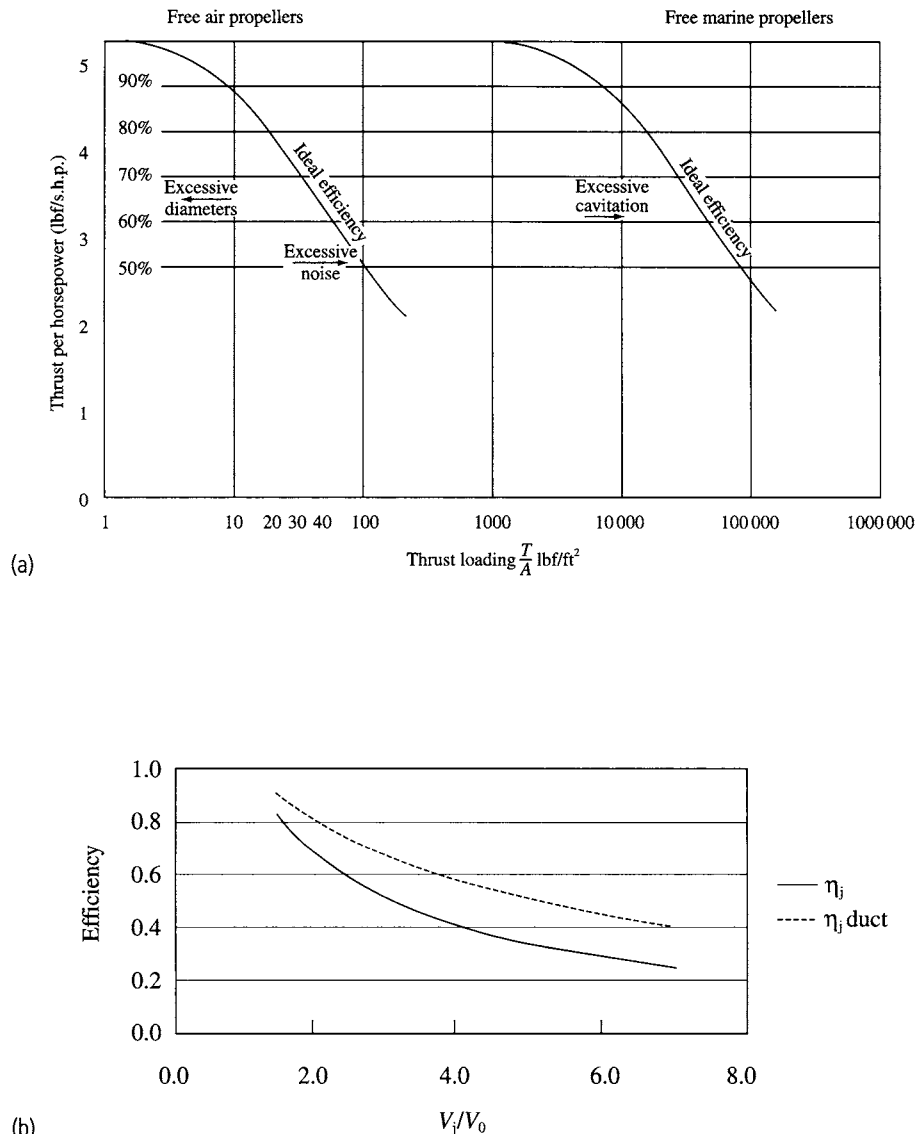


Fig. 15.6 Trends of ideal efficiency with disc loading and jet velocity: (a) trends with disc loading; (b) trend with jet velocity.

approaching the ideal curve as closely as an air propeller; see section 15.4 for a detailed discussion.

It can be seen that as disc loading is increased, η_i drops away. To minimize installed power, a value of a between 0.2 and 0.5 appears desirable. The thrust for a ducted propeller is also given for comparison, see section 15.3 for further discussion.

Blade element theory

Our discussion has so far ignored the form of the propeller itself. The ideal efficiency and therefore the characteristics discussed above are based on the assumption that the only loss of energy is that represented by the kinetic energy of the slipstream along the propeller axis. In addition to this there are three main sources of energy loss:

- drag forces on the propeller blades (see Fig. 15.5(a));
- variation of the pressure distribution radially along the blades, and circumferentially between blades;
- kinetic energy losses due to the slipstream rotating vortex.

In order to derive realistic performance curves of absorbed power and produced thrust against craft speed, the individual aerofoil blades must be taken into account. The blades must be designed with an appropriate form and angle of attack along their length to provide the lift force which accelerates the fluid to provide the thrust.

The lift generated by a propeller blade tapers to zero at its tip. In addition, the blades create parasitic and pressure-induced drag as well as lift. Absorbed power will therefore be increased compared to an ideal impeller due to the drag forces, and the total thrust developed will be less. This will reduce efficiency by 15% or so compared to the ideal for an air propeller. Water screws face a more difficult problem with cavitation, which limits the effective lift force as well as limiting the lift which can be generated close to the blade tips, reducing efficiency by as much as 30% compared to the ideal.

Consider each blade of a propeller rotating around its axis with angular velocity Ω , in an airstream velocity of V . At any section, the element creates a lift force due to the circulation around the section. This will vary along the blade and will create vortices at the axis and the tip of the blade similar to those at the root and tip of a wing and which pass downstream in the propeller wake following helical paths. These vortices create an interference flow which alters the circulation around the blade section. The blade element thrust may be represented by

$$dT/dr = 4\pi r \rho V^2 (1 + a) a \quad (15.15)$$

and torque by

$$dQ/dr = 4\pi r^3 \rho V \Omega (1 + a) a' \quad (15.16)$$

where a is the interference flow axially (same as for momentum theory) and a' the interference flow in rotation. The forces on a blade element are therefore

$$\begin{aligned} \text{axial} &= V(1 + a) \quad \text{at disc (note also that } V = V(1 + 2a) \text{ in propeller slipstream)} \\ \text{rotational} &= r \Omega (1 - a') \end{aligned}$$

The resultant, W is at angle ϕ to the rotation disc plane, where

$$\tan \phi = [V/r\Omega] (1 + a)/(1 - a') \quad (15.17)$$

If we resolve lift and drag to thrust and torque, then

$$\delta T = C_L \cos \phi - C_D \sin \phi \quad (15.18)$$

$$\delta Q = C_L \sin \phi + C_D \cos \phi \quad (15.19)$$

so that

$$dT/dr = \delta T \times 0.5 \rho W^2 c \, dr \quad (15.20)$$

$$dQ/dr = \delta Q \times 0.5 \rho W^2 c r \, dr \quad (15.21)$$

If we consider the propeller disc rather than a single blade, then in place of the area of the blade, we need to integrate to the effective area of all blades, so a non-dimensional quantity s is introduced, the solidity, where

$$s = nc/(2 \pi r)$$

then

$$dT/dr = \pi s r \rho v^2 (1 + a)^2 \delta T \cosec^2 \phi \quad (15.22)$$

or

$$\pi s r^3 \rho v^2 (1 - a')^2 \delta T \sec^2 \phi$$

and

$$dQ/dr = \pi s r^2 \rho v^2 (1 + a)^2 \delta Q \cosec^2 \phi \quad (15.23)$$

or

$$\pi s r^4 \rho v^2 (1 - a')^2 \delta Q \sec^2 \phi$$

Comparing with the earlier expressions for dT/dr and dQ/dr it can be shown that

$$a/(1 + a) = 0.5 s \delta T / (1 - \cos^2 \phi) \quad (15.24)$$

and

$$a'/(1 - a') = 0.5 s \delta Q / \sin^2 \phi \quad (15.25)$$

the efficiency of the blade element is therefore

$$\eta = \frac{V}{\Omega} \frac{dT}{dQ} = \frac{V}{r\Omega} \frac{\delta T}{\delta Q} = \frac{1 - a'}{1 + a} \frac{\tan \phi}{\tan(\phi - \gamma)} \quad (15.26)$$

where $\tan \gamma = C_D/C_L$. This can be compared to the ideal efficiency from momentum theory of $1/(1 + a)$, illustrating the additional losses from the slipstream rotation a' and the effect of profile drag of the blades γ .

The characteristics of a blade element can be calculated knowing r/R , s , θ and the aerofoil characteristics (a , C_L , C_D). Starting with a series of a , the values of a , a' , J and η can be calculated. It can be seen in Fig. 15.7(a) that η typically reaches a maximum at J of 0.5–0.6 whereas if the drag force were zero then efficiency would increase to 1.0 at J of 1.0. If the blade angle is increased or decreased, this will alter the efficiency curve as shown in Fig. 15.7(b), due to the blade lift coefficient changing as its angle of attack is changed. High blade pitch gives the highest efficiency. For a given propeller diameter, this will also lead to the smallest number of blades.

A two-bladed propeller is the simplest to construct. At the forward speeds typical of an ACV, a two-bladed propeller would require relatively large diameter to produce the desired thrust. While this may be accommodated on very small craft (Fig. 15.8), propellers with between three and six blades are generally selected for larger ACVs. The most common design is a four-bladed propeller.

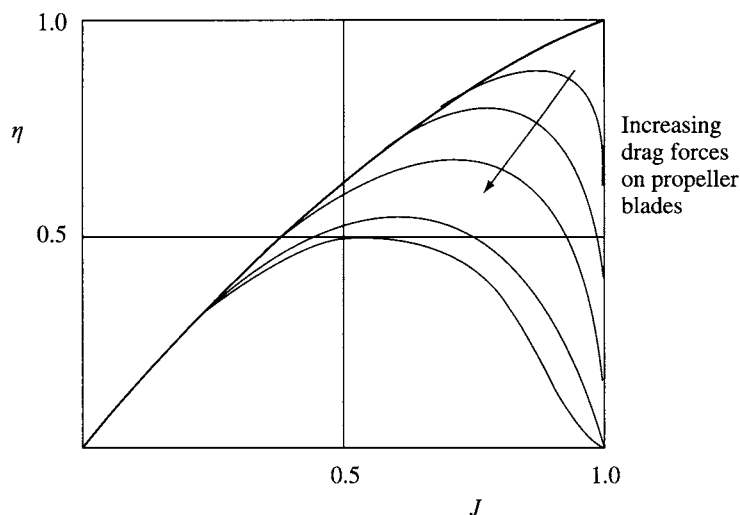


Fig. 15.7(a) Propeller efficiency vs speed of advance, J .

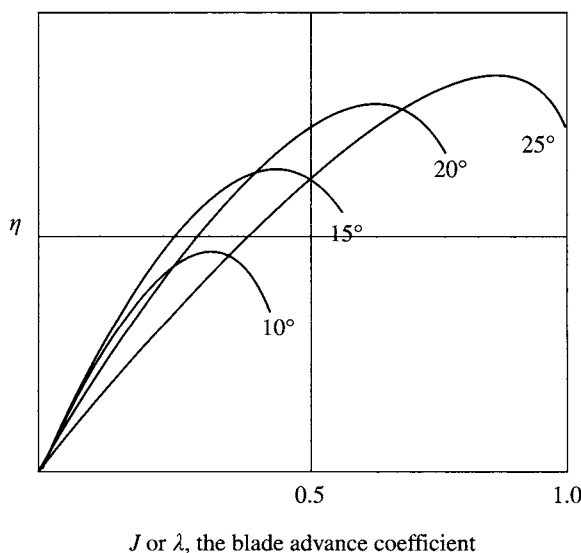


Fig. 15.7(b) Efficiency variation at different blade angles.

Static thrust

Propellers, fans and water jets operating when a craft is static or at very low speed will have streamlines looking something like those shown in Fig. 15.9. Air or water flow in the area of the blade tips will move forward before travelling through the impeller. Flow contraction will be rather different from the momentum theory presented above and so the generated thrust will not be as high.



Fig. 15.8 View of a small craft with large two-blade propeller, the Universal Hovercraft UH-15P.

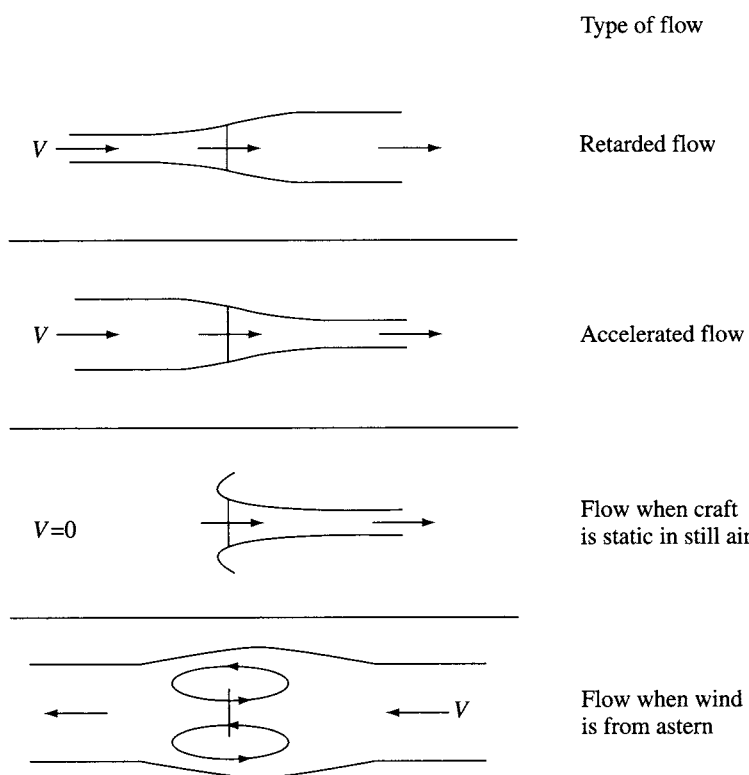


Fig. 15.9 Velocity streamlines at low speed.

An open propeller will experience turbulent flow over the outer part of the blade. Ducted systems can be designed with these outer radius streamlines in mind, so maximizing thrust at low speeds, but then at high speed the bell-shaped intake will not be optimum. Clearly a compromise is required. The duct nose geometry is generally developed using a camber line which forms a bell radius forward of the impeller plane. A thick section, of 12–18% chord is used, to minimize flow breakaway, both at high forward speeds and when the craft is yawed.

Based on experience gained from helicopter rotors, ACV designers often use a figure of merit (FoM) to characterize a propeller performance at a particular speed of advance into the fluid V_0 , defined as the ratio of ideal power input to actual power input, i.e.

$$\text{FoM} = N_i/N_a = \eta_i/\eta_a \quad (15.27)$$

Real propeller characteristics are determined from wind tunnel or cavitation tunnel testing, where thrust and power coefficients C_T , C_N are determined at given rotational speeds, n . Dimensional analysis may be used to verify the following relationships:

$$C_T = T/[\rho_a n^2 D^4] \quad (15.28)$$

$$C_N = N/[\rho_a n^3 D^5] \quad (15.29)$$

now

$$\begin{aligned} T &= \rho_a A V_{\text{act}} V_j = m V_j \\ &= \rho_a A V_{\text{act}} V^* \end{aligned} \quad (15.30)$$

where

$$V^* = V_j/V_{\text{act}}$$

also

$$V_{\text{act}}^2 = T/(\rho_a A V^*)$$

(If craft forward speed is V_0 this must be deducted from V_{act} and V_j when determining the thrust.) Now

$$\begin{aligned} N_i &= 0.5 \rho_a V_{\text{act}} A V_j^2 \\ &= 0.5 \rho_a V_{\text{act}}^3 A V^{*2} \\ &= 0.5 \rho_a A V^{*2} [T/(\rho_a A V^*)]^{3/2} \end{aligned} \quad (15.31)$$

so

$$T = N_i^{2/3} [2 \rho_a A]^{1/3} \quad (15.32)$$

or

$$N_i = T^{3/2} / [2 \rho_a A]^{1/2} \quad (15.33)$$

thus

$$\begin{aligned} \text{FoM} &= N_i/N \\ &= [C_T^{3/2} \rho_a n^2 D^4]^{3/2} / \{[C_N \rho_a n^3 D^5] [2 \rho_a A]^{1/2}\} \\ &= [C_T^{2/3}/C_N] \{2/\pi\}^{0.5} \end{aligned} \quad (15.34)$$

also

$$\text{FoM} = T^{2/3} / \{N [2 \rho_a A]^{1/2}\} \quad (15.35)$$

so

$$T = \text{FoM}^{2/3} N^{2/3} [2 \rho_a A]^{1/3} \quad (15.36)$$

thus

$$T/N = \text{FoM}^{2/3} [2 \rho_a A/N]^{1/3} \quad (15.37)$$

from which it can be seen that thrust per unit power is inversely proportional to the cubed root of the disc loading. Since

$$A = \pi D^2/4$$

$$T = \text{FoM}^{2/3} N^{2/3} [\pi \rho_a/2]^{1/3} D^{2/3}$$

and

$$T/N = \text{FoM}^{2/3} [\pi \rho_a/2]^{1/3} D^{2/3} (1000/g)^{2/3} 1/N^{1/3} \quad \text{in kW} \quad (15.38)$$

or

$$T/N = \text{FoM}^{2/3} [\pi \rho_a/2]^{1/3} D^{2/3} (550)^{2/3} 1/N^{1/3} \quad \text{in hp} \quad (15.39)$$

These expressions can be reduced as follows:

$$T/N = 1.26891 \times \text{FoM}^{2/3} [D^2/N]^{1/3} \quad \text{in kW} \quad (15.40)$$

or

$$T/N = 1.04216 \times \text{FoM}^{2/3} [D^2/N]^{1/3} \quad \text{in shp} \quad (15.41)$$

which allows a plot of thrust/power against $[D^2/N]^{1/3}$ for a given FoM, as shown in Fig. 15.10. Typical FoM for four-bladed open propellers may be between 0.7 and 0.75, so that T/N may be estimated for a given diameter.

From momentum theory (see section 15.3) the relationship between ideal thrust available from a ducted propeller compared to a free propeller at zero forward speed can be shown to be approximately

$$T_{sp}/T_{fp} = 1.26 (D_s/D_t)^{2/3} \quad (15.42)$$

where D_s is the duct inside diameter, ignoring the blade tip clearance, for the ducted propeller. If the shroud section thickness is 15% of diameter and outer diameters are the same (shrouded propeller diameter 85% of free propeller, which is typical) T_{sp}/T_{fp} is 1.13062, so that T/N becomes

$$T_{sp}/N = 1.43466 \times \text{FoM}^{2/3} [D^2/N]^{1/3} \quad (N \text{ in kW}) \quad (15.43)$$

If FoM is again assumed as between 0.7 and 0.75 then the static thrust exclusive of induced thrust from the duct itself can be estimated for given powers, to gain some idea of the appropriate duct diameter for a given craft. It should be noted this assumes a duct which has ideal inflow and no flow contraction in the slipstream.

Air jet propulsion

If we consider alternatives to a propeller to create a jet of air for propulsion or manoeuvring of an ACV, the following might be used:

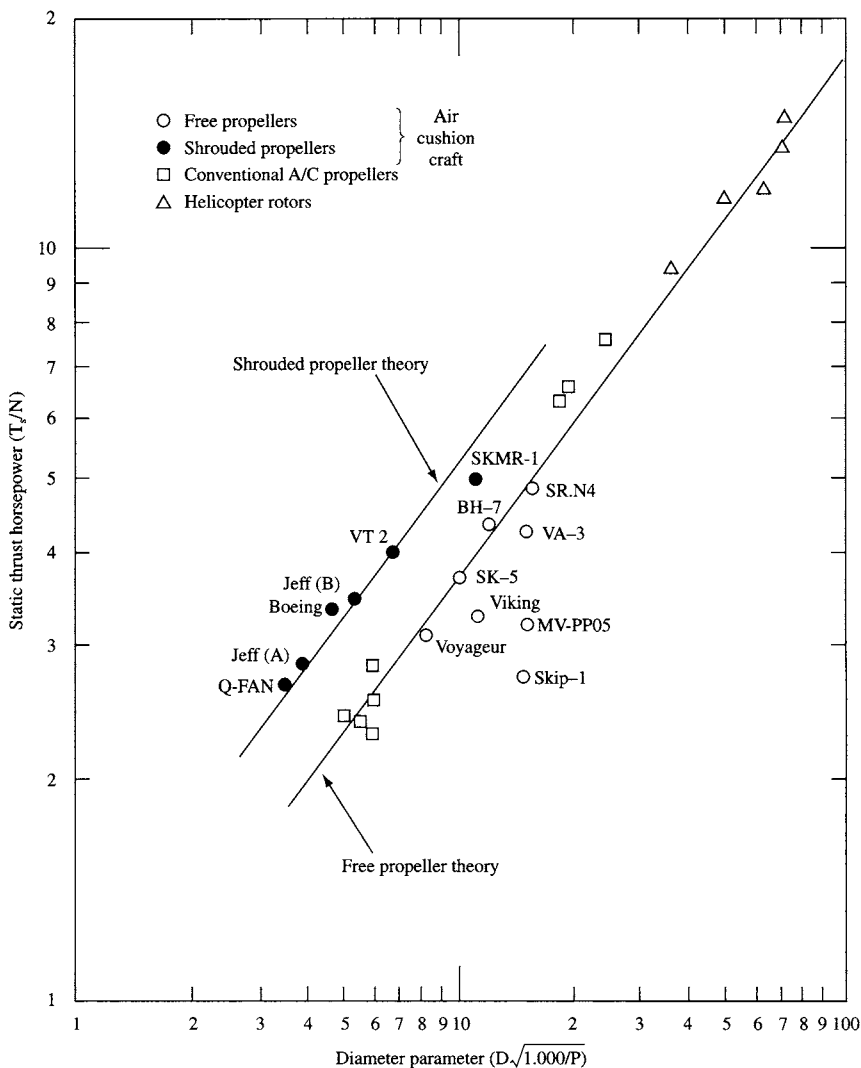


Fig. 15.10 T/N vs $D/N^{0.5}$ [4].

- cushion air
- air ducted from a mixed flow or centrifugal fans
- ducted axial fans

A small component of thrust is often present from the gap under stern skirts. To prevent scooping through hump speed a positive gap under stern segments is desirable anyway, usually about 10% of the segment height. The thrust developed from this air jet is

$$T = Q \rho_a (V_j - V_c) \quad (15.44)$$

where V_c is the craft speed air speed and V_j the air jet speed

$$V_j = [2 p_c / \rho_a]^{0.5}$$

$$Q = A C_j V_j$$

where C_j is the discharge coefficient for the air jet under the skirt segments. At zero speed in still air equation (15.44) reduces to

$$T = A C_j 2 p_c \quad (15.45)$$

Cushion static pressure is converted to kinetic energy at free stream pressure to develop thrust. The V_j available from typical cushion systems is shown in Fig. 15.11. At zero speed, the discharge coefficient for the skirt 'nozzle' reduces the available thrust. At increasing craft forward speeds, the thrust simply diminishes, in contrast to

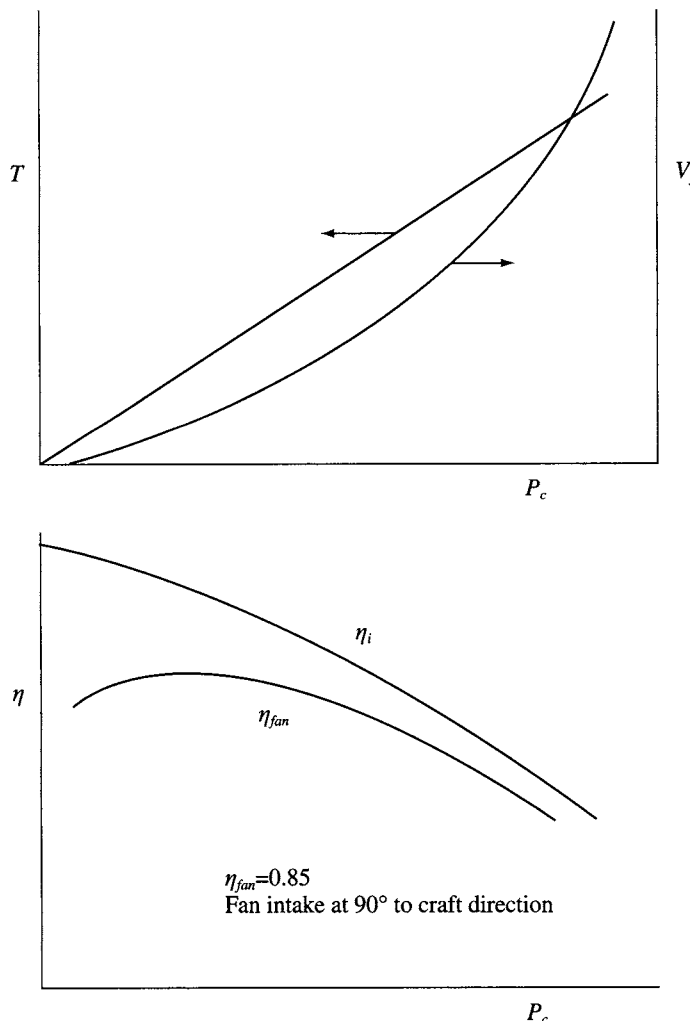


Fig. 15.11 V_j from cushion systems.

a propeller or ducted axial fan, which may be designed for a given forward speed. This loss may be correlated with acceleration of lift fan intake air to craft forward speed, which is normally calculated as momentum drag and represents a comparative efficiency loss of 50%.

Cushion system fans are selected for maximum efficiency when at mean cushion flow, at cushion pressure. In order that the lift fans operate at their most favourable point, the cushion system design should account for the desired stern skirt discharge.

Rather than using cushion air, it is more convenient to use dedicated air ducts and fans. The SR.N1 in its original configuration used a system with ducts to each corner of the craft, see Fig. 1.9. In the 1960s this was developed further on a number of craft, for example the Cushioncraft CC5, Fig. 15.12, used centrifugal fans for propulsion. The primary design objective for this craft was a low noise signature. In this case the fan operating point is adjusted to a discharge pressure sufficient to balance the intake and diffuser duct losses. A fundamental problem exists, which is that at craft forward speeds there is an intake loss as the air is first accelerated to craft forward speed and in addition centrifugal fans have low efficiency at high flow rates. While not the most power efficient, fan jet craft were extremely quiet.

More recently, ducted air has been used for rotatable bow thrusters on the LCAC, and AP1.88, for example, see Fig. 15.13 and Fig. 6.9. Optimization follows the same logic as for a centrifugal fan propulsion system, at craft speeds close to zero. While the thrust at high speed is low, this can be used to assist control of yaw in side winds. Low efficiency is accepted based on the utility of the control forces made available. The air jet exhaust velocity should be selected to be higher than the craft cruise speed, so as not to create unnecessary additional drag force in normal operation.

Ducted axial flow fans are discussed further below. For the purposes of ACV design these may be considered a subset of ducted propellers with higher solidity.

15.2 Air propellers

It is assumed at this point that the designer has used momentum theory with approximate values of expected efficiency to estimate his desired propeller diameter, as in Fig. 15.14. The propeller design itself is now to be selected, including the number of



Fig. 15.12 The Cushioncraft CC5 – a very quiet centrifugal fan propelled craft.



Fig. 15.13 A rotating thruster unit (AP1.88).

blades and their form. We will first give some background, before discussing propeller selection itself. Example data for hovercraft propellers are given in Table 15.2.

Table 15.2 Hoffman air propeller summary data

Propeller	No. blades	Pitch change mechanism	Power (kW max.)	RPM (max.)	Diameter (max. m)	Weight (kg)	Application
HO-V123O-DOR	3	H/M	225	2400	1.8	32	SAH 1500, Hovertrans PH11, PH12
HO-V1440-DOR	4	H/M	300	2500	2.0	45	Griffon 2000 TDX
HO-V1550-DO	5	H	300	3600	1.5	34	
HO-V1830-DO	3	H ground adjustable	320	2500	2.2	42	
HO-V194P-DFR	4	H	640	2200	4.0	173	Wartsila Larus
HO-E214	4	ground adjustable	800	2200	2.75	108	BHC AP1-88
HO-V225Q-VR	5	H	1200	1200	4.0	220	Chaconsa SA36
HO-V254P2-DFR-0	4	H	640	2200	3.0	150	BHC AP1-88 ABS
HO-V285	5	H	2450	960	3.6	600	Korea Tacoma Marine

Design methodology

A design methodology has been developed over many years for aircraft propellers, based on interpretation of results from wind tunnel testing, in a similar way to the original development of data on aerofoil forms. Non-dimensional coefficients C_T (thrust coefficient), C_N (power coefficient) and J (advance ratio) are determined

experimentally in the wind tunnel by propeller designers, based on a given blade angle at a station 70% of the propeller diameter from the centre.

$$C_T = T/[\rho_a/g n^2 D^4] \quad (15.46)$$

$$C_N = N/[\rho_a/g n^3 D^5] \quad (15.47)$$

$$J = V_0/[n D] \quad (15.48)$$

where T is the propeller thrust (kg), ρ_a the air density (kg/m^3), n the propeller speed, rps (l/s), D the diameter (m), N the propeller power (kg m/s) and V_0 the free stream velocity (m/s). Propeller efficiency can be determined as

$$\eta = T V_0/N = C_T J/C_N \quad (15.49)$$

The propeller characteristics are normally plotted against variations in the propeller diameter, number of blades, the activity factor AF and blade-integrated design lift coefficient $C_{L,Di}$ [104] where

$$AF = 10^5/D^5 \int_{r=0.1D}^{r=0.5D} c r^3 dr \quad (15.50)$$

where c is the local blade chord

$$C_{L,Di} = 10^4/D^4 \int_{r=0.1D}^{r=0.5D} C_{L,D} r^3 dr \quad (15.51)$$

where $C_{L,D}$ is the local lift coefficient at zero blade incidence for the aerofoil. Activity factors for propellers which have been used on existing hovercraft are usually in the range 100–150 and have $C_{L,Di}$ values in the region 0.55–0.7.

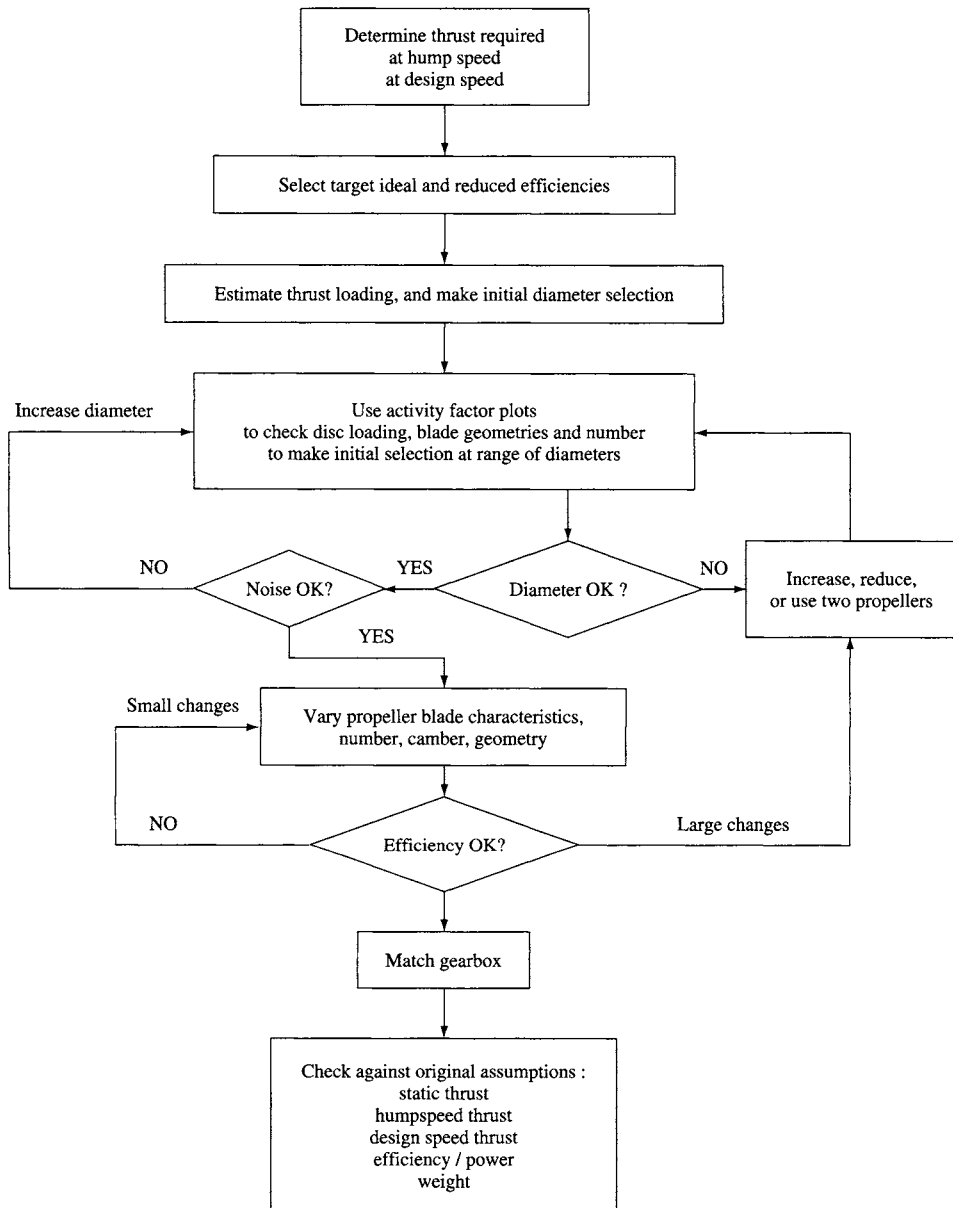
Blade types and efficiency

High activity factor blades (above 150) have more of a paddle appearance, while low AF (e.g. SR.N4 at 108) blades are tapered. High AF propellers are more suited to lower tip speed, 120–170 m/s, which also helps limit emitted noise. High $C_{L,Di}$ blades are more cambered and so give very little reverse thrust if constructed as a variable pitch propeller.

Early ACVs used low AF propellers direct from aircraft, which had high tip speeds. Experience has shown that unless tip speed is kept below about 50% of the speed of sound ($C = 330$ m/s) then propeller noise can be a nuisance to the environment, with external levels in excess of 90 dBA at 150 m from the source. If we consider the desired propeller speed for a moment, if we limit tip speed to 175, 165 and 150 m/s, this gives the results shown in Table 15.3, for different diameters.

It can be seen that above around 1.5 m diameter, reduction drive is required for high-speed diesels. For installations up to around 400 kW (550 shp) toothed belt drives may be used to achieve the reduction, while above this, a gearbox is unavoidable.

The noise limitation requirement effectively limits the power which may be absorbed by a propeller of a given diameter. The designer then has a choice between increasing blade number or changing the blade geometry to maximize efficiency. If a

**Fig. 15.14** Air propeller selection.

variable pitch propeller is to be selected, to give reverse thrust, then blades with low camber (low $C_{L,D}$) need to be chosen. With camber of around 4% and lift coefficient 0.7, similar to SR.N4 propellers, reverse thrust of 45–50% can be generated. If camber is increased to 5%, with lift coefficient at 0.9, then reverse thrust drops to 35–40%, for the same forward thrust rating. If the propeller is a fixed pitch unit, then higher camber may be selected, to reduce the blade number or dimensions for a given power rating.

Table 15.3 Propeller diameter/tip speed relationship

Diameter (m)	RPM at tip speed			Typical power	
	175 m/s	165 m/s	150 m/s	kW	shp
0.5	6685	6303	5730	13	17
1.0	3342	3151	2865	51	68
1.5	2228	2101	1910	115	154
2.0	1671	1576	1432	204	274
2.5	1337	1261	1146	319	428
3.0	1114	1050	955	459	616
4.0	836	788	716	817	1095
5.0	668	630	573	1276	1711
6.0	557	525	477	1838	2464
7.0	477	450	409	2501	3353

Selection procedure

The starting point to select a propeller for a given craft is to consider two forward speed conditions, hump speed into a wind of say 25 knots and the desired maximum operating speed, e.g. 60 knots in a head wind of 10 knots or so. At hump speed, sufficient thrust margin for acceleration is required, between 20 and 50% depending on the design maximum speed. Propeller selection is shown diagrammatically in Fig. 15.14.

Propeller power loading in the region 50–75 kW/m² is typical of ACVs which have been built to date. Choice of diameter is dictated by available blades and hub assemblies from the specialist suppliers. If a practical efficiency level for a typical propeller is assumed as 15% below the ideal curve to estimate thrust, this will provide a start for sizing and enable initial enquiries to be made to suppliers.

Typically characteristic plots for propellers with three to six blades should be available. A good starting point will be to use the data for a four-blade propeller and check first how close this is to the desired characteristics. Once AF, C_N , C_T and J data plots have been obtained it is possible to select a series of AF and check the C_N and C_T at differing J . A sample plot is shown in Fig. 15.15 for the Dowty LCAC propeller. From these data a compromise for propeller speed, blade angle and shape may be chosen to fit the craft operating envelope.

Some experimentation between blade number and blade chord is usually necessary before the desired combination of propeller speed and diameter can be selected. Normally four-blade propellers provide a realistic selection, while ducted propellers for high powered craft may require six blades to limit diameter and emitted noise.

This approach assumes that the ACV designer will select a propeller from a range of standard components available from a specialist supplier (Messier-Dowty, Hoffman, Hamilton Standard or Air Vehicles for example). Development by these suppliers of a new propeller is very expensive, partly because the new design would be required to be prototype tested for certification by authorities prior to use on a commercial ACV. Several propeller designs are now available based on standard hubs and blades, which can be assembled to fulfil a range of possible requirements. Designers should nevertheless bear in mind that in most cases, the selection of a propeller will be between a series of available units, in the same way as selecting an engine.

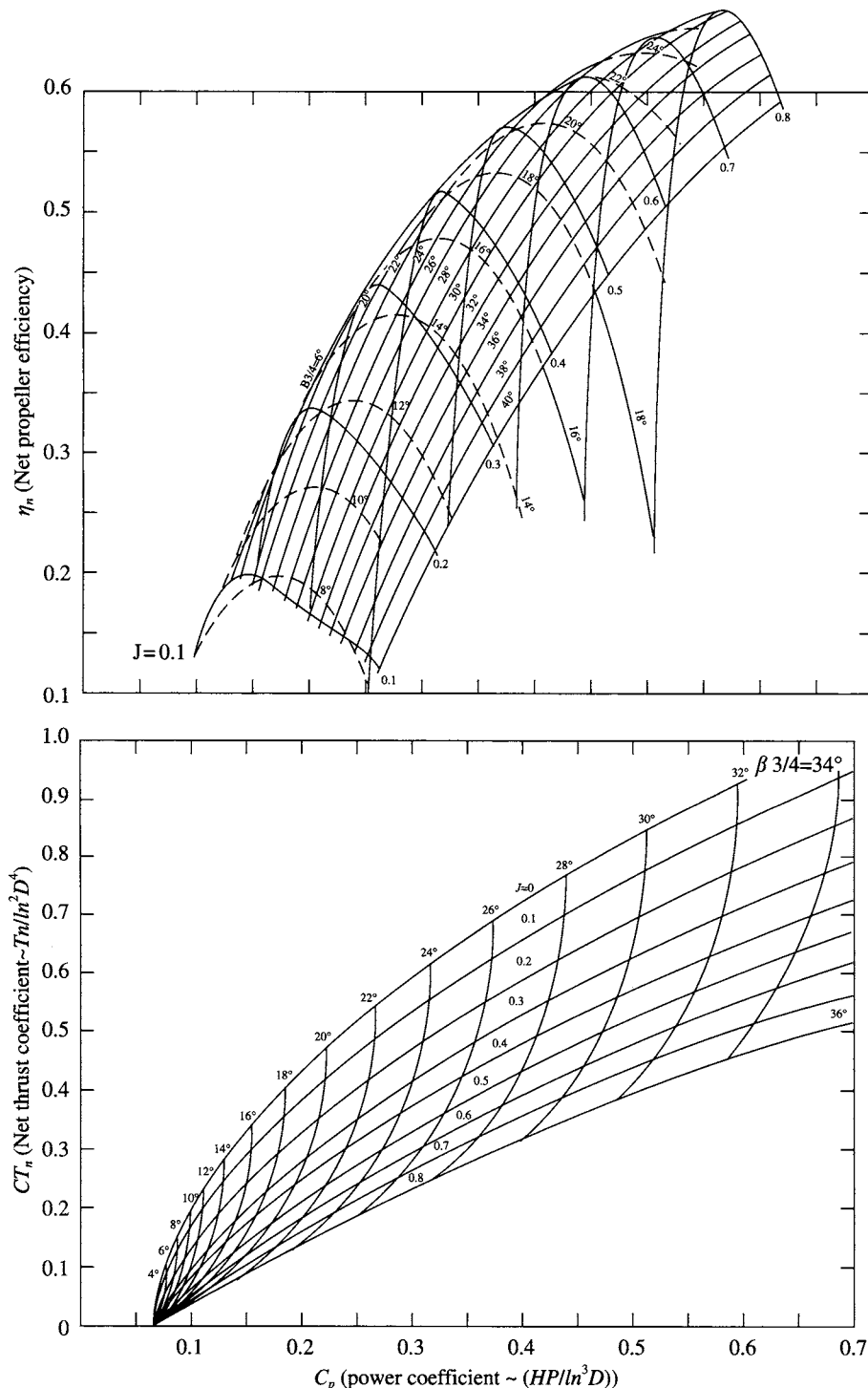


Fig. 15.15 Example plots of efficiency and CT_n against varying blade angle for the Dowty LCAC ducted propeller with exit area ratio 1.18, stator vanes and blade erosion protection.

Construction and weight

Air propellers are constructed in three ways. Fixed pitch propellers for smaller craft can be manufactured in wood laminated with epoxy resin. Larger propellers used to be made from solid aluminium alloy forgings, while very large propellers, for example the 5.8 m diameter SR.N4 propellers, are made from an inner aluminium alloy spar surrounded by a blade section formed from polyurethane foam with a glass/epoxy outer sheath. Since the mid 1980s, composite propeller blade design has been developed and this is now the most likely candidate for a utility ACV, in 'ground adjustable blade angle' form, or as variable pitch propellers. Such propellers are significantly lighter than aluminium propellers. Due to the complexity of their construction aluminium and composite propellers are expensive to procure, particularly in variable pitch form. Dependent therefore on the craft size and mission, fixed pitch propellers combined with air-jet thrusters may be considered as a first option, and variable pitch propellers if craft manœuvring demands this choice.

Propeller weight may be estimated from the diameter. An initial estimate for craft design purposes may be based on:

4-blade VP propellers	100 kg/m diameter in aluminium 75 kg/m diameter in epoxy composite
6-blade VP propellers	120 kg/m diameter in epoxy composite
4-blade fixed pitch	20 kg/m diameter in wood laminate (to 3 m)
2-blade fixed pitch	10 kg/m diameter in wood laminate (to 3 m)

Variable pitch propellers have a hub structure and control system such as that shown in Fig. 15.16(a) and (b), a Dowty propeller hub. A system of hydraulic pistons is used to rotate the blades via crank pins. Fig. 15.16(b) shows a Hoffman ground adjustable propeller hub which allows static optimization of a fixed pitch propeller to a craft.

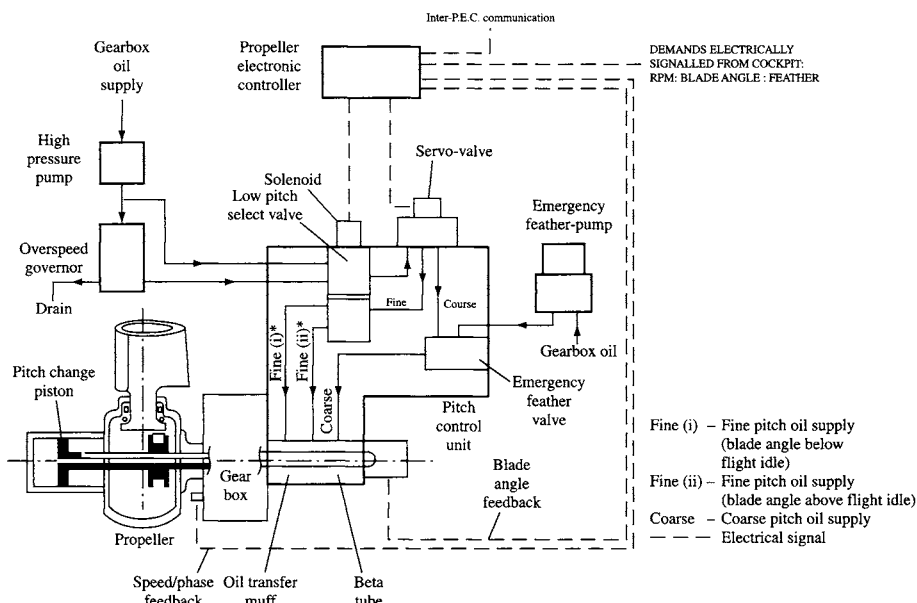


Fig. 15.16(a) Variable pitch air propeller control system schematic.

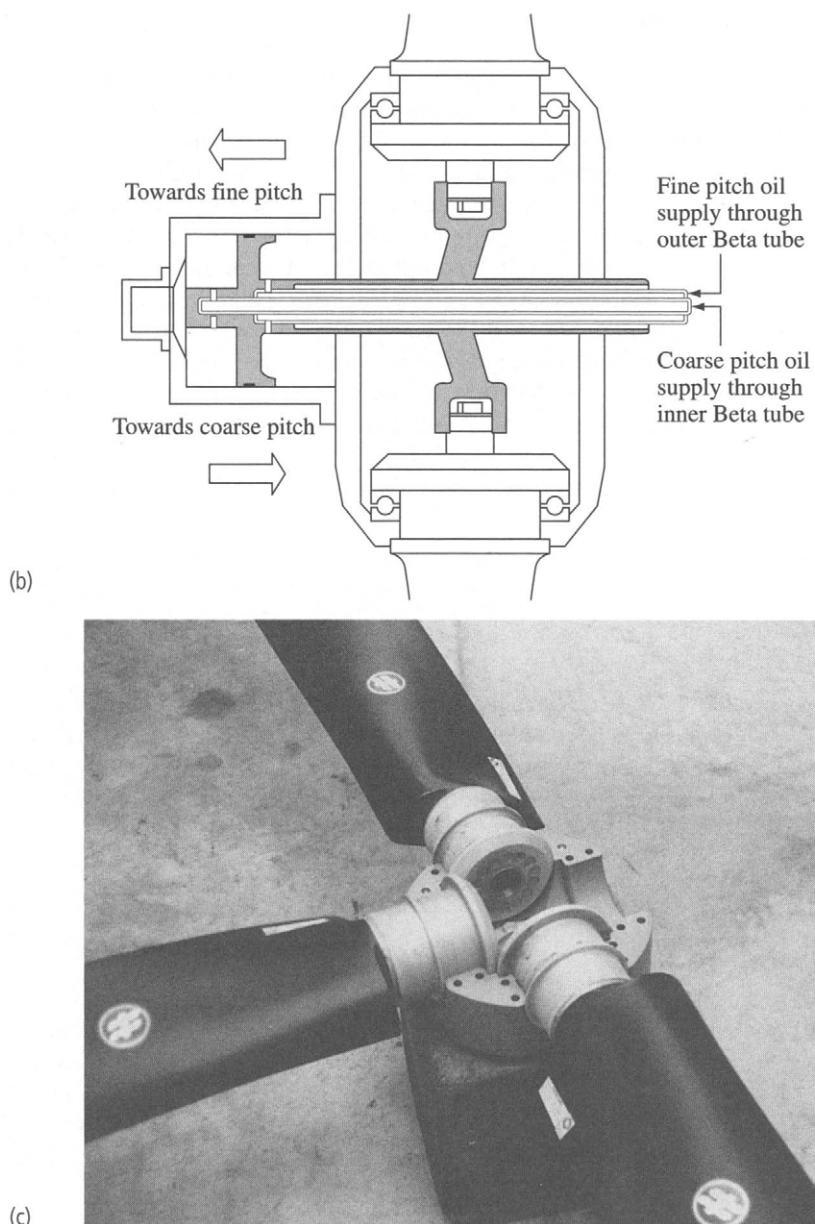


Fig. 15.16 (b) Variable pitch propeller hub construction and control system; (c) Hoffman ground adjustable hub from an API-88 propeller.

Blade erosion and its mitigation

Sand and salt water can cause rapid leading edge erosion to propeller blades unless protective strips are fitted. Wooden blades are normally protected by a thin metal

plate over the outer half of the blade length. Aluminium blades require nickel-plated leading edges, while composite blades are usually fitted with thin metal plates bonded into the resin.

15.3 Ducted propellers and fans

The primary purposes for installing ducted air propulsors are to reduce diameter so as to reduce noise level for a given thrust and to provide higher thrust levels at low speeds giving greater thrust margin for acceleration through hump speed.

The penalty is that of duct weight. With efficient cushion systems now making the use of heavier hull structures and diesel engines practical, this should not be a significant penalty and the advantages can be maximized. Other benefits include the physical protection of the propulsor afforded by the duct.

Ducted propellers

If a propeller is installed in a duct, the inflow conditions are changed so that the jet velocity behind the duct is the same as velocity at the impeller disc (or possibly slightly below, if the duct has an internal flare), i.e.

$$V_j = V_0(1 + a) \quad (15.52)$$

In this case the ideal efficiency may be derived again from equation (15.11a)

$$\eta_i = 2/[2 + a] = 1/(1 + a/2) \quad (15.53)$$

Table 15.1 illustrates the variation of η_i with V_j in comparison with open propellers. It can be seen that as V_j increases, the relative gain from installing a ducted propeller also increases.

Ducted fans

The main difference between a ducted fan and a ducted propeller is that a fan generally has much higher solidity, operates at lower J values and employs static flow straightener vanes behind the impeller to remove the swirl imparted to the air flow, recovering the energy which would otherwise be wasted. A ducted fan with stator system should therefore give higher T/N than a ducted propeller of the same diameter.

Since the stator blades are fixed, the designer has to make a choice of what craft operating condition should be optimized. Craft cruising conditions may be taken as a start. At lower craft speeds there will be some residual swirl in the slipstream, while above cruising speed thrust will simply diminish since there will be no additional power available.

Ducted fan propulsion has been developed to the greatest extent for small craft, based on using industrial HVAC fan components, in the power range between 15 and 150 kW (20 and 200 shp). The commercial availability of a variety of aerofoil cross-section moulded plastic blades and hub designs in this power range allows acceptable efficiency to be achieved while maintaining minimum cost and installed weight. The designer may then concentrate on design of an effective stator system and duct in order to maximize craft performance.



Fig. 15.17(a) The VT2 hovercraft propelled by Dowty variable pitch ducted fans.

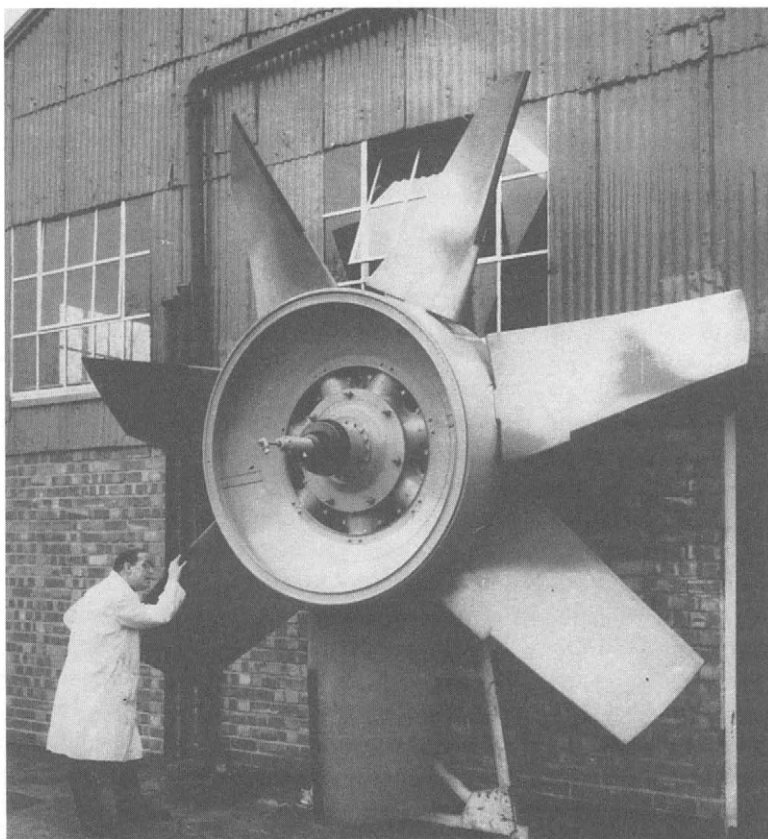


Fig. 15.17(b) The Dowty T2 ducted fan impeller.

At the opposite end of the size scale, Vosper Thornycroft and Dowty Rotol co-operated together in the mid 1970s to design a ducted fan propulsion system for the 100 t VT2 hovercraft, see Fig. 15.17. These fans, designed to absorb 3000 shp each from Rolls-Royce Proteus gas turbines, were installed in integrated lift and propulsion powertrains. The fans had variable pitch mechanisms on the impeller blades to allow thrust variation while maintaining cushion lift and to give some reverse thrust capability.

When operating a fan and stator system in reverse flow, it is clear that efficiency will be relatively low and so the obtainable thrust will be lower than from a variable pitch ducted propeller. Due to the number of blades, the pitch change mechanism will also be very complex.

In general, if a designer selects a ducted fan propulsion system, the initial approach will be to look at fixed impeller designs, with separate powering to the cushion system, and consider alternative means for reverse or manoeuvring thrust. Where installed power is higher than around 150 kW, a ducted propeller is more likely to offer the best balance of design parameters.

Fan selection

Fan characteristics of power, pressure and efficiency are normally determined by fan manufacturers in relation to the volume flow at a given diameter and speed of rotation. Dimensional analysis [110] can be used to show that the laws relating volume flow and pressure are

$$Q = k_q d^3 n \quad (15.54)$$

$$p = k_p \rho_a d^2 n^2 \quad (15.55)$$

and

$$N = p Q = k_N \rho_a d^5 n^3 \quad (15.56)$$

where k_q , k_p and k_N should be constant for geometrically similar units. Once the values of these coefficients have been obtained from a manufacturer for a given fan, it is then possible to plot power and thrust curves against rotational speed, at a pressure equal to the free stream dynamic pressure. Since

$$T = Q \rho_a V$$

and

$$V = (2 p / \rho_a)^{0.5} \quad \text{if we assume fan total pressure can be used as basis.}$$

It is assumed here for simplicity the craft is static and that a stator system is installed such that slipstream swirl is removed.

Axial fans are normally designed with hubs which allow the blades to be set at a range of different angles, measured at the blade root, commonly between 20 and 50°. Each blade design will have an optimum root angle where the characteristics are most favourable, which will be evident from inspection of the characteristic curves. Data are often presented also for different numbers of blades in a given hub, 3 blades in a 6-blade hub, 4 out of 8, 5 from 10, etc.

Fan hubs are considerably larger than propeller hubs, between 0.1 and 0.3D rather than 0.05–0.15D and require nose and tail fairings to avoid significant loss of efficiency due to turbulence.

Stators

Consider the velocity triangle diagram for an axial fan shown in Fig. 15.18. The aerofoil blade operates at an angle of attack relative to the ideal vane and imparts a mean velocity of w_∞ to the flow which is the mean of the entry and exit velocities w_1 and w_2 at a vane. The induced rotational velocity V_u is therefore

$$V_u = w_\infty C_L 0.5c/s \quad (15.57)$$

where c is the individual blade chord and s the blade spacing, $= 2\pi r/z$, where z is the number of blades.

If drag forces on the aerofoil blade are included, then it can be shown [110] that

$$V_u = w_\infty C'_L 0.5c/s \quad (15.58)$$

where

$$C'_L = C_L [1 + C_D/C_L \cot(\beta - a)]$$

Typically the value of C_D is of order 0.015 to 0.02 [111] while C_L is between 0.7 and 1.0 and the design angle of attack would be 4–6°.

The stator vane or aerofoil will have a velocity triangle as shown in Fig. 15.18 where the induced rotational velocity is $-V_u$. The stator blades will require significant camber and in order to avoid turbulence problems at off-design conditions it is advisable to use a reasonably thick aerofoil section.

In order to avoid problems of ‘beating’ between impeller and stator and the associated noise generation, it is advisable to use an odd number of blades (if impeller has 6 blades, stator should have 5, 7 or 9).

Design of stator systems requires fan blade aerodynamic data to be available to the designer for the design conditions. This can be obtained from the manufacturer, or calculated based on direct measurement of the fan blade geometry, so long as the aerofoil is a known design, for example one of the NACA series [111]. Where the fan used as basis for the propulsion system is an industrial unit, an improvement of between 10 and 20% in developed thrust compared to a unit without stators is normally achievable.

Stators should be located as close to the trailing edge of the impeller blades as possible. There are limitations to this in order that stator blade geometry is practical to fabricate. Blade flexure and vibration in service mean that an average of 20% of impeller chord is a likely minimum, while if the gap exceeds the impeller blade chord, then the stator effectiveness will be significantly reduced.

Duct design

Ideally a propulsor duct should be as short as possible, to minimize weight, but there are practical limitations to this. The duct section is an aerofoil formed around a camber line which follows a parabolic or hyperbolic curve in front of the impeller and either a cylinder behind, or an expanding cone with angle of 5–10°.

A realistic dimension for the intake section will be between 10 and 15% of the diameter. The impeller should be located at the aerofoil ordinate with maximum suction, which is usually just ahead of the maximum camber, at about 0.3c, thus the chord

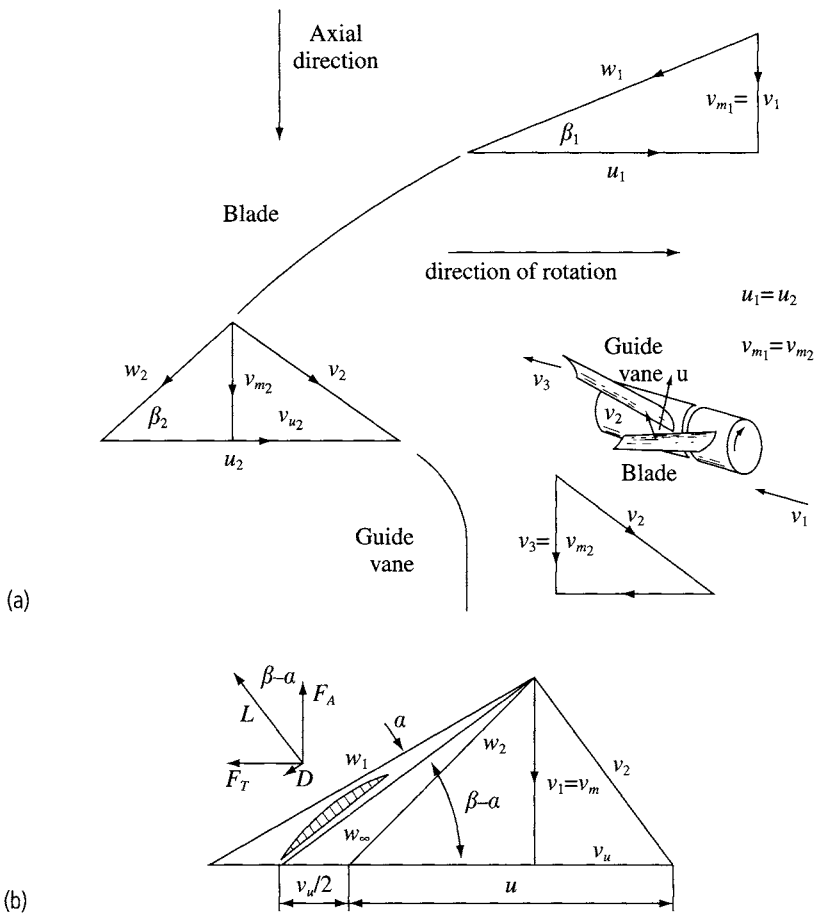


Fig. 15.18 Axial fan velocity diagrams, ideal vane and aerofoil. [110]

should be between 0.3 and 0.5D. If stators are installed, the duct may be between 0.4D and 0.6D in length. NACA 63 series aerofoils are a useful starting point [111].

The intake bell-mouth geometry will require some thought regarding the craft speed for which it is optimized. The camber line cone angle for inflow to the leading edge is related to the chosen value of a for the impeller. If a is 0.2 then the the cone angle should be $\tan^{-1} 0.2$, i.e. 11.5° , while at $a = 0.5$ the angle should be 26.5° . At zero speed, when a is infinite, the inflow streamlines will converge from a wide angle, so that the ideal geometry is a radius, typically of 0.1–0.2D. The intake clearly has to form some compromise between these two conditions.

Experience suggests that if the designer begins with a cone convergence angle of 15° for high-speed craft and 30° for low-speed craft and fits a camber mean line similar to NACA 63, followed by a 63-012, 015 or 018 basic thickness form, this should provide an efficient aerodynamic basis for a duct; this is because of the favourable pressure profiles of both the mean line and aerofoil. The final form is likely to be altered slightly from this so as to optimize fabrication.

Integrated controls

Ducted propulsors have rudders and elevators directly mounted to the trailing edge of the duct. This minimizes supporting structure, but places stresses on the duct which need to be accounted for when designing the duct structure.

Interaction with ACV hull form

ACV propellers operate in a non-uniform air flow caused by disturbance from the hull form. The lower part of the propeller or fan will be operating in a region of lower velocity and will produce less thrust than predicted above. The reduction depends very much on the ACV hull and superstructure profile.

The most practical approach to account for this effect is to consider the loss of thrust in the same way as a naval architect considers the wake deduction for a marine propeller behind the hull of a ship. Propellers mounted on pylons, such as those of the SR.N4, may have a thrust reduction factor of around 2–5%, while units mounted behind a superstructure, such as the AP1.88 may have slightly higher losses of order 4–8% compared to the free stream performance. This should be accounted for by a designer when first specifying the desired thrust and installed power to avoid the final craft performance being less than that contracted with the customer.

15.4 Marine propellers

Marine propeller design developed from the same momentum and blade element theories reviewed above [88]. The denser fluid in which they operate allows the blades to have much higher chord length and solidity than an air propeller. Marine propellers have total blade area which is between 50 and 120% of the disc area (solidity, or blade area ratio 0.5–1.2). The blade pressure distributions interfere with each other, reducing lift force compared to isolated aerofoil theory. Chord length at $0.7R$ and blade length are of similar dimensions and the chord itself varies rapidly and so the pressure distribution over a marine propeller blade is therefore very much three-dimensional.

Marine propeller design has therefore been founded on tests of propeller designs in closed circuit water tunnels ('cavitation tunnels') to provide correction coefficients to the available theory. As an example, ref. 109 details testing of a parametric series of propellers for operation at high speeds characteristic of SES.

Marine propellers most often have three or four blades. Two-blade propellers are difficult to balance and the pressure variations tend to create vibration under the hull. Larger numbers of blades tend to require a larger boss which reduces efficiency for high-speed propellers. At forward speeds below about 35 knots it is possible to achieve efficiency levels in the range of 70%, but this drops sharply as suction pressure on the blade back surface reduces towards the local vapour pressure. Figure 15.19 shows a plot of approximate efficiency which may be expected from different types of marine propellers and water jets.

Subcavitating propellers must operate with a blade tip speed constrained below a limit (approximately 170 fps or 52 m/s) to maintain the suction side pressure above the

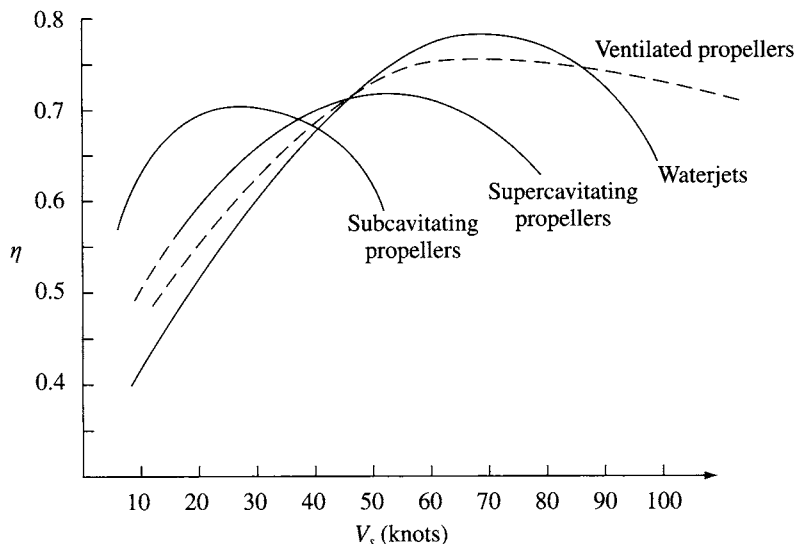


Fig. 15.19 Marine propeller and water-jet efficiency.

level where cavitation begins, while supercavitating propellers should have a minimum tip speed to ensure cavity formation (approximately 300 fps or 92 m/s). If a propeller is to reliably operate in the fully cavitating regime (often also referred to as ‘supercavitating’), the suction pressure must be low enough to generate a steady cavity over the full blade forward surface.

Marine propeller blade sections are thinner than air propellers. Leading edge geometry and orientation are critical to whether turbulence in the real fluid will cause local cavitation. The three-dimensional flow regime combined with this sensitivity created many challenges for analysts until computing power was sufficient to allow calculation based on lifting surface theory rather than two-dimensional analysis. Development of successful blade geometries has therefore been by derivation from parametric series tested in cavitation tunnels.

Marine propellers are normally installed on inclined shafts at an angle of 5–15° (see Fig. 15.27 showing example SES installations). The propeller disc will have a clearance below the SES hull which is minimized in order to give least floating draft. The exposed shaft, shaft supports and rudder mounted behind the propeller all create drag forces (see section 3.10, Figs 15.2 and 7.15) which reduce the propulsive efficiency of the system. They also affect the propeller inflow and so its efficiency directly. At high speeds, these effects become much more significant. Figure 15.19 shows fully submerged cavitating propeller efficiency reducing above about 65 knots. This is because of the rapidly increasing propeller shaft and boss drag.

To reduce this problem the propeller boss may be ventilated, or the propeller may be placed behind the transom with its centre-line closer to the water surface and most or all of the shaft internal to the hull. The blades may be designed to emerge from the water over part of their rotation, in which case propeller sizing has to be carried out for the immersed blades area. Such propellers can be efficient at speeds as high as 100 knots. This design technique is typical of racing craft such as hydroplanes.

Water jets have no external appendages and so can offer higher system efficiencies than supercavitating propellers in the speed range to 65 knots. This is also partly due to the same effect as with ducted air propellers whereby loading on the outer part of the blade may be higher, more closely approximating the assumptions of momentum theory. At present there is not enough experience to clarify whether water jets or ventilated propellers provide the optimum propulsor for ultra-high speeds. The challenge for cavitating or ventilated propellers is structural design, while for water jets design of the intake duct system and a change to inducer-type impellers are the main issues.

In the following paragraphs we will outline the main issues affecting propeller selection for SES, beginning with propellers in the subcavitating regime. Examples of propellers designed for SES are shown in Table 15.4.

Table 15.4 Marine propellers

Craft	Propeller manufacturer or design	Type	Dia (m)	No. off	No. blades	RPM	SHP	Thrust (kg)	Weight (kg)	Material	Remarks
HM.2	Gawn Burrill	Sub FP	0.385	2	3	2600	300	818		Stainless steel	
HM.5	Gawn Burrill	Sub FP		2	3					Stainless steel	
VT.1	KaMeWa	Super VP	0.640	2	3	2200	1100			Ni Al bronze	Outboard rotation
SES-100B	Hydronautics	Semi VP	1.067	2	6	1900	class.	class.	1045	Titanium	Inboard rotation
BH.110	Mekat Escher Wyss	Super									
		Super FP	1.067	2	3					Stainless steel	
		Semi VP			2	7				Stainless steel	
Norcat		Super									
		Trans FP		2	3					Ni Al bronze	

Sub: subcavitating; Super: supercavitating; Semi: semisubmerged design; FP: fixed pitch; VP: variable pitch; class.: classified data (US Navy).

Cavitation

Marine propellers for SES are likely to be subject to cavitation. Variation in local pressure at the blades due to proximity of the hull surface and varying advance coefficient due to shaft inclination will also make cavitation more likely due to the unsteady flow regime.

Dissolved air in the water tends to come out of solution as bubbles (cavities), as pressure reduces towards atmospheric over a propeller blade upper surface. The cavities are initially water vapour saturated. Cavitation damage occurs when the local pressure reduces below the saturation pressure of the water at that depth so that water vapour in the cavities recondenses. The rate at which this happens is sufficient to cause mechanical damage to the propeller blade surface.

The propeller cavitation number is given by the ratio of local static pressure ($P_a + \rho gh$), normally measured at the propeller centre-line, to the local water vapour pressure P_v , divided by the dynamic pressure through the propeller plane:

$$\sigma_p = \frac{P_a + \rho gh - P_v}{0.5\rho V_p^2} \quad (15.59)$$

where h is the immersion of propeller centre-line to static water level, P_v the water

vapour pressure (36 lbf ft^2 or 176 kgf/m^2 approximately), P_a the atmospheric pressure (2116 lbf/ft^2 or 10348 kgf/m^2),

$$V_p = V_a + U'_a$$

where U'_a is the induced axial velocity component at the propeller plane and V_a the free stream velocity. Since U'_a is a function of propeller loading, so σ_p reduces as propeller loading is increased. If the calculation of cavitation number is extended to include the induced velocity at a blade section represented by $\sigma_{0.7}$ (see Figs 15.20 and 15.26) rather than simply the induced axial velocity, it can be stated that below $\sigma_{0.7} = 0.05$ the blade section will fully cavitate, while above $\sigma_{0.7} = 0.12$ cavitation should be limited to vortex shedding from blade tips.

At values of advance coefficient J typical of fast craft, between 0.6 and 1.4, the cavitation number based on free stream velocity, σ_0 , should be above the upper line of Fig. 15.20 for subcavitating propellers. As craft speed increases, it becomes more difficult to restrict blade loading to achieve this.

In the central zone of Fig. 15.20 it is particularly important to consider measures to mitigate the effects of cavitation, including selection of materials with good cavitation resistance, application of cavitation-resistant coatings and improvements to the hydrodynamic design of the hulls. Titanium alloys, followed by stainless steels, are the most resistant, but also the most expensive. The most widely used material, aluminium bronze, has reasonable resistance, but has shown insufficient life for SESs and so it is normally recommended to use stainless steel as a minimum specification, unless operations can allow regular change-out of propellers.

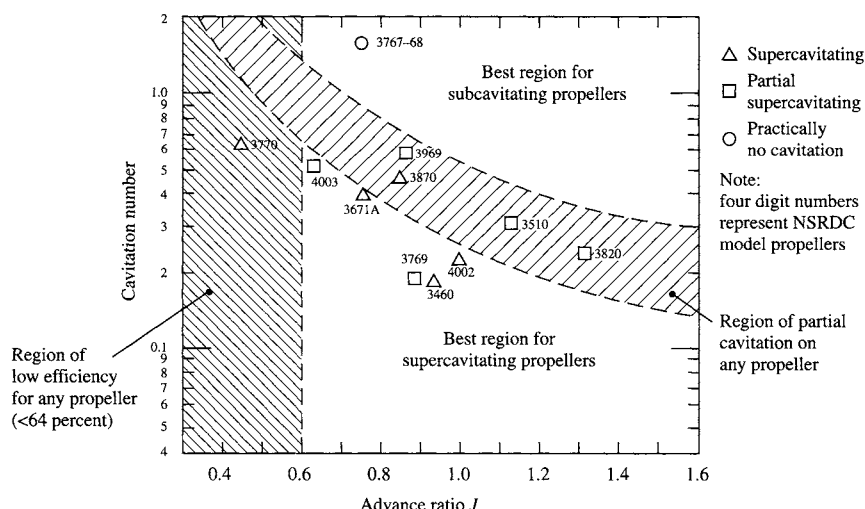


Fig. 15.20 Subcavitating >> fully cavitating regions vs. J . [4]

Momentum theory

Momentum theory as developed in section 15.1 can be used to carry out initial selection of propeller diameter based on a scheme such as shown in Fig. 15.23.

Blade element theory

Blade element theory for marine propellers needs to account for the much lower aspect ratio of the blades than air propellers. Subcavitating marine propellers commonly use flat-faced circular arc blade sections, or thin aerofoil sections such as NACA 16 or 66 series which have a relatively fine leading edge profile [111].

Determination of lift and drag by integration of properties along the length of the blade is straightforward, except that for a marine propeller, the blade chord changes rapidly with diameter and blades form a cascade where interference is significant. The consequence of this is that significant corrections are needed to the blade lift coefficients both with diameter and along the chord at each station of the blades, based on the vortex theory.

Vortex theory

The concept of lift force being generated as a function of circulation around a body developed by Lanchester and expanded later by Prandtl, was applied to propeller design by Helmbold and Goldstein. It was found that marine propellers designed using this theory had too low blade pitch in practice (assumed efficiency as a lifting surface was too high) and so empirical corrections were developed from testing, later followed by theoretical treatments. This work produced correction functions for the inflow and for the effective characteristics of the propeller blades for lightly loaded propellers.

If we consider the lift produced by a propeller's blades:

$$L = \rho V \Gamma \quad (15.60)$$

where Γ is the circulation of a blade element, and if we integrate along the blade, the thrust and power coefficients for the whole propeller may be represented as

$$C_{Tl} = 4Z \int_{x=x_h}^{x=1} G(x/\lambda - U_t/2V_a) dx \quad (15.61)$$

$$C_{Ni} = 4 Z/\lambda \int_{x=x_h}^{x=1} G(1 + U_a/2V_a) dx \quad (15.62)$$

where Z is the number of blades, initially assumed infinite, λ the advance ratio (becomes λ_i for finite number of blades), U_t the tangential induced velocity in slipstream ($U_t/2$ at propeller disc), U_a the axial induced velocity in slipstream ($U_a/2$ at propeller disc), V_a the axial velocity at propeller plane and G the non-dimensional circulation, $G = \Gamma/\pi D V_a$. For a finite number of blades, G must be modified to account for the non-uniform velocity over the circumference. Goldstein derived a relation for this as follows:

$$\Gamma_z = \{2 \pi K(r)/Z\} U_t \quad (15.63)$$

so

$$G = \{2 K(r) x/Z\} U_t / 2V_a \quad (15.64)$$

The Goldstein function for three-blade propellers is shown in Fig. 15.21. For an optimum propeller, the axial and tangential induced velocities at the propeller blades are

$$\begin{aligned} U_a/2V_a &= [\cos \beta_i \sin (\beta_i - \beta)]/\sin \beta \\ &= \{[1 - \eta_i]/\eta_i\} \{x^2/(x^2 + \lambda_i^2)\} \end{aligned} \quad (15.65)$$

$$\begin{aligned} U_t/2V_a &= [\sin \beta_i \sin (\beta_i - \beta)]/\sin \beta \\ &= \{[1 - \eta_i]/\eta_i\} \{\lambda_{ix}/(x^2 + \lambda_i^2)\} \end{aligned} \quad (15.66)$$

Kramer solved these equations to obtain λ_i as a function of λ (J/π) and C_{Ti} . The results for a three-bladed propeller are shown in Fig. 15.22. The area relevant to propellers for high-speed craft is indicated.

If the effects of viscosity are added in the expressions for C_T and C_P become

$$C_T = \int_{x=x_h}^{x=1} \frac{dC_{Ti}}{dx} (1 - \varepsilon \tan \beta_i) dx \quad (15.67)$$

$$C_N = \int_{x=x_h}^{x=1} \frac{dC_{Ni}}{dx} (1 - \varepsilon/\tan \beta_i) dx \quad (15.68)$$

where ε is the lift/drag ratio for each blade section, which may be approximated by using the value at $r = 0.7R$ to characterize the blade performance. The efficiency can be expressed as

$$\eta = C_T/C_N = \eta_i \eta_e \quad (15.69)$$

where η_e is the blade element efficiency due to viscous flow. If an approximation for ε at the blade element at $0.7R$ is used ($\bar{\varepsilon}$):

$$\eta_e = (1 - 2 \bar{\varepsilon} \lambda_i)/(1 + 2 \bar{\varepsilon}/3\lambda_i) \quad (15.70)$$

These relations allow a lightly loaded propeller to be assessed by representing the propeller by its performance at the $0.7R$ ordinate. Assumptions implicit in the method so far are those of two-dimensional theory. The effects between adjacent blade elements with rapidly changing chord, both radially and tangentially, cascade interference and the highly curved flow of the fluid through the propeller all alter the blade element performance. Computer programs have been developed to carry out iterative solution of the pressure distribution over the blade surfaces. These have improved the analytical predictions, but still require calibration with cavitation tunnel tests to avoid errors. The unsteady fluid dynamics of cavitating propellers further increases the dependence on test data.

The consequence of the additional three-dimensional effects is in general to reduce the lift which is generated and to increase the drag forces, making it necessary to adjust the blade incidence and allow for reduced efficiency. The changes will vary with advance coefficient λ and blade loading C_T for a given propeller.

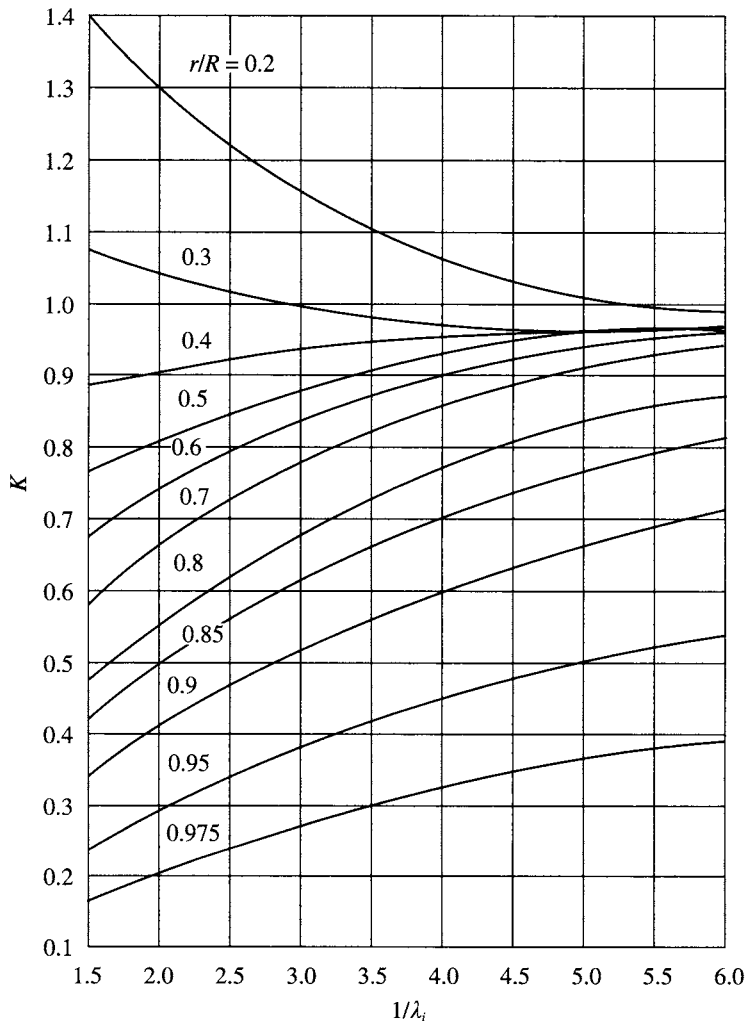


Fig. 15.21 Goldstein function plot for three-blade propellers. [88]

Propeller selection procedure

We consider first a subcavitating propeller. The designer follows a procedure similar to that in Fig. 15.23. An initial estimate of propeller diameter from momentum theory is made, by first determining the required thrust

$$T_r = R_{\text{tot}}/(1 - t) \quad (15.71)$$

where t is the thrust deduction factor, often assumed at 0.92 for twin propeller installations. Approximate data for high-speed craft, based on FoM = 0.7, are given in Fig. 15.24. The propeller speed can be estimated from a formula given by Burtner [88]

$$n = [50 \times 0.2 N/D] 1.667 \quad (15.72)$$

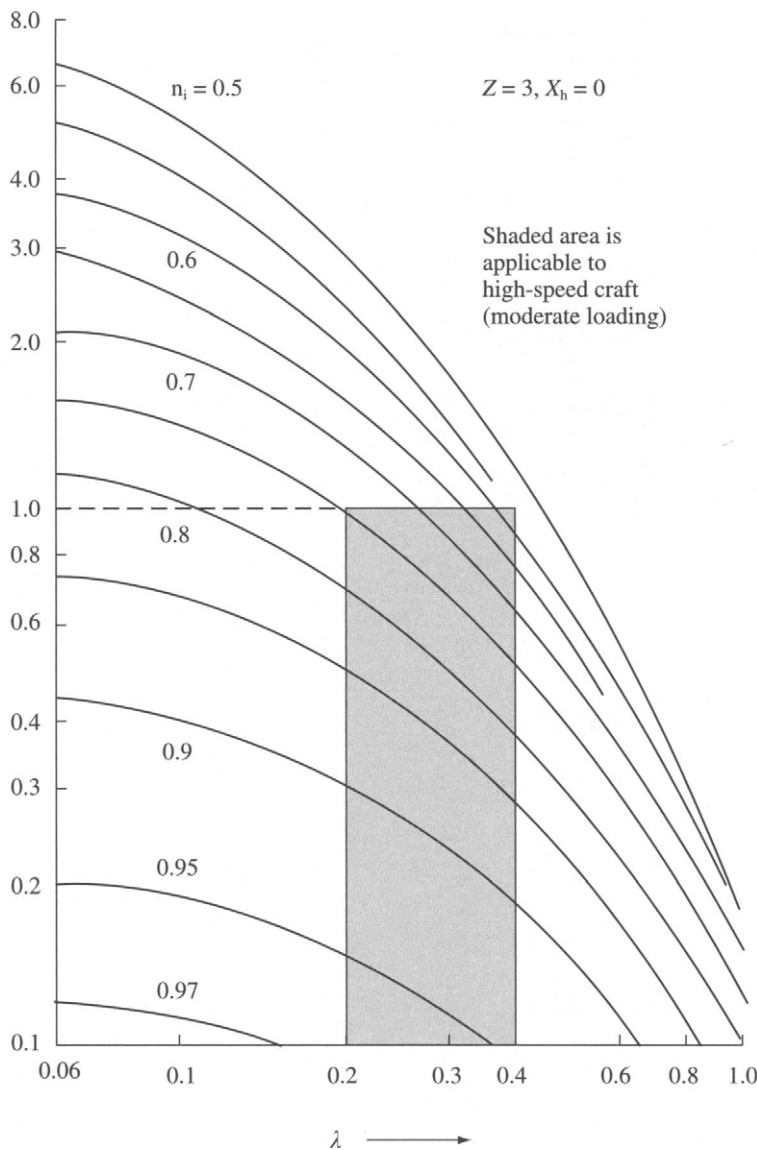


Fig. 15.22 Kramer's chart for three-blade propellers. [88]

where D is the diameter in feet and N the power in shp. If the tip speed ($n D$) is below 55 m/s (180 fps) and the advance ratio ($J = V_c/n D$) is in the region of 0.8–1.0 a successful start has been made.

Propeller blade pitch needs to be adjusted from the advance ratio J , which represents the ideal situation, to include the blade angle of attack necessary to develop lift. This is referred to in propeller design as the slip. High-speed propellers operate with slip in the range 10–15%. During initial design 15% is recommended to be used. The flow regime past SES hull aft bodies is not significantly decelerated

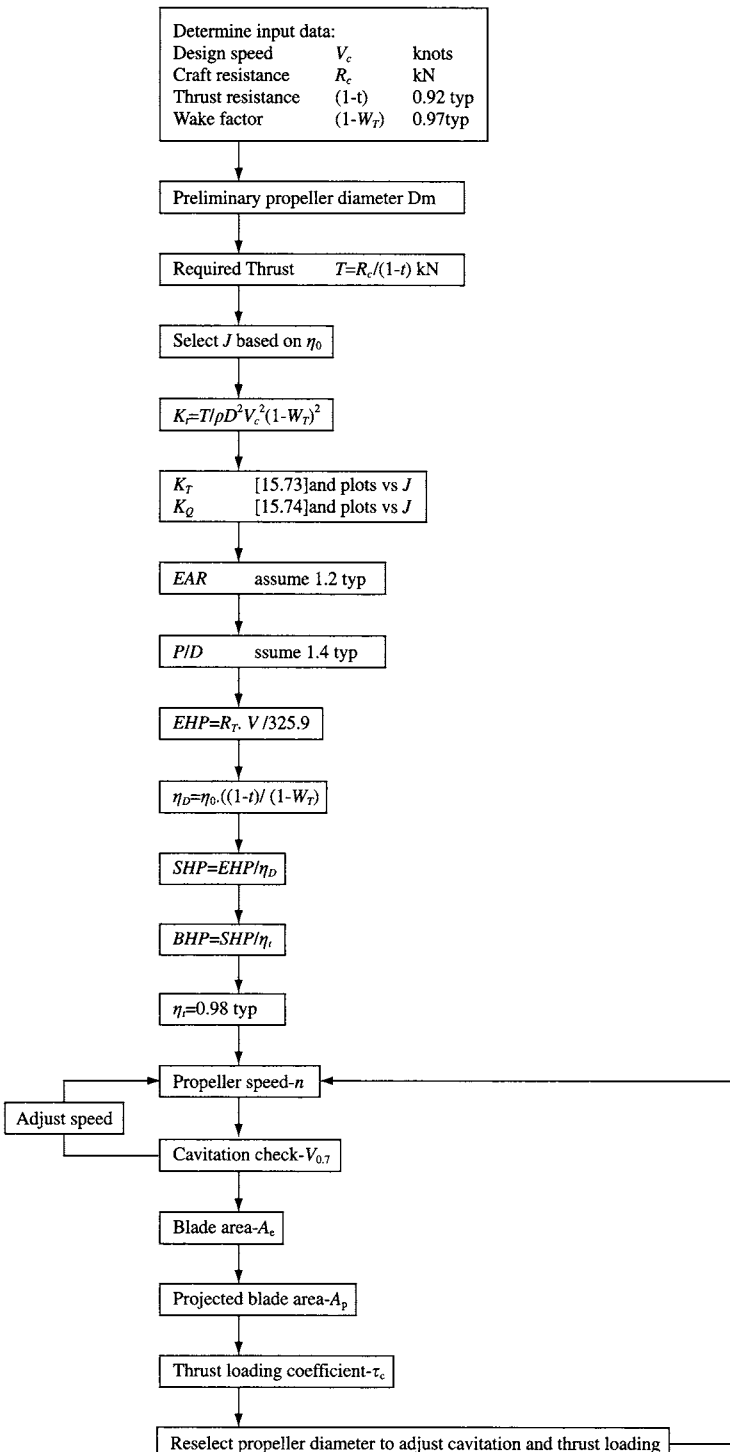


Fig. 15.23 Marine propeller selection procedure.

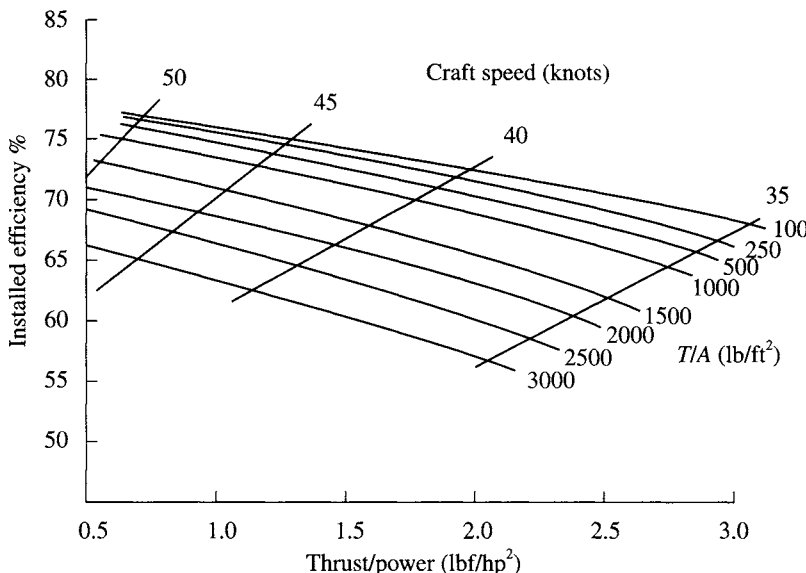


Fig. 15.24 Table of effective πA , $\pi H P$ for FoM 0.7 for 35–50 knots.

as for displacement vessels and so the effect of wake fraction on propeller design can be ignored for the moment.

The next step is to check the performance of standard blade series for which data are available, for example Gawn–Burrill [87, 112], Newton–Rader [87, 109], or the Troost [142] series. The values of K_T and K_Q can be investigated for different blade area ratios and the related values of J , D , N and η determined. An example plot for a three-blade subcavitating propeller is shown in Fig. 15.25. More extensive data are presented in the reference papers.

K_T and K_Q are related to C_T and C_N as follows:

$$K_T = (\pi J^2/8) C_T \quad (15.73)$$

$$K_Q = (J^3/16) C_N \quad (15.74)$$

$$\eta = C_T/C_N = K_T/K_Q J/2\pi \quad (15.75)$$

A designer will often have limited options for engine selection and reduction gearbox ratio. The propeller selection will therefore be a matter of iteration to an acceptable diameter, pitch ratio and blade area ratio which will develop the required thrust within the available engine power rating.

Propeller suppliers will perform this matching process, possibly offering alternative blade sections which may improve efficiency. Previous experience with similar craft can also be used to advise the SES designer on minimum advisable clearance between the sidehill keel and the propeller tip, which as a starting point should not be less than 0.1D.

Use of standard series, or similar data via propeller suppliers, has the advantage of obtaining a reliable solution quickly, but has limitations. The blade pressure

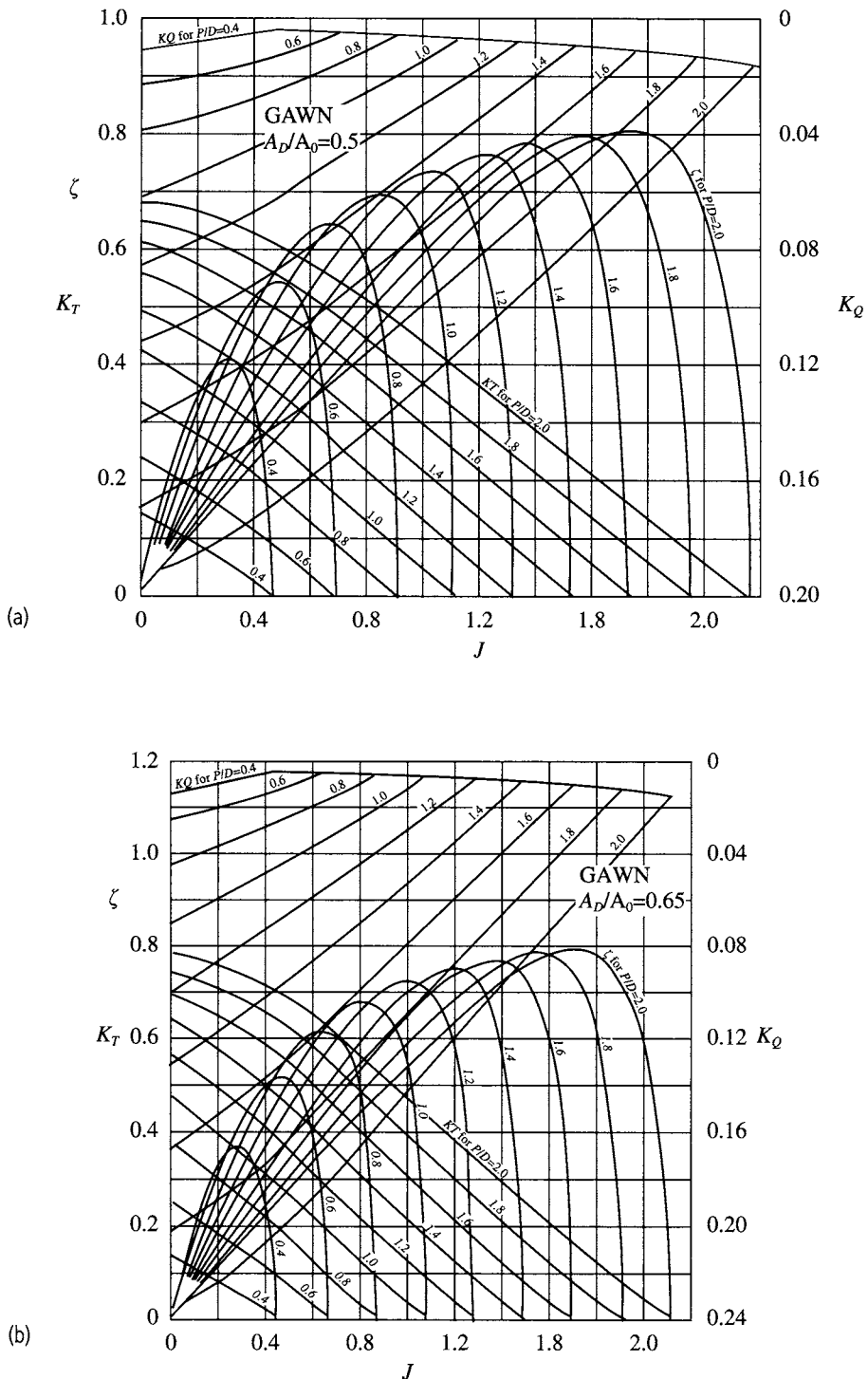


Fig. 15.25 K_T and K_Q diagrams for marine propellers. [112]

distribution for these propeller series is developed generally with high cavitation number in mind. For high-speed craft a different distribution may be more appropriate, with lower loading towards the blade tips.

The design method for such propellers [88] involves determining C_{Ti} and C_{Ni} based on assuming $\eta_i = 0.75$ and $\epsilon' = 0.08$ as a starting point and subsequently calculating the forces on each blade element using aerofoil section data having derived the hydrodynamic pitch β and the blade angle of attack ($\beta_i - \beta$). The blade chord at any section can be determined from the relation

$$C_L C/D = (4 \pi K/Z) \sin \beta_i \tan (\beta_i - \beta) \quad (15.76)$$

where K is the Goldstein function (Fig. 15.21). The cavitation number at any section should be kept above the critical level. For deeply submerged propellers this may be approximated to

$$\sigma_x = \sigma_0 [1 + (x \pi/J)^2] \quad (15.77)$$

The blade camber should be restricted to ensure shock-free flow. For NACA sections this is approximately $(0.06 C_L c)$, where C_L is typically 0.8 and C_D about 0.015 for angles of attack between 6 and 8°.

Having determined an acceptable pressure distribution over the blades, a check on the blade strength is made using cantilever beam theory and adjustments made to section thickness if this indicates problems of fatigue at the blade root.

Supercavitating propellers

Where craft speed is higher than 35 knots and so σ_0 is below 0.5, cavitation will be impossible to avoid and so a different approach needs to be taken. Propeller blade section and geometry are chosen with the aim of developing a steady cavity over the leading surface of the propeller.

First consider the development of cavitation over a propeller blade as speed is increased. In the subcavitating regime thrust increases with J in relation to speed squared. A single K_T vs J characteristic can be defined. Once σ_0 is low enough that cavitation begins to grow from the blade tip in towards the root as shown in Fig. 15.26, K_T will be reduced. At a given σ_0 (craft speed), as propeller speed is increased (reducing J), cavitation will grow across the blade until the K_T characteristic again forms a single curve. This characteristic for a fully cavitating section has an optimum K_T in the region of $J = 0.55\text{--}0.6$.

A fully developed cavity creates a blockage to flow between the blades, reducing the inflow on the pressure side of the adjacent blade, so reducing lift generated. A higher propeller speed, compared with a subcavitating propeller, is thus needed to generate similar thrust. The cavity developed will depend on the propeller speed and the blade characteristics.

Momentum theory can be used to develop equivalent expressions for efficiency to the non-cavitating regime, by introducing a term η_c to represent the effect of the cavities on inflow and η_b to represent the efficiency of the blades in cascade flow, giving an expression of the form

$$\eta = 2/(1 + (1 + C_T/\eta_b)^{0.5})(1 + C_T/\eta_b \eta_c)/[\eta_b (1 + C_T/\eta_b)] \quad (15.78)$$

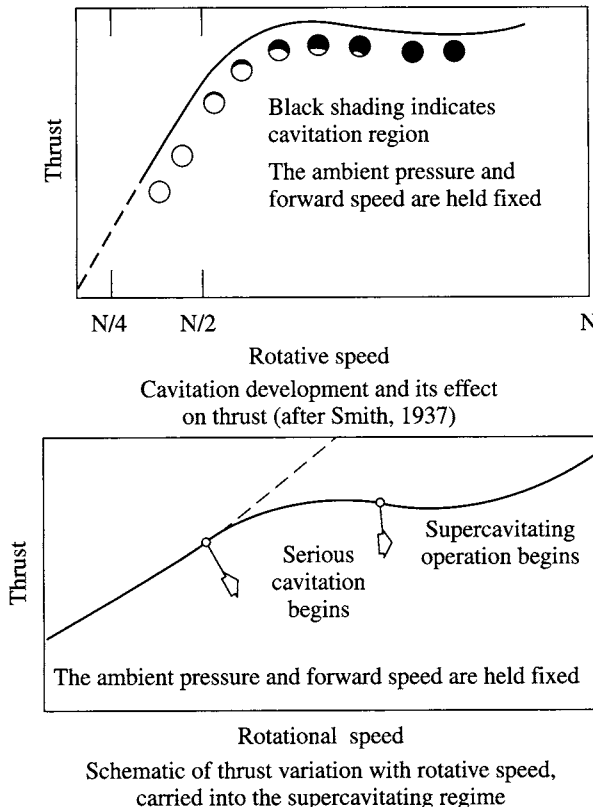


Fig. 15.26(a) Growth of cavitation across propeller blade. [88]

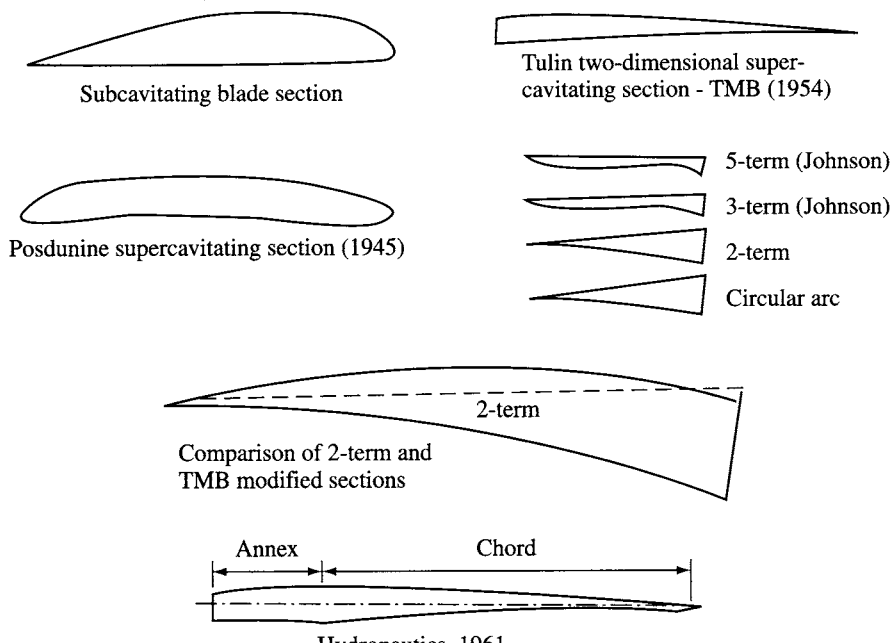
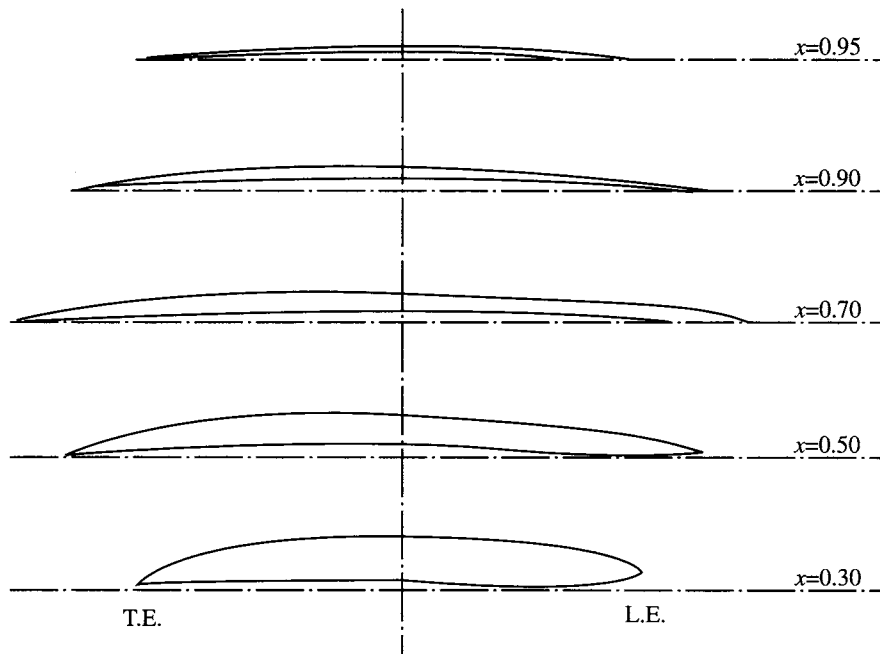
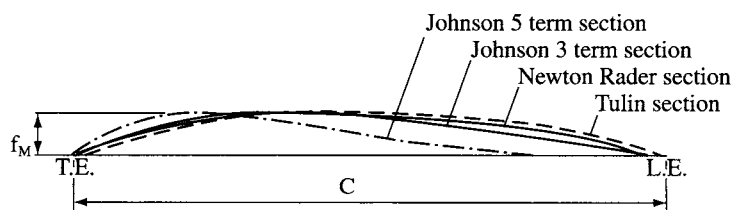


Fig. 15.26(b) Examples of supercavitating blade sections.



Newton-Rader blade sections



Comparison of camber lines

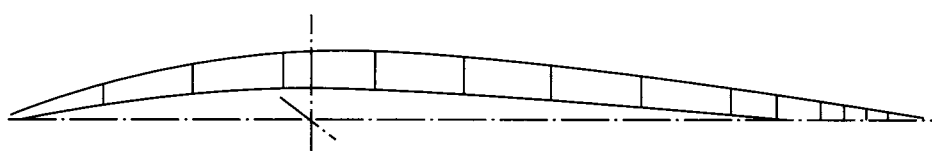
Sulzer-Hydro ventilated partially submerged propeller
installed on Mekat SES

Fig. 15.26(b) cont. Examples of supercavitating propeller blade sections.

which reduces to the expression

$$\eta = 2/(1 + (1 + C_T)^{0.5}) \quad (15.79)$$

for non-cavitating flow, where η_c and η_b are both 1.0.

Newton and Rader [109] carried out tests of a parametric series of three-bladed propellers at σ_0 values down to 0.25 (craft speed of approximately 55 knots). The blade sections used were an elliptic section profile based on a NACA $a = 1.0$ mean camber line, covering blade area ratios of 0.48, 0.71 and 0.95 and P/D of 1.05, 1.25, 1.66 and 2.05. The base design had BAR of 0.71 and P/D of 1.25.

The leading edge profile of the base propeller had to be modified during initial trials so as to remove face cavitation (Fig. 15.26(b)). A sharp leading edge section is needed so as to encourage clean cavity initiation, while at low angles of attack this can lead to cavities on either side of the section.

Principal conclusions from Newton and Rader's work were:

1. The efficiency of cambered blade sections in cavitating conditions approach that of non-cavitating sections, in contrast to flat-faced sections which have much lower efficiency.
2. The optimum blade incidence range is similar between cavitating and non-cavitating conditions.
3. When fully cavitating, obtained when $a_{0.7} = 2.5^\circ$ and $\sigma_{0.7} < 0.08$ for the series, the lift coefficient depended only on the angle of incidence, the face shape and the local cavitation number and not on the thickness form, in conformation with the theory of cavitating flow.
4. The drag-lift ratio followed an increasing trend with t/c , which is in conflict with theory, probably due to the finite thickness of the leading edge. The ratio was also higher than that for non-cavitating sections. This was attributed to the need for high camber ratio to achieve the necessary lift, which in turn necessitated higher angles of incidence to achieve sheet cavitation from the leading edge. These angles are higher than consistent with minimum drag. Further experimentation with the leading edge profile was proposed as a means to reduce the drag.

This work demonstrated that in the range to 55 knots it is possible to design open propellers with efficiencies close to that of subcavitating units and provided performance data for selection which have been successfully applied to a number of fast craft.

For higher speeds, a further investigation of hydrofoil sections is required. Since it is the face geometry which controls the section performance, researchers have investigated a number of possible forms, usually as isolated foils. Examples of these are the Johnson '3 term' and '5 term' sections [88] as shown in Fig. 15.26(b). While the lift coefficient can be optimized somewhat, the main challenge in development of these forms has been the leading edge geometry, the thinness of which is limited by strength considerations. In practice therefore, the designer has to accept reduced efficiency in order to achieve high craft speeds.

The reduced efficiency can in part be accommodated by raising the shaft close to the water-line and designing the propeller to be only partially submerged. While this introduces higher varying stress amplitudes at the blades, it reduces the appendage drag, which will be significant at high speeds. Design of partially submerged propellers follows the approach for a fully submerged propeller except that the thrust

developed is assumed proportional to the immersion. For SES such propellers have the advantage that at low speeds, higher thrust can be generated by increasing immersion (reducing lift) to assist acceleration through hump speed.

Performance data for a number of propellers are now available from the main international hydrodynamics laboratories such as DTNSRDC in the USA and MARIN in the Netherlands. DTNSRDC has for example extensively tested a propeller designated No. 4281 at a range of P/D , J , σ , shaft inclination and yaw, blade skew, rake and shaft immersion. For craft with speed requirements above 55 knots, consultation with these institutions is a useful starting point.

Outline design procedure

Design of supercavitating propellers is an iterative process. A typical procedure will include the steps shown in Fig. 15.23. Differences compared with subcavitating propeller design include:

1. greater sensitivity of the blades to both radial and chordwise stress distribution, so that development of the blade profile using blade element analysis may require some iteration before an acceptable profile is achieved for both hydrodynamic and structural criteria;
2. 'off design' conditions, including SES hump speed require full analysis since σ changes, rather than the check which can be carried out for subcavitating propellers.

Special considerations for SES

A propeller mounted at the stern of an SES hull is influenced by the proximity of the air cushion water surface and of the stern skirts, see Fig. 15.27. For lower speed craft (35 knots or less), fully submerged propellers need to be checked against free stream cavitation number based on the cushion water-line and cushion pressure to ensure this does not change the predicted performance. Propellers may become ventilated in a seaway due to craft motion if the rear seal is soft and so either the seal stiffness may need to be high, which is generally not optimum, or propeller immersion might be increased, or performance when ventilated may need to be investigated.

Higher-speed craft will generally require variable pitch propellers so as to optimize the power absorbed at both hump speed and service speed. In this case a further iteration of the design process is required for the hump speed condition. If partially submerged propellers are to be used, then the designer also has the choice of varying this relationship between hump and full speed.

Large high-speed craft with partial immersion propellers at the stern may require wider sidewall width than optimum from the resistance point of view in order to accommodate the propeller transmission and afford some physical protection during manoeuvring. The design problem becomes progressively more difficult as SES size increases. Above around 1000 t displacement, the advantages of internal arrangement for water jets encourage the designer to consider these in preference to supercavitating propellers.

Open propellers are most suited therefore to low- and medium-speed SES in the

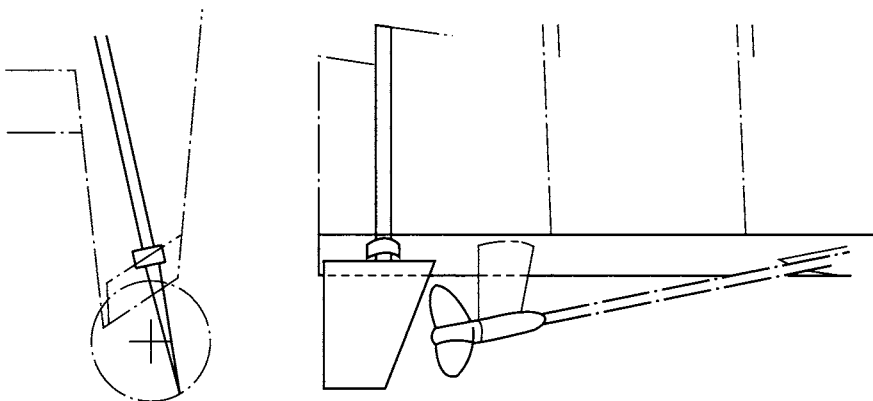


Fig. 15.27(a) Bell Halter BH 110 propeller arrangements [88].

range 20–55 knots and for sizes up to 1000 t displacement. Within this application range, propulsive efficiency between 0.65 and 0.75 should be achievable and propeller designs sourced from a number of suppliers. Where fixed pitch propellers can be selected, the installation will be relatively simple, lightweight and of low cost. Careful selection of blade geometry can achieve surprisingly high efficiency at speeds up to 55 knots. Beyond this speed, reduced efficiency has to be accommodated. Given that this is compatible with the mission, for example fast military strike craft, ventilated partially submerged propellers can offer effective propulsion to speeds in excess of 100 knots.

15.5 Water jets

Water jets for marine propulsion have a similar background to marine screw propellers. Reference 113 gives a comprehensive description and bibliography for water-jet history. The British Navy carried out parallel trials of a water-jet powered and a water screw driven vessel, the Waterwitch vs the Viper, in 1863. At that time pumps used as water jets were found to be less efficient than screw propellers and so the British Royal Navy concentrated on water screw development as an alternative to paddle wheels.

Development in the recent past was initially encouraged by a market for very shallow draft small pleasure craft in the 1950s and for propulsion of larger high-speed hydrofoils during the 1960s. Since then development has been primarily driven by applications for SES and a rapidly expanding high-speed ferry market in the 1980s and 1990s.

In the early 1970s the US Navy carried out initial design of a 3000 t water-jet propelled high-speed SES. This followed competitive trials of two 100 t displacement prototypes, the SES-100A (water jets) and SES-100B (supercavitating propellers). The programme was taken as far as preliminary design of water jets for the ship, aimed at a power rating of 40 000 kW, and a design ship speed of 80 knots. The project

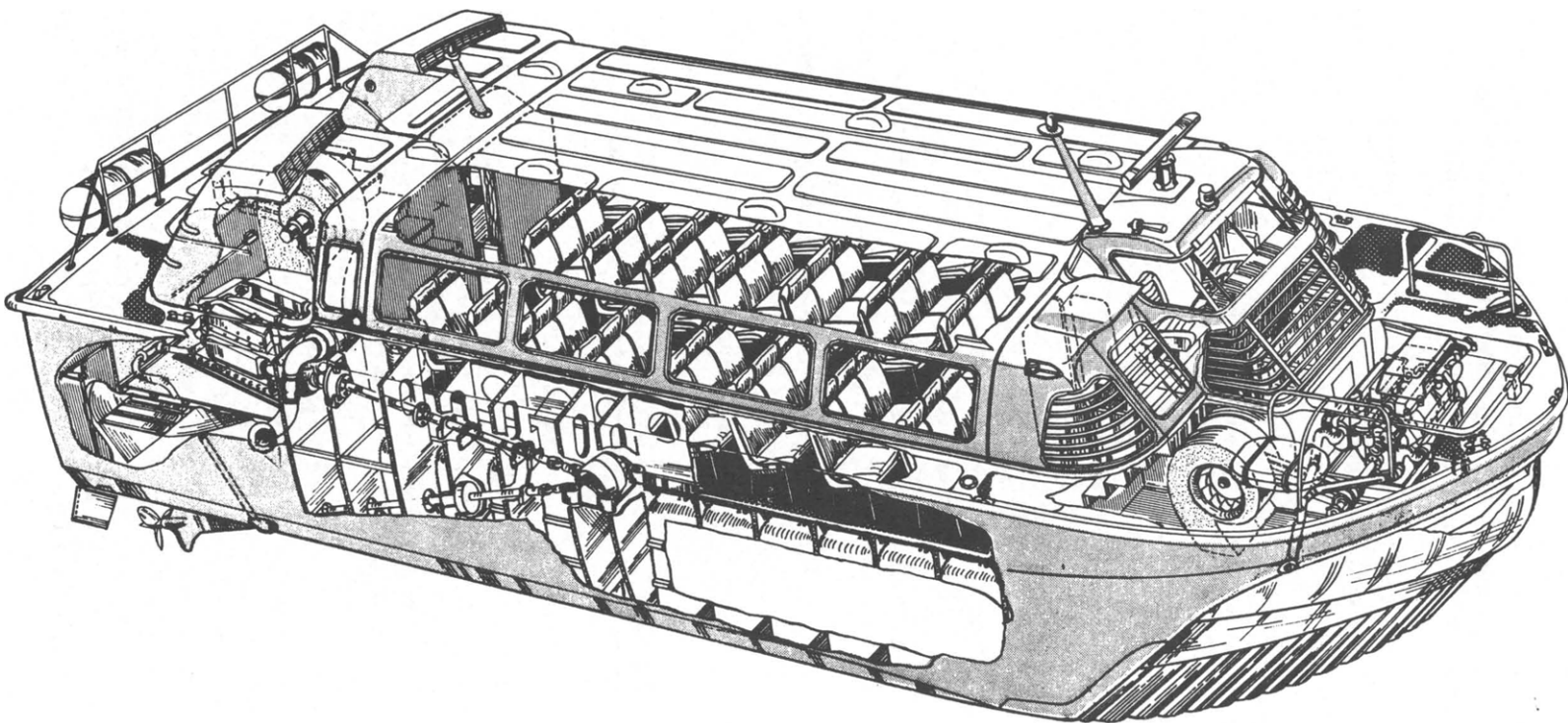


Fig. 15.27(b) Hovermarine HM 216 SES showing propulsion shaft and propeller arrangement.

was cancelled before ship construction started, but significantly improved the understanding of technical requirements for large water-jet units for high-speed craft. The water-jet system designed by Rocketdyne still represents the highest power rating attempted to date.

Overall propulsive efficiency (OPC) of between 0.45 and 0.55 were a realistic expectation at that time, using centrifugal pumps (USN hydrofoil Tucumcari), or inducer pumps such as proposed for the 3KSES, both designed for high jet exit velocity compared with craft speed.

It can be shown (see below) that if the jet velocity can be reduced closer to ship speed the efficiency can be much increased. There are two problems with this. Firstly, similarly to air propellers, the propulsor diameter has to increase exponentially as design ship speed is lowered. The second problem is that for craft operating at above about 40 knots cavitation begins to become a problem just as for marine propellers, unless the inlet pressure to the main pump can be maintained above that at which cavitation occurs.

For applications in the speed range 30–50 knots it has been found that water-jet systems with mixed flow pump impellers can give OPC in the range 0.5–0.75 (Fig. 15.3). This is clearly most attractive for designers compared to open propellers, particularly when a number of other advantages are accounted for:

- Flush inlet water jets have no appendage drag (shafts, supports, rudders).
- Steering is achieved by deflection of the jet itself, which is much more powerful than rudders.
- Reverse thrust is achieved by jet deflection rather than via a gearbox or variable pitch blades.

Other advantages associated with water jets include:

- reduced draft;
- reduced underwater noise, see Fig. 15.28 for an experimental comparison;
- reduced vibration and inboard noise from water-jet impeller, see Fig. 15.29 for a comparison;
- high power able to be applied at low ship speeds.

Water jets are products procured from specialist suppliers. Development of a new jet system from scratch is a process only open to large projects such as the US 3KSES programme. This section is therefore aimed at outlining for the SES designer the typical characteristics of water-jet systems, what opportunities there are for optimization relative to SES hulls and what may also be expected from the water-jet supplier.

Suppliers, see for example Table 15.5, have developed their ranges in a stepwise manner as the market has grown. The basic building blocks of inlet, pump and stators, nozzle and steering gear are scalable within a range of speeds, which has assisted improvements over the current speed range of 30–50 knots. At higher speeds where different pump types are required, a similar approach will need to be taken.

SES hulls lend themselves to the flush-type water-jet inlet (see Figs 15.30 and 15.31 for example), so long as some measures are taken to guard against ingestion of cushion air in heavy seas. Many detailed studies have been carried out by the suppliers for this type of inlet, through model testing and analysis.

SES designers will most likely make an initial selection of candidates based on their

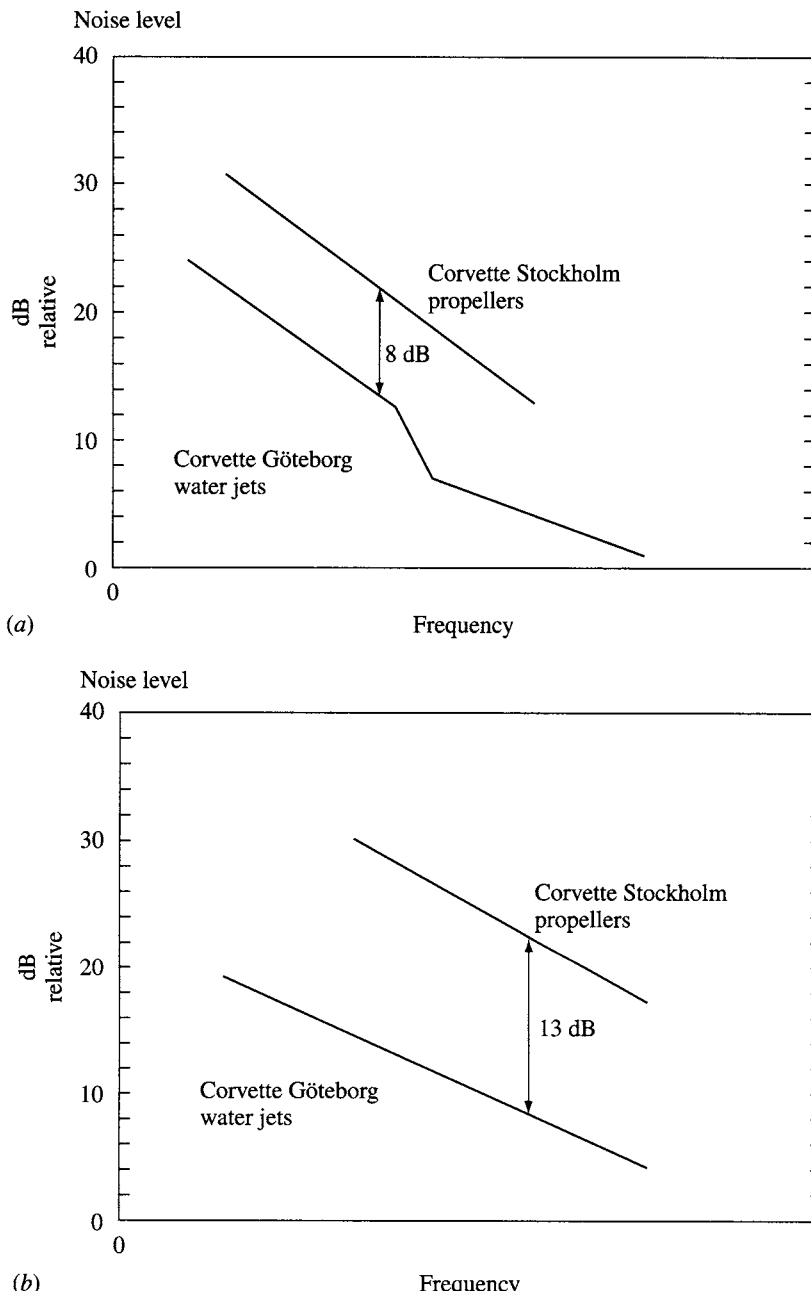


Fig. 15.28 Underwater noise comparison for water jets vs open propellers.

own powering estimates. The supplier will then need hull lines, resistance curves, predicted wake and craft dynamic trim through the speed range in order to begin the optimization process. The SES designer can expect that a water-jet supplier will provide a recommended geometry for the system based upon the craft hull lines together

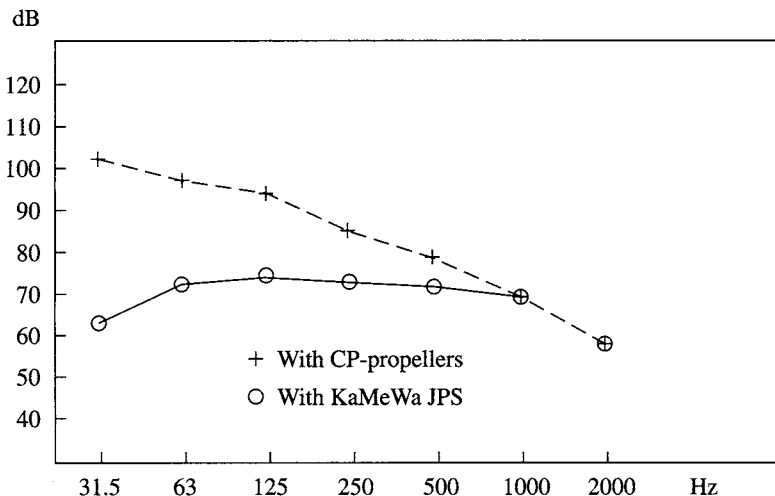


Fig. 15.29 Internal noise and vibration comparison for water jets vs open propellers.

with an indication of the allowable power input at the range of craft speeds, and the predicted thrust performance of his unit. Final integration of the SES hull and water-jet design will be an iterative process from this point, as SES detail design proceeds.

A summary of physical dimensions for various waterjet units is shown in Table 15.5(a) and (b). The designer can determine required water-jet performance using the logic shown in Fig. 15.32 by calculating:

Table 15.5a KaMeWa water jets

Size	A	B	C	D	E	F	G	H	J	K	L	M
40	1095	2530	440	300	20	75	415	480	790	900	480	2000
45	1400	3350	493	350	20	80	410	640	840	1220	540	2200
50	1520	3750	550	375	25	100	635	695	945	1350	600	2200
56	1670	4200	620	395	35	110	635	760	1030	1510	670	2500
63	1900	4700	695	465	35	120	675	860	1120	1700	760	2500
71	2115	5300	772	535	35	130	745	965	1280	1900	850	2900
80	2395	5970	875	535	40	140	810	1085	1450	2140	960	3300
90	2615	6720	972	630	50	165	1030	1185	1610	2410	1080	3500
100	3000	7470	1100	670	50	180	1020	1360	1820	2680	1200	4130
112	3360	8360	1230	750	60	200	1140	1520	2030	3000	1350	4620
125	3750	9390	1370	840	65	220	1270	1700	2230	3350	1500	5160

A Overhang length from transom.

B* Minimum length transom to forward foot of intake.

C Nozzle outlet behind transom.

D Location of interface between intake and pump inlet casing.

E Minimum transom plate thickness.

F Nominal shaft diameter.

G Extended depth of reversing bucket in stowed position.

H Maximum width when jet deflected 30°.

J Diameter of transom mounting flange.

K* Minimum distance of intake rear lip from transom.

L Height of pump centre-line from keel.

M Distance from transom to shaft connection.

* These dimensions will vary with craft installation. In general the intake will be longer.

Table 15.5b MJP Mark II water jets

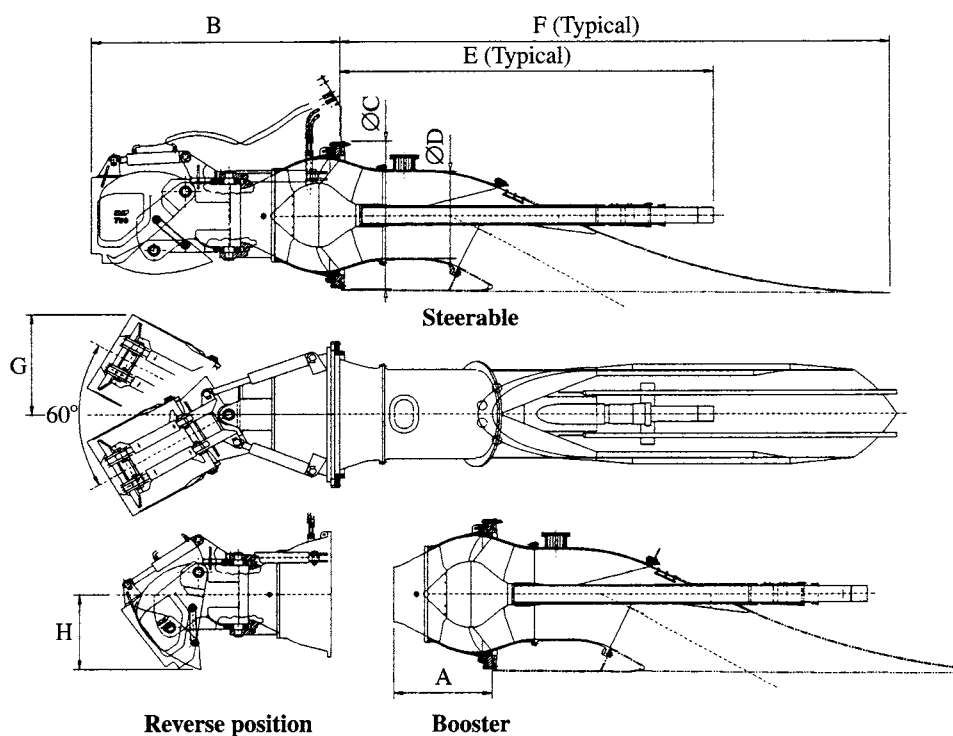
Size	Nom. kW	Max. kW	A	B	C Dia.	D Dia.	E	F	G	H	Weight steerable	Weight booster
500	1200	1800	510	1290	855	500	2050	3400	575	460	815	57
550	1500	2250	560	1412	940	550	2250	3790	630	505	1090	71
650	2100	3150	665	1680	1120	650	2675	4510	750	600	1560	103
750	2800	4200	765	1900	1255	750	3075	5180	860	690	2105	146
850	2700	5550	880	2100	1440	850	3540	5890	990	795	3145	212
950	4900	7350	1010	2460	1610	950	4070	6590	1100	915	4330	300
1100	6950	9750	1200	2845	1890	1100	4820	7630	1350	1090	6040	408
1350	9200	13800	1355	3490	2110	1350	5560	9370	1555	1250	8450	583
1550												

Dimensions in mm.

Weights in kg, including hydraulics, but excluding intake duct and shafting.

All data are nominal, and would be adjusted based on client discussions.

- required thrust by determining and applying the thrust deduction factor to the drag;
- velocity approaching the inlet by applying the wake factor to the ship speed;
- inlet/jet velocities and mass flow to achieve required thrust, via momentum theory;
- initial estimates for system component efficiencies;
- net positive suction head and pump head based on assumed inlet and nozzle efficiencies;

**Fig. 15.30** Water jet geometries (MJP designs).

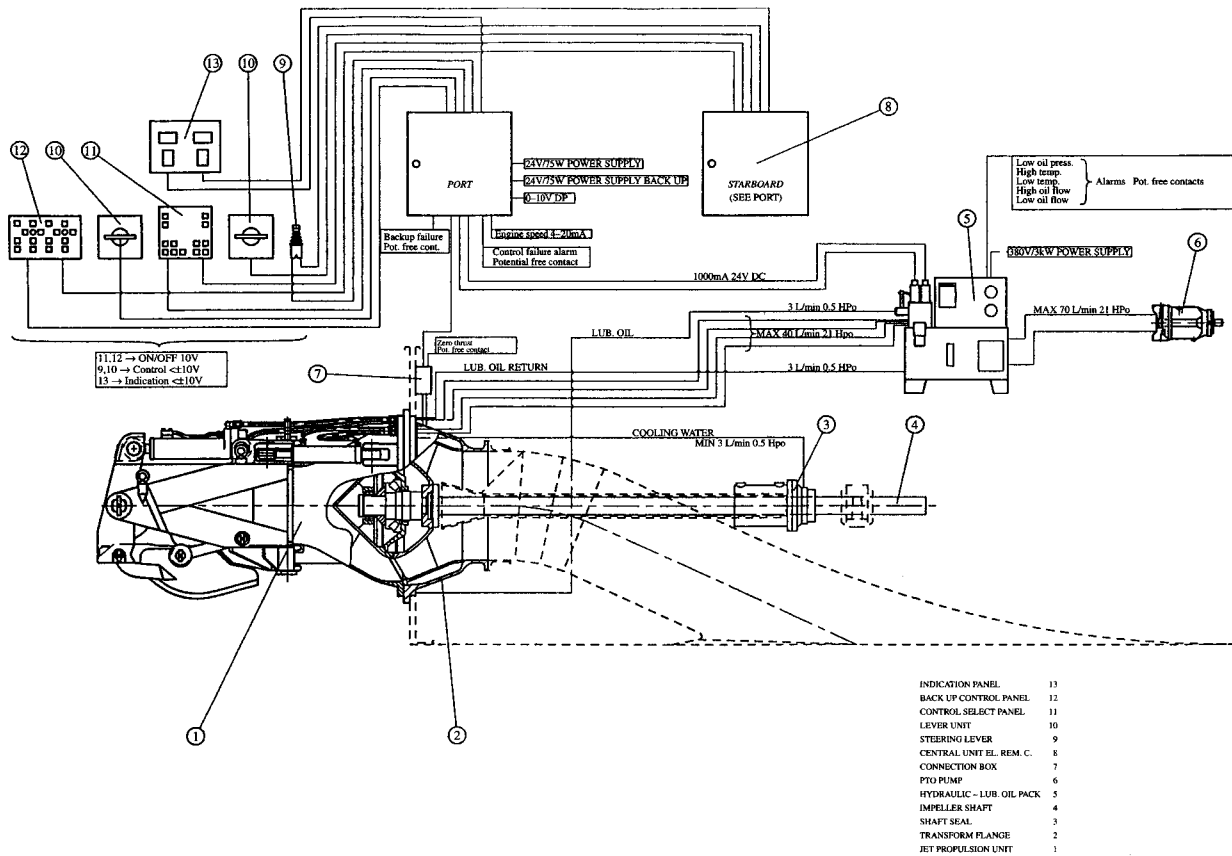


Fig. 15.31 KaMeWa waterjet system drawing.

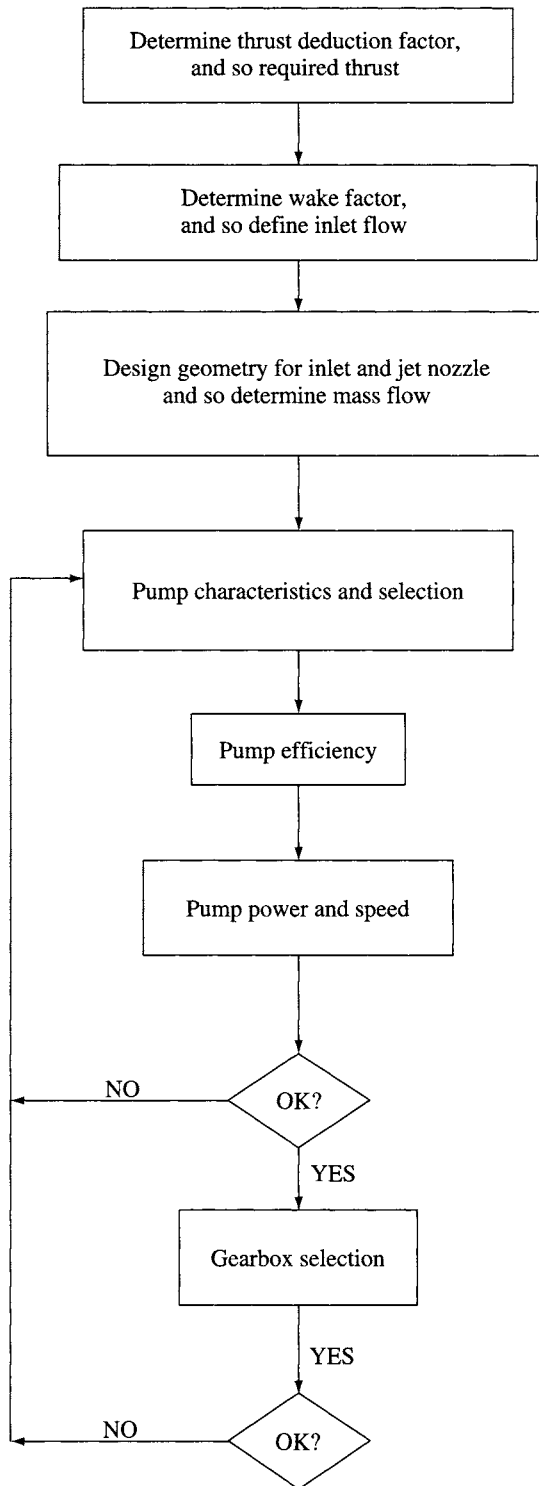


Fig. 15.32 Water jet selection procedure.

- non-dimensional operating point for the pump (ϕ , ζ , η_p);
- pump dimensions and rotation speed;
- system component efficiencies and therefore installed power, as a cross-check.

Once the desired characteristics have been determined, a selection can be made of units with closest performance and physical dimensions checked to ensure they will fit to the SES hull dimensions. At this point the designer may choose to revise the hull lines if the selection of water jet, transmission and engine are not fully compatible and so may repeat powering predictions before involving the suppliers in the design. Advice can then be sought of the suppliers to take the next step of verifying or revising the selection and optimizing the system. This will include adjustments to the inlet geometry and position in the sidehull, optimization of the pump itself, design of the power train, the nozzle installation outboard of the transom, and the water-jet control system.

We will look at each of the steps above in turn beginning with a review of system losses, including some discussion of their effect on component and system design.

Thrust deduction and wake factors

Ship resistance is normally determined from scale model test data or analysis of the basic hull form. The actual required thrust will normally differ from this due to unaccounted scale effects. In addition, appendages will add drag components to the overall resistance. These components are particularly important for propeller-driven craft. The effect of this increase in overall resistance is accounted for as a thrust deduction factor during initial design, where

$$T = R_p/(1 - t)$$

The thrust deduction factor ($1 - t$) for a water-jet propelled craft with flush type inlets is normally in the range 0.97–1.03. Pod inlets have a higher drag and will result in ($1 - t$) of between 0.9 and 0.97.

At low speeds a water-jet inlet will accelerate flow in the region of the intake in a similar manner to the velocity field behind a propeller (see Fig. 15.9), except that part of the boundary layer will be ingested, reducing the thrust deduction compared to open propellers. At higher speeds flow will be gathered from a much smaller volume and the flow behind the intake will be at close to free stream velocity so that the overall effect will be a reduction in required thrust. During the initial design stage of an SES it is recommended to use 1.0 for ($1 - t$).

The hull wake factor ($1 - w$) ranges between 1.02 and 0.8. At the upper bound of this range, the water jet is assumed to remove or reduce the boundary layer under the hull by accelerating water into the inlet duct rather than the deceleration which is normal in the afterpart of a fast semi-displacement or planing craft hull. This will be most effective at slow speeds and for SES where the hulls themselves are very slender. At design operational speed the effect will be governed by the jet velocity ratio. Since water-jet systems for high-speed craft tend to have high V_j/V_c , the wake factor will still be close to 1. During initial design a value of 0.97 is recommended for SES.

In the same way as for propeller design, the required thrust to be developed takes account of these two factors by

$$T = T_i(1 - w)/(1 - t) = T_i \eta_H \quad (15.80)$$

where η_H is often equated to 'hull efficiency'.

Inlet losses

If we consider the flow into an open propeller, as craft speed is reduced from the design conditions, streamlines will enter from a widening area (see Fig. 15.9). Water-jet systems face the same issues as ducted air propellers for design of the intake system. The duct centre-line normally follows an S curve from the hull base-line, while the duct geometry itself is a parabolic or hyperbolic curve, with an intake lip having similar geometry to an aerofoil leading edge at the front and a sharper edge on the aft part, similar to a supercavitating propeller leading edge.

Water-jet inlets normally have a geometry based on the normal operating condition (SES cruise speed), so that below this speed flow velocity will be higher at the inlet intake and losses will increase relative to the ideal. Inlet losses will reduce the available head at the pump suction and the practical limit for thrust developed will be controlled by the net positive suction head (NPSH) below which the pump starts cavitating. Above normal operating speed, flow into a fixed inlet geometry will be decelerated over the initial part of the duct, producing a similar effect to hull wake.

While a variable geometry inlet would optimize flow into the pump, removing turbulence at the intake lip at low speeds and in the throat at high speeds, the costs of such an installation are normally prohibitive. Instead, water-jet manufacturers have found from model testing that inlet geometries can be defined which minimize the turbulence in off-design conditions, particularly at lower speeds.

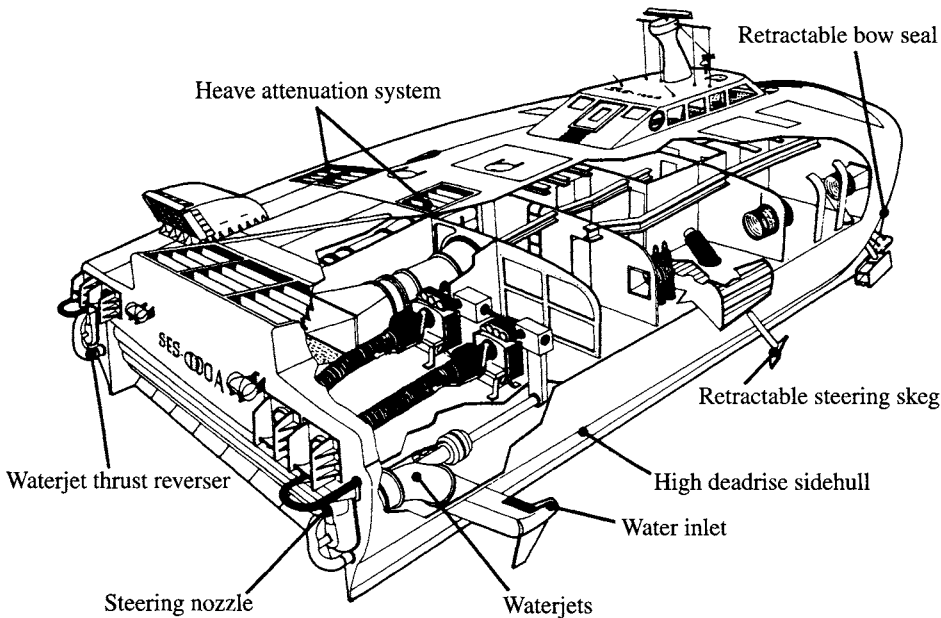


Fig. 15.33 Water jet inlet with secondary slow speed intake.

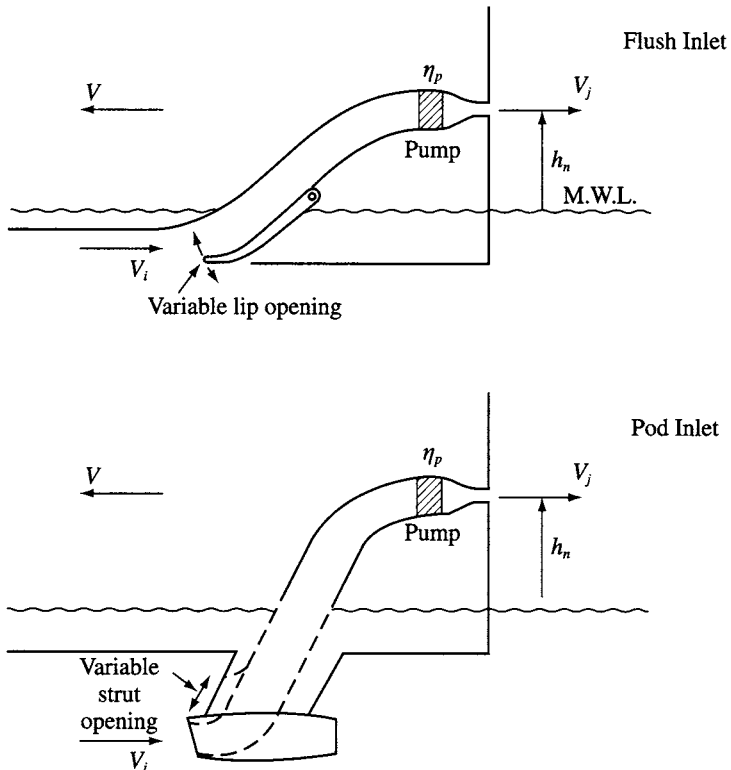


Fig. 15.34 Variable area water jet inlets.

Water-jet inlets can either be flush to the base-line of the SES hull, or extended as a 'pod' to capture flow from the area undisturbed by the hull boundary layer. Pod inlets are used on hydrofoils. The SES 100A test craft was originally fitted with pod inlets (see Fig. 15.33). These comprised a main high-speed intake and auxiliary inlets allowing greater flow at lower speeds. Performance was less than projected and so the craft was retrofitted with variable area flush inlets. These initially had problems with air ingestion in a seaway and so various geometries of 'fence' between the intakes and the sidehull lower chines were experimented with until performance was satisfactory. Further studies were then carried out on the variable geometry inlets, which did not behave according to design predictions. It was found to be very difficult to set the ramp position for optimum thrust and at the same time avoid cavitation either internally or externally. Eventually it was found that a round fixed area inlet could give a reasonable compromise without the complexities of the variable ramp operating mechanism and so this design was selected for the 3KSES as a design basis.

At craft speeds of 30 knots, V_i/V_c variation between 0.5 and 0.95 can occur without cavitation on a typical well-designed flush type inlet (see Fig. 15.41). This range narrows to V_i/V_c of 0.66–0.82 at 70 knots and further to 0.7–0.8 at around 100 knots. Below the lower boundary cavitation occurs under the rear intake lip, while above the upper boundary, flow separates from the intake roof or the inside of the lower lip.

It can be seen therefore that if a craft is designed for V_i/V_c to be 0.66 at 70 knots, this will become 1.54 at 30 knots and cavitation will occur on the inside of the inlet unless the pump flow is reduced to about 60% of design. This may be acceptable so long as the SES drag hump is not too high, i.e. for high L/B craft. For craft with higher hump drag and those with very high design speed (above 60 knots), it may be beneficial to install a secondary inlet system which can be closed above hump speeds, along the lines of Fig. 15.34. For craft speeds in the 40–60 knot range, it is realistic to design the inlet based on the design speed and accept reduced efficiency at lower speeds.

The inlet for an SES will generally be constrained in width by the sidewall. Ideally, the transition forwards from the pump impeller to the inlet should be as smooth as possible, with an elliptical cross-section at the entrance. If the width is restricted, the elliptical entrance will naturally be extended forward and aft. If this becomes too extreme, there may be a tendency to flow breakaway at the sides of the inlet, so if necessary the SES hull width should be adjusted to give a greater beam at the keel.

If smooth geometry can be achieved for the inlet system and the inlet width can be kept wide, approximately 1.0–1.2 times the impeller diameter, it is realistic to expect efficiency between 0.8 and 0.9 for a flush inlet system. A starting point for initial design may be 0.825 for craft speed 30 knots increasing to 0.9 at about 55 knots. Above this speed cavitation problems may reduce inlet efficiency again so that at 100 knots 0.85 might be assumed as a starting point.

Nozzles and efficiency η_n

Nozzles may be of two types. The Pelton type has an exhaust duct outer wall which follows the geometry of the stator hub fairing as used by MJP (Fig. 15.30) and KaMeWa (Fig. 15.31). In this case the vena contracta of the jet will occur just downstream of the nozzle. Alternatively the duct may be extended as a parallel section, in which case there will be no external vena contracta. The latter nozzle is more often used on small water jets used for pleasure boats and jet ski craft.

Nozzle design, including flow through the system of stators behind the pump and the duct formed by the hub rear fairing and the outer casing, is aimed at uniform axial flow. In fact there will be some variation due to the boundary layers at the casing and hub fairing, see Fig. 15.35, but these effects are usually very small and the nozzle efficiency should be close to 99% at design condition.

Nozzle elevation h_n

The water which travels through a water-jet system is elevated before entering the pump, incurring a head loss. This suction head loss is significant for a hydrofoil where the jet is located in the hull, but for an SES generally amounts to just a metre or so above the keel. This suction head must be taken into account when determining pump NPSH, see Fig. 15.34.

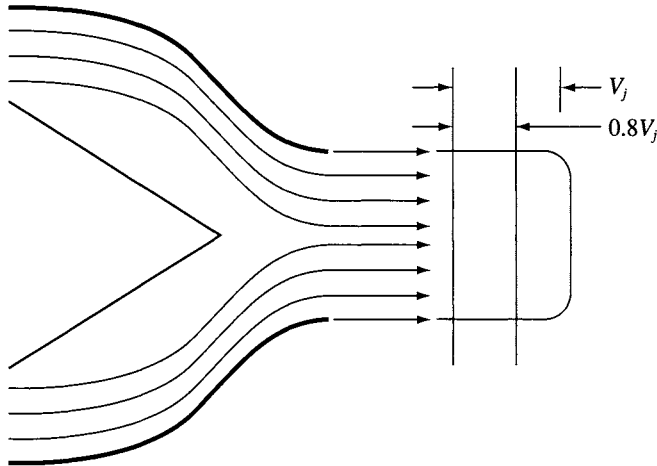


Fig. 15.35 Water jet vena contracta.

Momentum theory and jet efficiency

Having considered the main system losses, excepting the pump, we first consider the efficiency of a jet system, before looking at the pump itself in a little more detail.

Water entering the water-jet system is considered to be accelerated to the forward speed of the vessel, V_c before being accelerated through the pump and nozzle to V_j . The net thrust developed by a water jet is therefore

$$T = \dot{m} V_j - \dot{m} V_c \quad (15.81)$$

the energy applied by the pump to the water mass is

$$E = 0.5 \dot{m} (V_j^2 - V_c^2) \quad (15.82)$$

The propulsive efficiency is therefore

$$\eta_j = T V_c / [0.5 \dot{m} (V_j^2 - V_c^2)] \quad (15.83)$$

which reduces to

$$\eta_j = 2 V_c / (V_j + V_c) \quad (15.84)$$

if we equate V_c/V_j to μ then dividing terms in equation (15.83) by V_j :

$$\eta_j = 2 \mu / (1 + \mu) \quad (15.85)$$

which has a similar form to the equations for ideal efficiency of air propulsors. This is shown as the top curve of the series in Fig. 15.36. If losses are considered as a single factor ζ related to the inlet energy, i.e.

$$E = 0.5 \dot{m} (V_j^2 - V_c^2) + \zeta 0.5 \dot{m} V_c^2$$

then

$$E = 0.5 \dot{m} (V_j^2 - V_c^2 (1 - \zeta)) \quad (15.86)$$

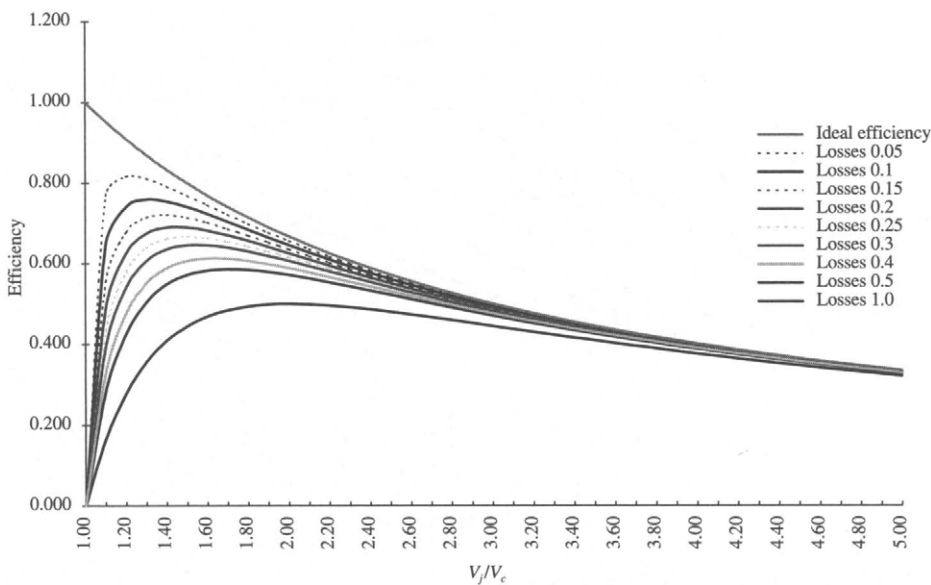


Fig. 15.36 Water jet efficiency.

since

$$\eta_j = T V_c / E$$

so

$$\eta_j = T V_c / [0.5 \dot{m} (V_j^2 - V_c^2 (1 - \zeta))]$$

or

$$\eta_j = 2 \mu (1 - \mu) / [(1 - \mu^2) (1 - \zeta)] \quad (15.87)$$

This is shown in Fig. 15.36 for values of ζ up to 1.0, where the inlet energy is completely lost.

It can be seen that if the system is to be efficient, losses from the inlet must be relatively low, of order 5–15%. The optimum jet velocity ratio is 1.2–1.4. Water jets with jet velocity ratios in this range would be relatively large, somewhat larger than an equivalent open propeller in fact, due to the relatively high boss diameter (see Fig. 15.30 for example).

In fact it is possible to design water jets to have pump outer diameters similar to that of open propellers, while maintaining high efficiency, as demonstrated by the KaMeWa performance data, Fig. 15.3. KaMeWa recommended selection of water-jet sizes for initial design as shown in Fig. 15.37. We need therefore to investigate interaction of a water jet with the hull, which can mitigate the losses which are apparent from momentum theory.

If the efficiency is expressed as a relation to thrust loading coefficient rather than the velocity ratio the following expression for ideal efficiency results. If

$$C_t = T / [0.5 \rho_w A_j V_c^2] \quad (15.88)$$

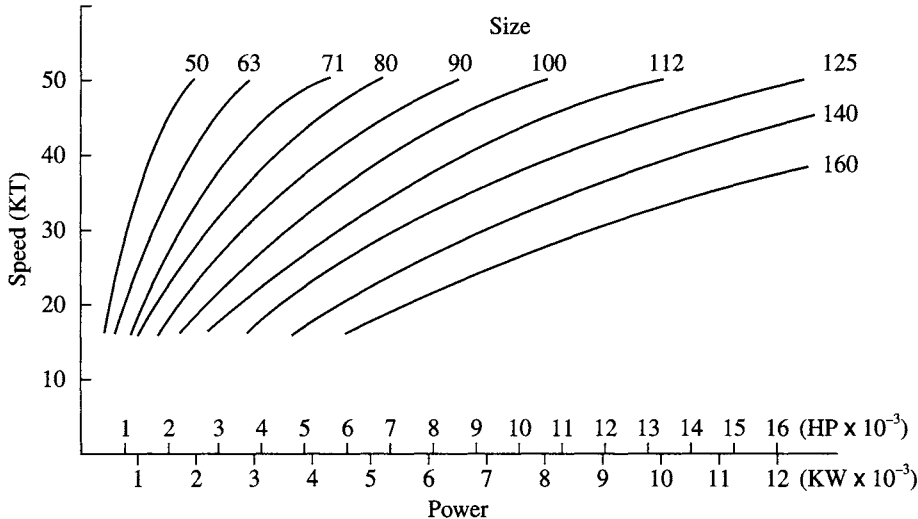


Fig. 15.37 KaMeWa water jet selection chart.

then

$$\eta_j = 4/[3 + (1 + 2 C_j)^{0.5}] \quad (15.89)$$

which may be compared with the equivalent expression for an open propeller; where

$$\eta_i = 2/[1 + (1 + C_j)^{0.5}] \quad (15.90)$$

this is shown in Figs 15.38 and 15.39. Clearly a water jet has improved performance at higher thrust loading, a result equivalent to the ducted propeller, suggesting that reduced disc area is possible while maintaining efficiency equivalent to an open propeller.

If we include system component losses in the expression for efficiency (15.87), i.e.

$$\eta_i = (1 - \zeta) \text{ inlet losses}$$

$$\eta_n = (1 + \psi) \text{ nozzle losses}$$

$$W_c = \dot{m} g h_j \text{ head loss due to nozzle elevation}$$

then the expression for expended energy becomes

$$E = 0.5 \dot{m} [(1 + \psi) V_j^2 - (1 - \zeta) \{(1 - w) V_c\}^2 + 2 g h_j] \quad (15.91)$$

now

$$\begin{aligned} \eta_j &= T V_c / E \\ &= \dot{m} (V_j - (1 - w) V_c) V_c / E \end{aligned} \quad (15.92)$$

if we divide through by V_j^2 and set $\mu = V_c/V_j$ as earlier, this expression becomes

$$\eta_j = \frac{(1 - (1 - w)\mu)\mu}{0.5 [(1 + \psi) - (1 - \zeta) \{(1 - w)\mu\}^2 + 2 g h_j/V_j^2]} \quad (15.93)$$

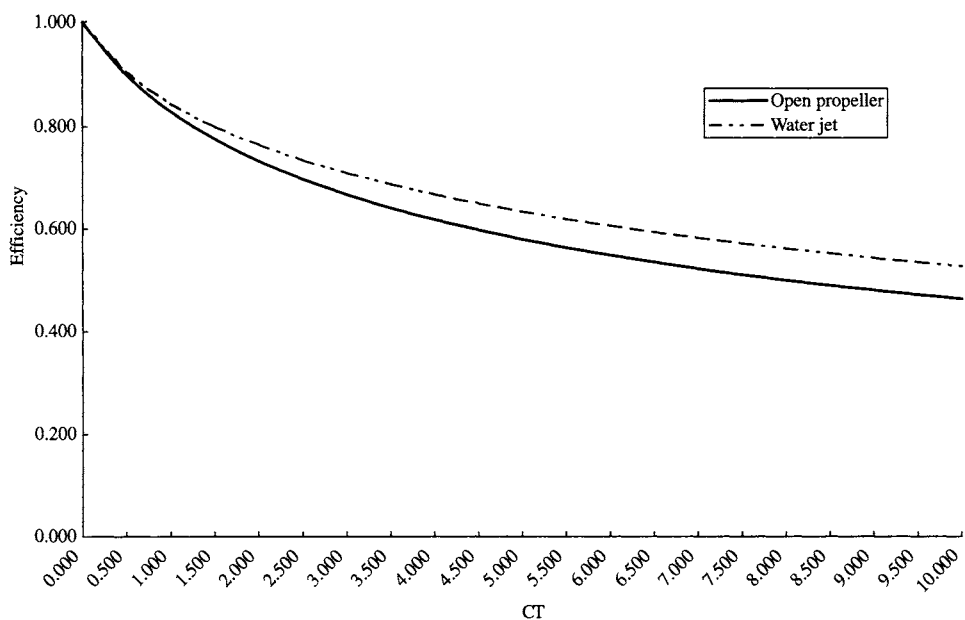


Fig. 15.38 Efficiency comparison: open propeller vs water jet.

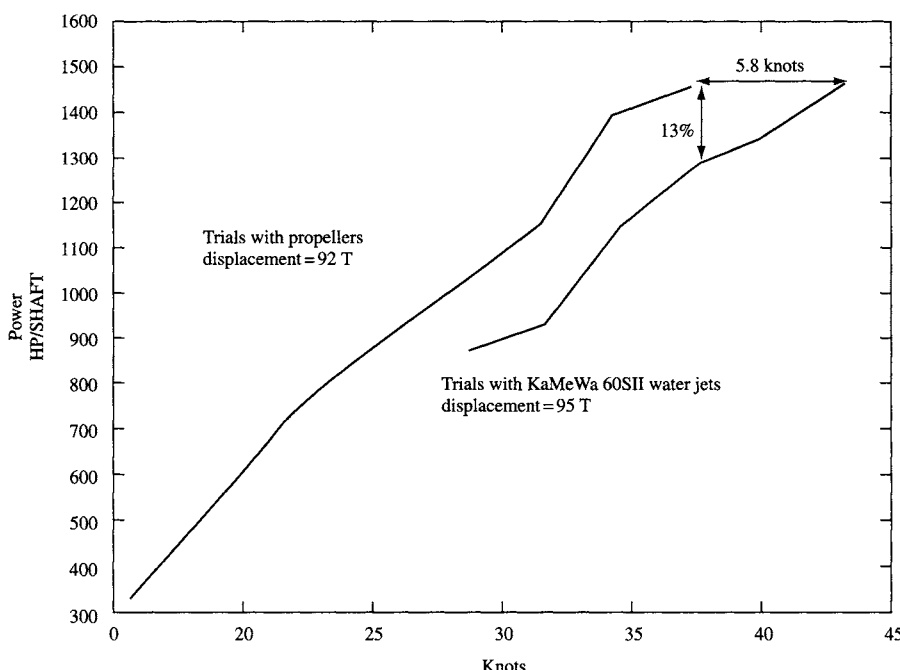


Fig. 15.39 Comparison between propellers and water jets from trials with SES Norcat.

If μ is considered relative to wake velocity at the jet intake, i.e. $\mu_w = (1 - w)V_c/V_j$ instead of relative to the craft speed, this becomes

$$\eta_j = \frac{2(1 - \mu_w)\mu_w/(1 - w)}{(1 + \psi) - (1 - \zeta)\mu_w^2 + 2gh_j/V_j^2} \quad (15.94)$$

This formulation is convenient to allow cavitation tunnel testing of a water jet in a facility similar to Fig. 15.40. When combined with the inclination of the jet pump this becomes

$$\eta_j = \frac{1}{(1 - w)} \cdot \frac{2\mu_w(\cos a \cos \phi - \mu_w)}{(1 + \psi) - (1 - \zeta)\mu_w^2 + 2g h_j/V_j^2} \quad (15.95)$$

since

$$T_{\text{eff}} = \dot{m} V_j \cos a \cos \phi$$

where a is the pump centre-line inclination to horizontal water-line (should include vessel trim) and ϕ the pump centre-line horizontal inclination to ship centre-line.

If the effect of inlet drag is included (this is more pronounced for pod type inlets) then, first

$$\begin{aligned} D_i &= C_{Di} 0.5 \rho A_i V_i^2 \\ &= C_{Di} 0.5 \dot{m} V_i \text{ since } \dot{m} = \rho A_i V_i \end{aligned} \quad (15.96)$$

We define an inlet velocity ratio (IVR) in terms of the wake velocity, where

$$\text{IVR} = V_i/V_w$$

then

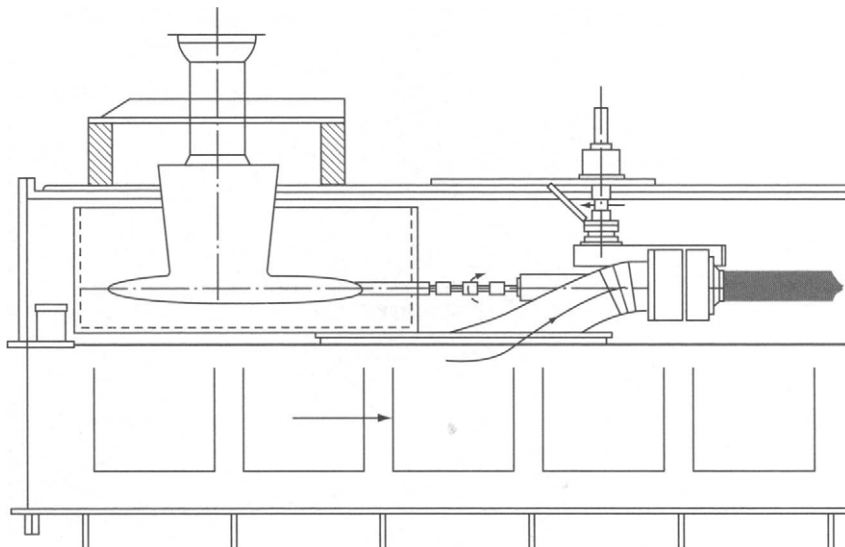


Fig. 15.40 Water jet model in cavitation tunnel (KaMeWa diagrammatic).

$$V_i = \text{IVR } V_w = \text{IVR } V_c (1 - w)$$

thus

$$D_i = C_{Di} 0.5 \dot{m} \text{IVR } V_c (1 - w) \quad (15.97)$$

If an inlet is truly flush and the flow around the rear inlet lip causes no turbulence, then D_i may be assumed as zero. Since for an SES it is likely that fences may be needed around the inlet and the rear lip will create drag, it is prudent to assume some losses. A value of C_{Di} between 0.008 and 0.03 may be considered representative of well-designed installations. Now

$$\eta_j = (T - D_i) V_c/E \quad (\text{from 15.91})$$

$$= \dot{m} [V_j - (1 - w) V_c - C_{Di} 0.5 \text{IVR } V_c (1 - w)] V_c/E \quad (15.98)$$

so by following the steps from (15.93) to (15.96), we obtain a revised expression as follows:

$$\eta_j = \frac{1}{(1 - w)} \frac{\mu_w \{2(\cos \alpha \cos \phi - \mu_w) - C_{Di} \mu_w \text{IVR}\}}{1 + \psi - (1 - \zeta) \mu_w^2 + 2g h_j/V_j^2} \quad (15.99)$$

Finally let us consider the local pressure effects around a water-jet intake, see Fig. 15.41. Based on physical measurements, Svensson [56] has shown that flow in the region behind a flush inlet produces an increased pressure which may exceed wake-affected stream pressure, causing a lifting force on the hull. This is the opposite to the flow field behind a propeller, which is accelerated, creating a relative suction on the hull compared to wake-affected stream pressure.

This effect is rather complex, varying with craft speed, IVR for the intake design, and the extent of the bottom plate behind and on either side of the intake. The altered velocity field will effectively reduce hull drag locally, so increasing jet efficiency. If the hull geometry is optimum in the region of the intake, then the velocity field itself will also be so, minimizing turbulence. It may be seen that optimization of the hull stern geometry and the jet intake position, together with the intake geometry itself, is important to a water-jet system. If we consider the pressure difference in the inlet area:

$$P_s - \rho g h_i = C_p 0.5 \rho V_c^2 \quad (15.100)$$

where P_s is the representative value of static pressure for the inlet flow field and h_i the water depth at inlet. At low craft speeds $P_s < \rho g h_i$ due to the large inflow capture area and so C_p will be negative, suggesting a reduced efficiency. At normal operating speeds the intake may be designed so $P_s > \rho g h_i$, whereby C_p becomes positive. A value of C_p of approximately 0.1 may be expected for optimized water-jet/hull combinations operating at design speed [113]. The term to be added into (15.100) will be a deduction from E . The form is similar to that for inlet drag (15.96) except that C_p is measured relative to craft speed rather than inlet velocity. Since the flow field around the outside of the inlet is a complex one, this is a logical approach. Equation (15.99) then becomes

$$\eta_j = \frac{1}{(1 - w)} \frac{\mu_w \{2(\cos \alpha \cos \phi - \mu_w) - C_{Di} \mu_w \text{IVR}\}}{1 + \psi - (1 - \zeta) \mu_w^2 + \frac{2g h_j}{V_j^2} - \frac{C_p \mu_w^2}{(1 - w)^2}} \quad (15.99a)$$

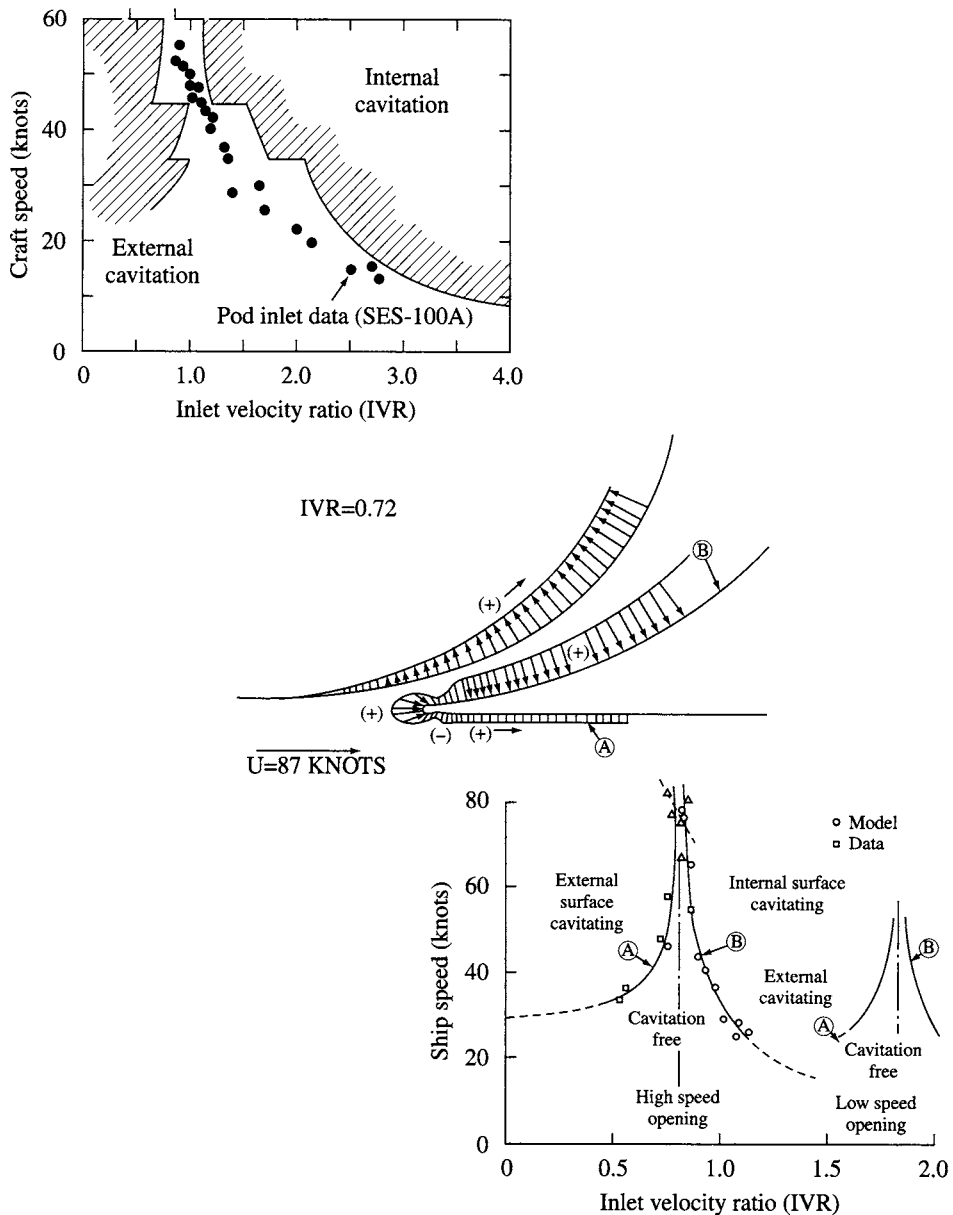


Fig. 15.41 Water jet inlet cavitation charts with craft data included. [4]

An expression for OPC including all significant loss components may now be stated as

$$OPC = \eta_p \eta_r \eta_t (1 - t) \quad (15.101)$$

where η_p is the pump impeller efficiency, η_r the pump relative rotative efficiency and η_t the transmission efficiency.

At the initial stage of design, the designer will generally exclude inlet drag and the hull interaction effects, using the form in equation (15.95) to estimate power and size the propulsors. These other effects can then be tested as sensitivities.

Pump characteristics, types and selection

Pumps may be of radial flow (centrifugal) type, axial flow or mixed flow. By considering the momentum theory, it has been shown above that a small velocity increment over the ship speed gives greatest efficiency. High flow rate with low-pressure head pumps are in principle the most efficient as water jets. The optimum pump type will vary according to the craft design speed. With exception of high speed craft, above about 60 knots, it is likely that the main design constraint will be the pump physical size inside the SES sidewall geometry.

A pump has the objective to deliver a specified flow Q , at a particular fluid pressure. The fluid pressure is equated to a static head of the fluid ρgH . Thus, the ideal pumping power is

$$N_i = Q\rho gH \quad (15.102)$$

and

$$N = N_i/\eta \quad (15.103)$$

Pumps are generally characterized by non-dimensional parameters which affect their efficiency, to allow scaling [114]. In general for a pump

$$\eta = f(Q, gH, \rho, n, D) \quad (15.104)$$

we can reduce the number of independent variables by dimensional analysis so that

$$\eta = f(\Phi, \Psi) \quad (15.105)$$

where

$$\Phi = Q/n D^3 \quad (\text{non-dimensional flow coefficient}) \quad (15.106)$$

and

$$\Psi = gH/(n^2 D^2) \quad (\text{non-dimensional head coefficient}) \quad (15.107)$$

Characteristic plots of Ψ vs Φ , or η against Φ should overlay one another for geometrically similar pumps. We may combine Φ and Ψ to obtain a non-dimensional power coefficient:

$$\Pi = \Phi\Psi = N/(\rho n^3 D^5) \quad (15.108)$$

In viscous fluids, the Reynolds number Re should be the same. Since $Re = VD/v = nD^2/v$ for a rotating machine, then the pump speeds should be related by $n_a/n_b = (D_b/D_a)^2$.

Two other dimensionless groups may be defined and are widely used in pump and fan selection, known as specific speed and specific diameter:

$$N_s = n Q^{0.5}/[gH]^{0.75} \quad (15.109)$$

where n is the pump speed (rps), Q the flow (m^3/s) H the pressure head (m), g is gravity = 9.81 m/s^2 , and

$$D_s = D (gH)^{0.25}/Q^{0.5} \quad (15.110)$$

Pump characteristics of N_s and D_s may be plotted together. Assembly of a wide range of data has led to a plot similar to that in Fig. 15.42, known as the Cordier diagram, showing regions where different rotating machines may be expected to have best possible efficiency.

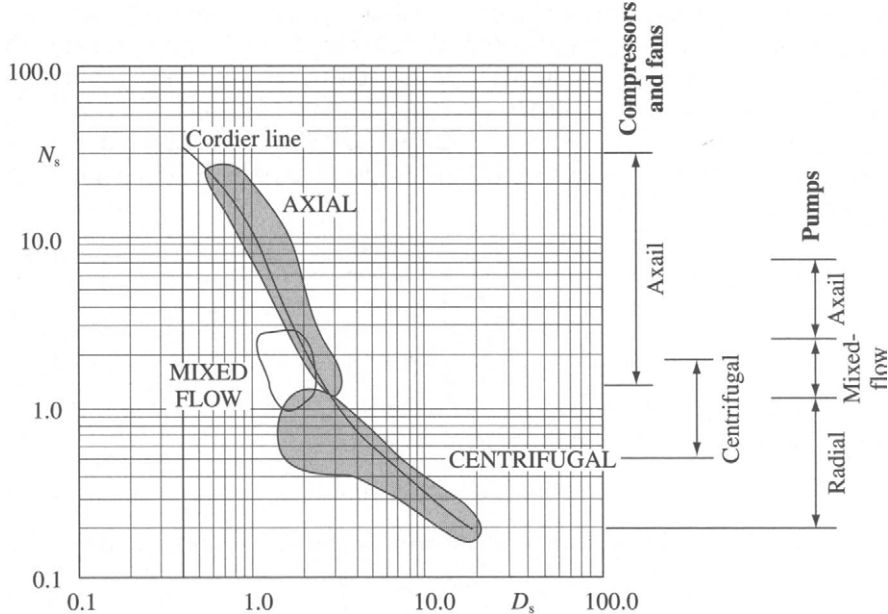


Fig. 15.42 N_s - D_s diagram [222].

Cavitation

A given water jet will cavitate and lose thrust if too much power is applied at low ship speed. An operating point marginally below this therefore defines the limiting thrust available at a given speed. Since jets are designed for maximum efficiency at the normal operating speed it is possible to plot contours of equal efficiency against craft speed and thrust, see Fig. 15.43. An important requirement for water-jet pumps is therefore that the suction head should not fall below the level at which cavitation would occur. Net positive suction head at the pump inlet is defined as follows:

$$\text{NPSH} = H_{\text{pi}} - H_v \quad (15.111)$$

where H_{pi} is the total head available at the entrance to the pump and H_v the water vapour pressure head. The total head in the free stream at SWL

$$H_{\text{fs}} = H_{\text{at}} + V_w^2/2g \quad (15.112)$$

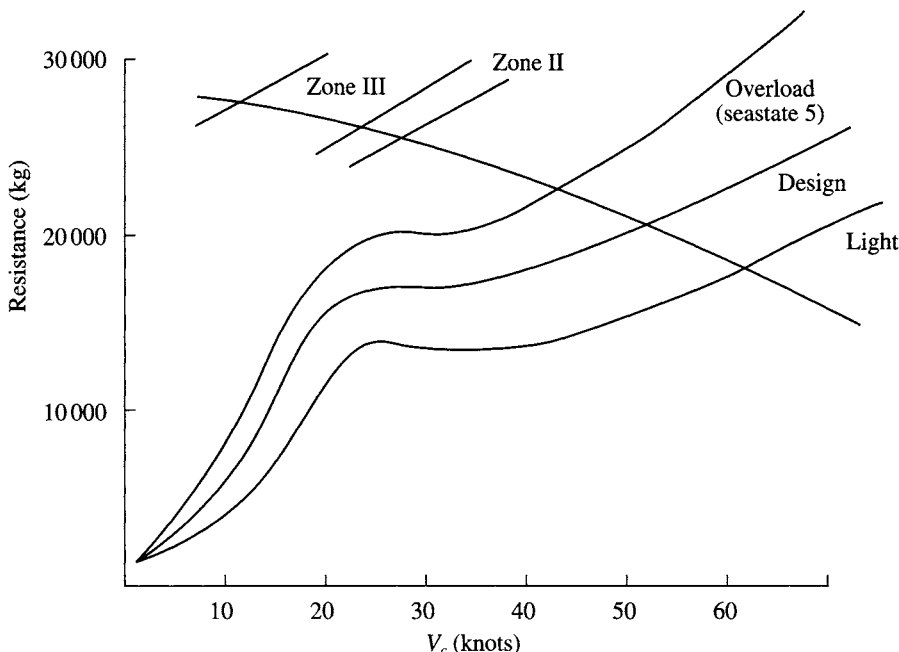


Fig. 15.43 Water jet efficiency vs V_c and T .

At the pump entrance this becomes

$$H_{pi} = H_{at} + (1 - \zeta) V_w^2 / 2g - H_i \quad (15.113)$$

where H_{at} is the atmospheric pressure (at SWL $H_v \sim 0.15H_{at}$) and H_i the height of pump inlet above SWL.

The water-jet inlet duct must be designed to supply an acceptable NPSH at design conditions and where possible allow the pump to operate close to its optimum at the lowest possible craft speed. Clearly from equation (15.113) a high duct efficiency is most important to maximize available NPSH. As craft speed reduces, if pump maximum power is maintained, the NPSH will drop below cavitation limits and the pump would overspeed as cavitation spread if power were not reduced. In cavitation tunnel tests, this point is determined by reducing fluid flow through the tunnel for constant pump speed, to the point where pump pressure head starts to fall off, typically by about 2%. The specific speed at this point is then defined as the suction specific speed, N_{ss} :

$$N_{ss} = n Q^{0.5} / (g \times \text{NPSH})^{0.75} \quad (15.114)$$

or

$$N_{ss} = n Q^{0.5} / [g (\eta_i V_w^2 / 2g - H_i - H_v)]^{0.75}$$

Limits of N_{ss} for operation without cavitation are around 1 for mixed flow pumps and as high as 3 for inducer type pumps. Water-jet pumps may be operated for short periods outside this limit so long as the pump is not allowed to reach severe cavitation

where overspeed may occur. Water-jet suppliers may provide plots similar to Fig. 15.44 showing lines of constant N_{ss} defining these regions. The limit for safe emergency operation may be in the region of $N_{ss} = 75$, with a red line limit at 80–90 for mixed flow units.

Centrifugal and radial flow pumps

These were used in early hydrofoil craft because of availability of pump units and have been successfully used for thruster units designed for low craft speed (Schottel units). They offer a compromise in that while the pump head is high, the unit is very compact for the static thrust generated.

Mixed flow pumps

The majority of water jets in use today use mixed flow pump units. The ratio of radial to axial flow varies between different manufacturers' designs. The range of pump specific speed N_s varies between 0.2 and 0.8. Mixed flow pumps can be optimized for craft speeds of 30 knots up to at least 50 knots.

There are a number of manufacturers now offering water-jet ranges of this type which extend up to 32 000 shp. Developments are currently ongoing to extend this as far as 50 000 shp, encouraged largely by the market for large fast catamaran ferries.

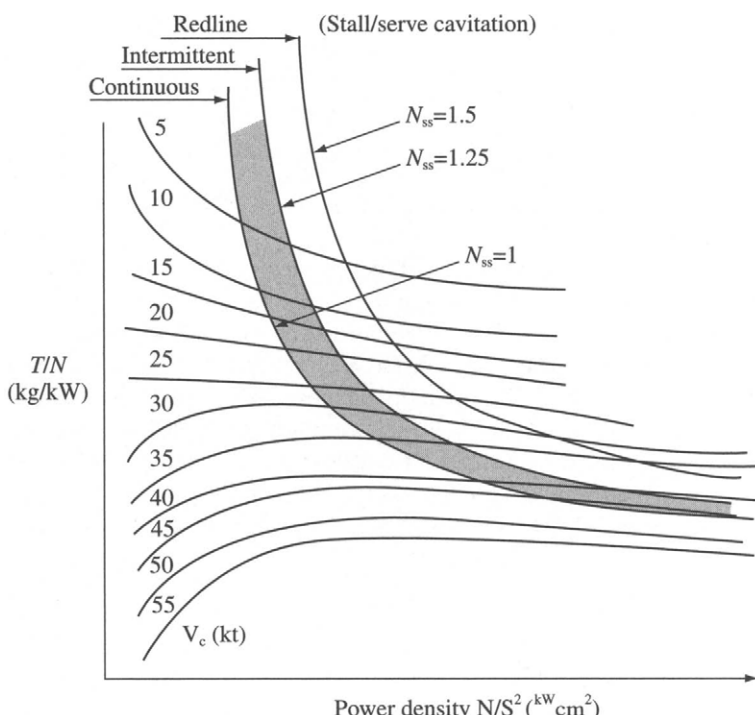


Fig. 15.44 N_{ss} boundaries on plot of water jet thrust vs craft speed.

Some mixed flow water jets use an inducer first stage to reduce the sensitivity to cavitation at high craft speeds.

Axial flow pumps

Axial flow pumps are high specific speed, high flow, low head machines. These pumps are often used for smaller units for pleasure boats in the power range 20–1000 shp. Higher power units generally use an inducer first stage or two axial stages in series where higher head is required.

Inducer pumps

The impeller for inducer pumps looks a little like an Archimedes screw. Pumps of this type were first developed for rocket motors, to increase the head sufficiently to prevent cavitation in the main impeller, of axial or mixed flow design at very high suction specific speeds ($N_s > 2$). Inducer pumps are less efficient than mixed flow pumps, typically $\eta_D = 0.5\text{--}0.65$ compared to 0.65–0.9 for mixed flow pumps. The optimum application is where an inducer is used to enable a mixed flow pump efficiency to be maximized for hump and operational conditions on a craft with design speed of 80–90 knots.

Pump efficiency η_p

Mixed flow pumps design for water-jet applications typically have hydraulic efficiency in the range 0.85–0.92. Inducer pumps may be expected to have efficiency in the region of 0.8. Axial flow pumps generally operate at efficiencies of 0.75–0.85, while centrifugal pumps may be expected to operate between 0.85 and 0.93. All pump types will normally be designed with downstream guide vane systems which recover energy by eliminating swirl from the jet flow.

These generalized data may be found useful for initial selection purposes, though information from the manufacturers themselves is recommended to be used during detailed design. There is a strong interaction between the impeller design and both the intake and the nozzle, so several iterations may be required before the optimum total system is found.

Water-jet selection

Preliminary assessment can be made using the procedure in Fig. 15.32. Having identified the desired thrust and power input, the pump characteristics need to be checked, so as to allow matching with power plant and gearboxes. Approximate sizing may be carried out based on charts such as the preliminary selection chart from KaMeWa, Fig. 15.37. A summary listing of larger jet units from the main suppliers is given in Table 15.5.

The ideal water-jet system should have the following characteristics:

- high hydraulic efficiency at design flow rate;
- freedom from cavitation over the desired range of operating craft speed and power;

- minimum pump diameter and so weight for a given nozzle size;
- pump speed to match standard (lightweight) gearboxes;
- tolerance to unsteady flows.

These requirements normally result in selecting a high specific speed N_s and also high suction specific speed N_{ss} . The procedure is best illustrated by an example.

Example

Consider selection of a water jet to power the SES with resistance curves as shown in Fig. 15.44. Two waterjet units will be selected, one in each sidehull, so craft resistance/2 is used for selection.

Required thrust at design operating point of 50 knots (25.7 m/s) is

$$T_{pi} = 40\ 000 \times 0.5 \times 0.95/1.0 = 19\ 000 \text{ kg}$$

where $(1 - w) = 0.95$ and $(1 - t) = 1.0$. Assume the following system efficiencies for first pass estimating:

η_i	= 0.85	inlet efficiency
η_n	= 0.99	nozzle efficiency, leading to a first pass
η_j	= 0.72	jet efficiency (Fig. 15.31)
η_p	= 0.91	pump hydraulic efficiency
η_r	= 0.99	relative rotative efficiency
η_t	= 0.97	transmission efficiency

$$\text{OPC} = \eta_p \eta_r \eta_j \eta_H \eta_t = 0.662 \text{ (based on } \mu \text{ rather than } \mu_w\text{)}$$

Then

$$\begin{aligned} T_p &= T_{pi}/(\eta_p \eta_r \eta_j) \\ &= 19\ 000/0.662 = 29\ 230 \text{ kg required} \end{aligned}$$

Power required is then

$$\begin{aligned} N &= T_p V_c / (1000/9.81 \eta_i) \text{ kW} \\ &= 29\ 230 \times 25.7 / (1000/9.81 \times 0.85) = 7770 \text{ kW} \end{aligned}$$

The thrust per kW, $T/N = 19\ 000/7770 = 2.44$. From Fig. 15.37, at this power loading and craft speed, a pump loading of 3100 kW/m^2 is appropriate, which suggests a pump inlet diameter of 2.25 m. The thrust loading can be estimated from Fig. 15.44 following a line of constant power loading. This line is shown in Fig. 15.43. It can be seen that between 23 and 25 knots for this craft, cavitation is likely at full power and so full power should not be applied until the craft has accelerated beyond 25 knots.

To check the validity of our original efficiency assumptions we may proceed as follows. Let nozzle area be 40% of inlet area, which is typical,

$$A_j = 0.4 \pi/4 \times 2.25^2 = 1.59 \text{ m}^2 (D_j = 1.423 \text{ m})$$

The inlet velocity to the water jet is

$$V_w = (1 - w) V_c = 0.95 \times 25.75 = 24.46 \text{ m/s}$$

From

$$T = \dot{m} (V_j - V_w) = \rho A_j V_j (V_j - V_w)$$

we can derive

$$V_j = 0.5 (V_w + [V_w^2 + 4 T / \rho g A_j]^{0.5}) \quad (15.115)$$

so

$$V_j = 48.8 \text{ m/s} \quad \mu = 0.5266$$

and

$$\begin{aligned} \eta_j &= 2\mu/(1+\mu) \\ &= 0.69 \quad \text{which compares to the 0.72 assumed initially} \end{aligned}$$

The actual jet efficiency will be slightly reduced by the height of the water jet above the keel, but is likely to be enhanced by the hull interaction effects so that the originally assumed 0.72 might be achieved after optimization.

The impeller diameter will be approximately 1.4 times the inlet diameter, i.e. 3.15 m. If cavitation is to be avoided then tip speed should be less than 46 m/s and so the pump speed should be less than 278 rpm (4.63 rps).

$$\begin{aligned} Q &= V_j A_j \\ Q &= 48.8 \times 1.59 = 77.6 \text{ m}^3/\text{s} \end{aligned}$$

The pump head is

$$\begin{aligned} H &= V_j^2 / 2g \eta_n - \eta_i V_w^2 / 2g + h_j \text{ m} \\ &= 0.99 \times 48.8^2 / 2g - (0.95 \times 25.7)^2 0.85 / 2g + 1.0 = 94.34 \text{ m} \end{aligned} \quad (15.116)$$

or

$$\begin{aligned} H &= 1000/g N \eta_p \eta_r \dot{m} \text{ m} \\ &= 1000/g \times 7770 \times 0.91 \times 0.99 / (77.6 \times 1000/g) = 90.2 \text{ m} \end{aligned} \quad (15.117)$$

We use $H = 90.2$ m. The pump dimensionless specific speed is then

$$\begin{aligned} N_s &= n Q^{0.5} / (gH)^{0.75} \\ &= 4.63 (77.6)^{0.5} / (g \times 90.2)^{0.75} \\ &= 0.25 \end{aligned} \quad (15.109)$$

Now

$$\text{NPSH} = \eta_i V_w^2 / 2g - h_i - H_v \quad (15.118)$$

We take $h_i = h_j$, so

$$\text{NPSH} = 0.85 \times 30.5 - 1 - 0.15 = 24.78 \text{ m}$$

where h_i is the height of inlet above SWL, assumed at 1m for this calculation, and H_v the vapour pressure head of water, approximately 0.15m above atmospheric ($H_a \sim 10$ m); then

$$\begin{aligned} n_{ss} &= n Q^{0.5} / (g \times NPSH)^{0.75} \\ &= 278 (77.6)^{0.5} / (g \times 24.78)^{0.75} = 39.8 \end{aligned} \quad (15.114)$$

also

$$\begin{aligned} \sigma_p &= NPSH/H \\ &= 24.78/89.57 = 0.28 \end{aligned} \quad (15.119)$$

Based on these data we can conclude that the pump is in a stable region for normal operation. As craft speed reduces, while H will remain almost constant at constant power, NPSH will reduce and the cavitation number will gradually reduce to the point where cavitation is unavoidable at the impeller. For our example this occurs at approximately 25 knots.

The water-jet unit weight for this example will be in the range 8000–9000 kg, see Fig. 15.45 which presents generic data which are applicable to the main manufacturers. For initial selection, the middle of the weight range may be used, until a design check against specific supplier pumps has been carried out.

Overall propulsive efficiency

If we consider the results of the calculation above and compare with open water propellers and the likely range for water jets, the following data are relevant:

Propeller	35 knots	Water jet typical	30–50 knots	Example 50 knots
η_0	0.663	η_{inlet} η_{jet} η_{pump} η_{nozzle}	0.80–0.95 0.70–0.85 0.85–0.95 0.99	0.85 0.72 0.91 0.99
η_t	0.97	η_t	0.97	0.97
η_H for $w = 0.05, t = 0.065$	0.985	η_H for $w = 0.05, t = 0$	1.052	1.052
η_D	0.633	η_{opc}	0.495–0.795	0.662

It can be seen that water jets have a large range of possible efficiency dependent on the system component performance. Careful integration of system components into the SES hull design is necessary, aimed at optimization of the intake geometry and jet nozzle velocity, in order to achieve OPC in the range 0.65–0.7 for an SES.

Once a typical water-jet sizing and OPC have been assessed, the designer should be in a position to make an assessment of the powering needs for the craft, including selection of reduction gearboxes and review candidate water jets from published information. Detail design would continue by making detailed studies in liaison with the suppliers.

Steering and reversing gear

Water-jet systems may be fitted with rotatable nozzles and deflector vanes to redirect the jet forwards under the hulls to give reverse thrust, see Figs 15.30 and 15.31. On large craft fitted with four water jets, it is normal to install this steering equipment on the outer jets only. This is because a relatively small deflection of a water jet produces

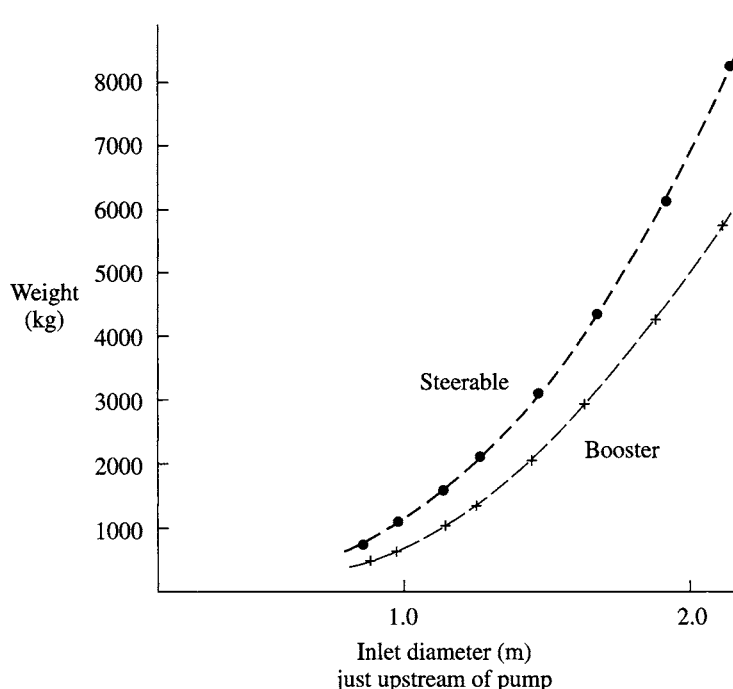


Fig. 15.45 Water jet weight vs inlet diameter.

high turning forces in comparison to a marine rudder. In addition, considerable weight is saved by installing non-steerable jets (see Fig. 15.45).

At full power, the side force generated by a jet deflected by 6° will be 10%. The available reverse thrust may be expected to be 30–40% of the maximum static thrust for the system. Reverse thrust can be selected at high speed, for rapid deceleration, though as the vessel slows, power must be reduced, to avoid cavitation at the impeller.

Reversing is achieved by a bucket or deflector plate system, depending on the supplier. Examples of two different approaches which both deflect flow under the hull transom can be seen in Figs. 15.30 and 15.31. Hydraulic cylinders are used to rotate the deflector bucket components about their hinge joints. Since relatively high forces are generated – the reactive force on the bucket itself may be as high as twice the design thrust – these components must be carefully designed. These loads are transmitted directly back to the transom flange mounting via the pump casing, thus the hull structure in this area must also receive careful attention.

If the deflector system is partially deployed, jet flow can be distributed so as to give zero net forward thrust, while engine power is set at the maximum allowable for the craft speed. Since operation of the deflectors is rapid, maximum thrust can be obtained very quickly, giving high craft acceleration to cruising speed.

Integrated control systems

Water-jet units are remotely operated from the wheelhouse via an electro-hydraulic system, an example of which is shown in Fig. 15.31. Operation can be designed

around combined thrust/steering levers, steering wheel, tiller, or a single joystick for all the water jets on a vessel controlling the units via a programmable system. Digital electronics are used to control engine/pump speed and monitor status of the system components. Back-up systems for operation of individual units by on/off levers and push buttons for steering, reversing and engine power are also provided. Examples of these systems are shown in Fig. 15.46.

While it is possible to control engine speed, thrust and steering manually, the convenience of a computer-controlled integrated control system has made it the primary choice for designers. These systems form an integral part of the water-jet system and so are designed by the same suppliers as the water-jet units themselves. It is now also possible to link this control system to an autopilot.

Prior to completing detailed design therefore, the SES designer will need to identify the hydraulic power, electrical power and electronic systems requirements for the units, to be included in the specification of auxiliary power and electrical services.

15.6 Power transmission

The power transmission system in an SES or ACV should be designed with minimum weight in mind. This approach implies that engine and fan, propeller or water jet are as close together as practical. The greater the distance between the two, the greater the challenge of providing transmission shafting which is stiff (to avoid whirling) and light (to minimize the problems of dynamic balancing).

There is often a trade-off between reduced distance and introduction of gearboxes in an SES for main propulsion engines, particularly for propeller-driven craft due to the narrow sidehull width. Where a reduction gear is needed anyway, this is not a particular problem. The design of smaller SES is also challenged by the vertical CG if engines have to be located above the sidehulls. It is common practice therefore to widen the hull towards amidships to accommodate engines within the hull depth. Water-jet systems require a significant keel width to optimize flush inlet design. This eases design of hull lines to accommodate engines immediately forward of the jet units.

ACVs are particularly sensitive to changes in CG. Since main engines are the largest mass apart from the passengers or cargo, their positioning influences the sizing of the ballast system for trim. Craft with separate lift and thrust engines are easier to optimize in this respect. The optimum position for propulsion devices is at the craft stern, while engines located towards the craft centre reduce required trimming ballast and craft rotational inertia so making it more manoeuvrable.

Designers will investigate different machinery arrangements at an early stage, to identify the sensitivity of their concept to payload variations and high/low fuel payload. The effect of layout changes on transmission arrangements may then be checked and an optimum chosen.

Before discussing transmission components, the design criteria should be stated. If the maximum operating torsional stress is q , the following factors for limiting stress design have been specified in the UK British Hovercraft Safety Requirements (the BHSRs) [115] (Table 15.6). The reasoning behind these design factors is to give an acceptable margin against unsteady stresses due to engine start-up and acceleration/

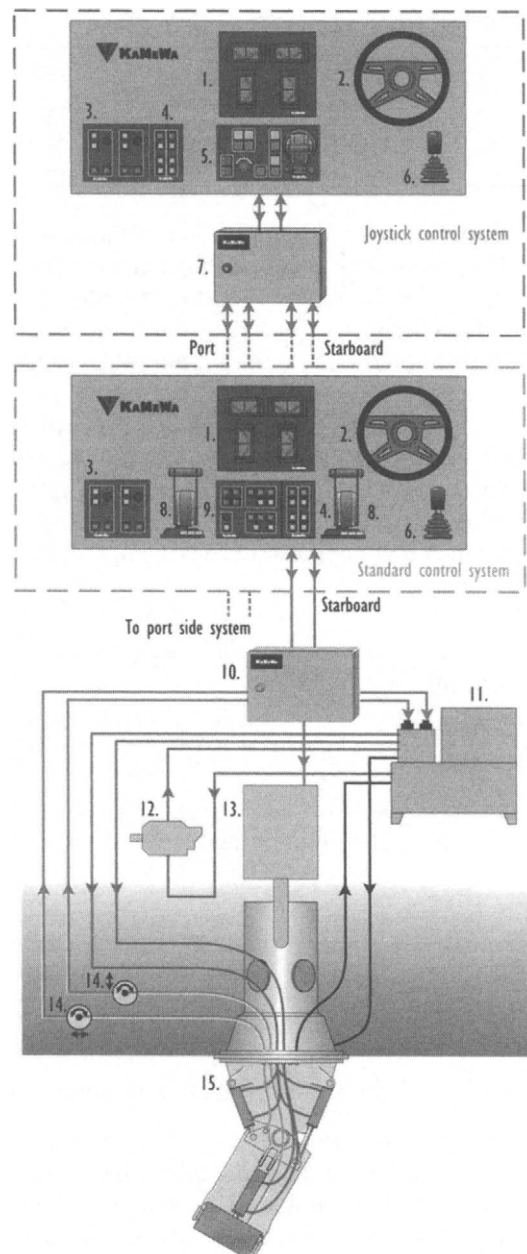


Fig. 15.46 KaMeWa control system components.

Table 15.6 Transmission shaft design factors

Engine type	Proof stress factor at q	Ultimate stress factor at q
4-cylinder engines	0.50	0.33
5-cylinder engines and greater	0.67	0.44
Gas turbine engines	0.75	0.50

deceleration of the propulsion device against its rotational inertia as power is increased or reduced. The response of reciprocating engines is much faster than a gas turbine, so exerting higher accelerations, demanding a higher design factor. In addition it is necessary to build in design margins against the uncertainty of material properties, approximately 15–20% of the 25% margin allowed for gas turbine engines in this case.

These factors are likely to control the design for steel transmission shafts, while for aluminium or composite shafting it may be found that fatigue will govern the dimensions. Lloyds, in their Special Service Craft rules, Part 13 – Shaft vibration and alignment [116], give empirical formulae for shaft design stresses including different couplings and bearings which will be useful to the designer at the detail stage.

Design stresses

A shaft is designed to transmit torque, where

$$T_q = \frac{N \times 746 g}{2\pi n} \text{ kg m} \quad \text{or} \quad \frac{N \times 33 000}{2\pi n} \text{ lb ft} \quad (15.120)$$

where T_q is the torque and N the transmitted power in kW or shp. The maximum stress in the outer fibre of the shaft is determined from

$$q = T r/J \quad (15.121)$$

where q is the maximum shear stress, r the shaft outside radius and J the polar moment of inertia of shaft cross-section,

$$J = \pi r^4/2 \quad \text{for a solid shaft} \quad (15.122)$$

$$= (r^4 - r_i^4) \pi/2 \quad \text{for a tubular shaft with inner radius } r_i \quad (15.123)$$

Since the polar moment of inertia is related to r^4 , clearly tubular shafts will be much more efficient than solid shafts. Larger diameter thin-walled shafts also have the benefit of greater stiffness. If high strength material (aluminium or steel) is used to further save weight, it is likely that welded joints may not be practical as the weld strength would control the design. In this case, shafts machined from solid may be required, with the consequent costs involved. Unless weight is critical, a compromise is usually reached between shaft diameter and material and the design of end connections.

A number of design cases need to be analysed for each section of shafting to establish acceptable dimensions from the quasi-static design approach, see Fig. 15.47, based on the design factors in Table 15.6. This will lead to a table similar to Table 15.7. The dimensioning load case will be identified by inspection, generally cases (3) or (5). Other load cases are needed for subsequent fatigue analysis. This analysis must be

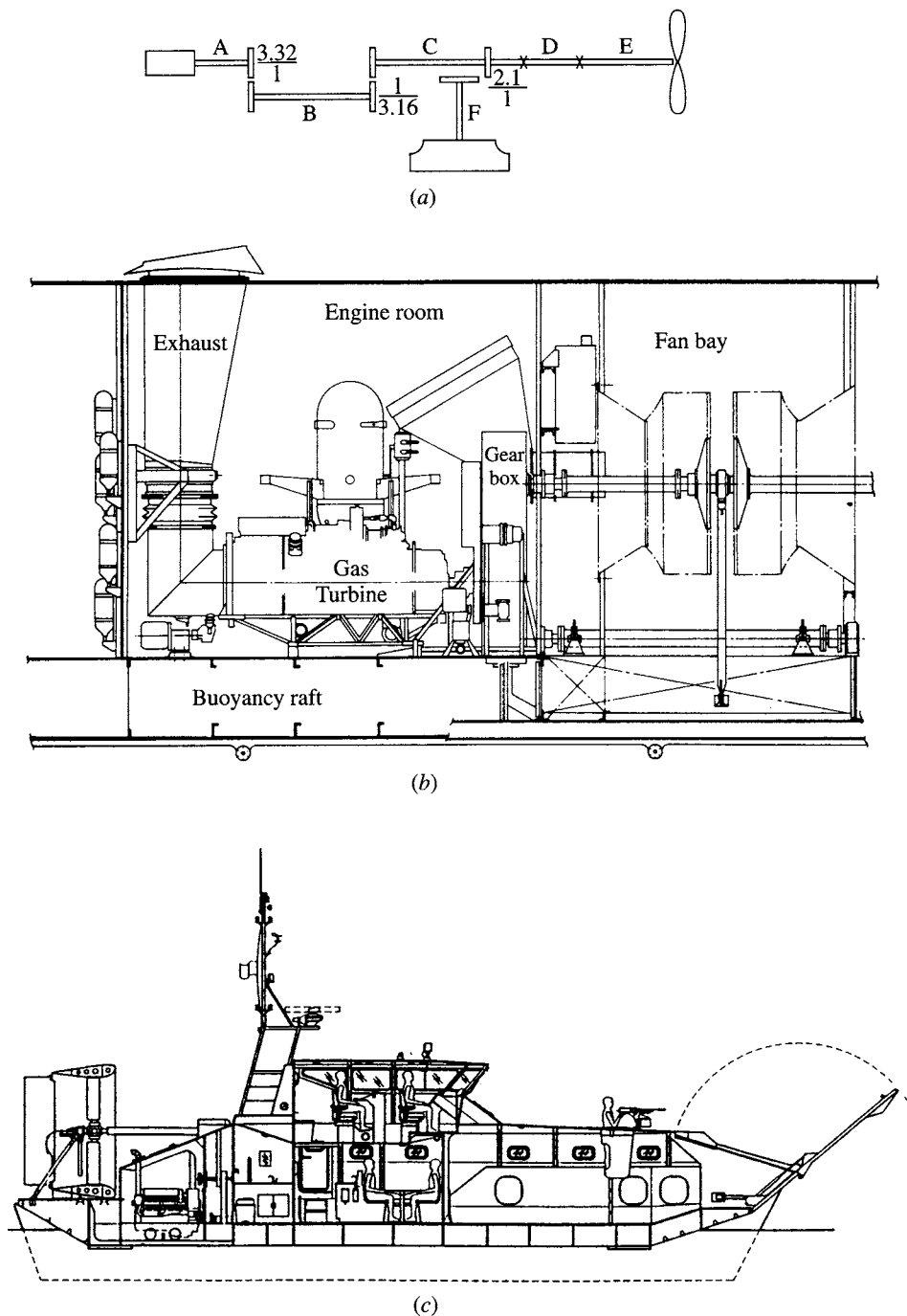


Fig. 15.47 Shaft sections for analysis: (a) BHC SR.N6; (b) Vosper Thornycraft VT.1; (c) ABS M10.

Table 15.7 Shaft design load case matrix

Load case	Engine (RPM)	Shaft (RPM)	Power (kW)	Shaft torque (kg. m)	Maximum stress (unfactored)	Running (Hours)
1 Static hovering						
2 Slow manœuvring						
3 Near hump						
4 Cruise light seas						
5 Cruise design seas						
6 Maximum speed calm						
Total						

repeated for each section of shafting between an engine and the fan, propeller, pump, or combination being driven. During detailed analysis once bearings and gearboxes have been selected, the power absorption by these devices can also be included.

Whirl speed

If a shaft is not exactly concentric, or has out of balance weights attached to it, a force will be generated as the shaft rotates, creating a bending moment along the shaft between its supports (the bearings). The shaft will deflect due to the force and this will increase the bending moment, so further increasing the deflection. The resistance generated by the shaft will be linear with deflection and proportional to its stiffness EI . The out of balance force due to a mass m , distance x from the shaft centre is

$$F = m x (2 \pi n)^2 \quad (15.124)$$

The force generated increases as shaft speed squared, so it may be seen that at low speed the deflections will be small and the shaft stiffness will enable a stable condition to be reached. It is normal to assume that the shaft behaves like a simply supported beam with pin joints to calculate the resisting forces. If the force is increased beyond the point where stresses generated in the shaft from its deflection reach yield (the limit of proportionality) the restoring force increment will be reduced and instability will occur. The response is called whirling and the speed at which instability occurs is known as the whirling speed, given by

$$n_w = 0.5 \pi (E I / (\mu L^4))^{0.5} \quad (15.125)$$

where n_w is the whirling speed in cycles per second, E the modulus of elasticity for the shaft material, I the moment of inertia of the shaft cross-section in bending $I_{x,y} = (r^4 - r_i^4) \pi/4$, μ the density of the shaft per unit length and L the shaft length between supports. The whirling speed is independent of eccentricity of the shaft and is inversely proportional to the distance between supports squared. Long transmission shafts therefore need intermediate supports to keep the design speed below whirling speed. Since the phenomenon is one of instability, it is normally recommended to stay at least 20% below n_w .

Shafts having very stiff bearings may behave more like a beam on fixed end supports, which would increase the whirling speed somewhat. SES and ACV design generally results in flexible rather than stiff structures, so it is more logical to employ self-aligning bearings to design the shafting runs so as to be well below whirling speed assuming pin-jointed supports at the bearings. For shafts with one or more intermediate bearings, it is preferable to have differing shaft lengths, so that vibration due to other dynamic forces will not affect all sections of a shaft at the same time.

Once acceptable shaft lengths between bearings have been determined, based on shaft dimensions derived from the torque requirements, an optimization might be carried out to find the lowest weight combination of shaft diameter, wall thickness, material and bearing distances.

A shaft should itself be balanced so that any exciting forces on the bearings are minimized, since the bearing life will be significantly reduced due to the unsteady loading of the rollers or balls on the bearing tracks. There will be unsteady dynamic loadings from both static imbalance and aerodynamic or hydrodynamic force variations at harmonics of the propeller blade frequency ($f = n n_b$, $2f$, $3f$, $4f$, $5f$, etc.). These excitations will be the main source of fatigue in the shaft.

A propeller or fan mounted on the end of a shaft will generate a vibration with a fundamental natural frequency as follows [87]:

$$n_1 = \frac{\pi}{2} \left[\frac{EI}{I_D(b + L/3) + (W_p b^2/g)(b/2 + L/3) + \mu(b^4/8 + Lb^3/9 + 7L^4/360)} \right]^{0.5} \quad (15.126)$$

where n_1 is the natural frequency in cycles per second, I_D the moment of inertia of propeller about its diameter (= half polar moment of inertia) (Note: add approx 60% for entrained water for marine propellers), W_p the propeller weight (Note: add approx 25% for entrained water for marine propellers), L the length between bearings and b the length of overhang.

This shaft section should be designed so that this frequency is higher than the design operating speed, again by a factor of 20%.

Fatigue endurance

Design for fatigue requires the dynamic fluctuations in stress in a shaft at nominally constant power to be determined. These are primarily at shaft rotation frequency and caused by out of balance causing shaft whirling and bending moments caused by masses attached to the shaft such as fans and propellers, including out of balance and dynamic vibration forces. The stress fluctuations are greatest for propellers or fans mounted on overhung shafting.

The operational profile for the craft has first to be determined, relative to the projected service hours, including cruise, slow-speed manoeuvring etc., which define the engine speed and torque applied to the transmission. The shear stress in the shaft due to the torque is first calculated, i.e. the mean loading, and then the alternating stress due to the static bending moment from the principal masses, plus any dynamic bending moments due to fan/propeller out of balance.

The number of cycles to failure at a given stress amplitude can be determined from a standard $S-N$ curve, for example Fig. 15.48. The degradation as a portion of the

total fatigue life of the shaft material is determined for that stress amplitude and number of cycles experienced by the craft. The total degradation is then calculated by summing the components of the craft operational profile, the Miner sum. The fatigue service life can then be estimated by the reciprocal of the degradation, assuming that the operational profile does not change. If N_i is the total number of cycles at σ_i for fatigue failure and n_i the number of cycles experienced by craft over operational period (days, months or years) then

$$D_i = n_i/N_i \quad (15.127)$$

$$D = \sum_{i=1}^n n_i/N_i \quad \text{referred to as the Miner sum} \quad (15.128)$$

$$L = 1/D \quad \text{endurance in days, years or operational cycles} \quad (15.129)$$

The accepted factors between calculated fatigue endurance and design fatigue life are 3 for components which can be regularly inspected and replaced and 10 for components which cannot be inspected. The reason for this is that crack initiation is rather uncertain in metallic materials. It is sensitive to microscopic inclusions, surface finish and surface corrosion, especially pitting.

ACVs and SES operate in an environment where corrosion is an important issue. The design factor of 3 represents the average uncertainty for the data in $S-N$ curves such as Fig. 15.48 and so if shafts are likely to be subject to surface corrosion in

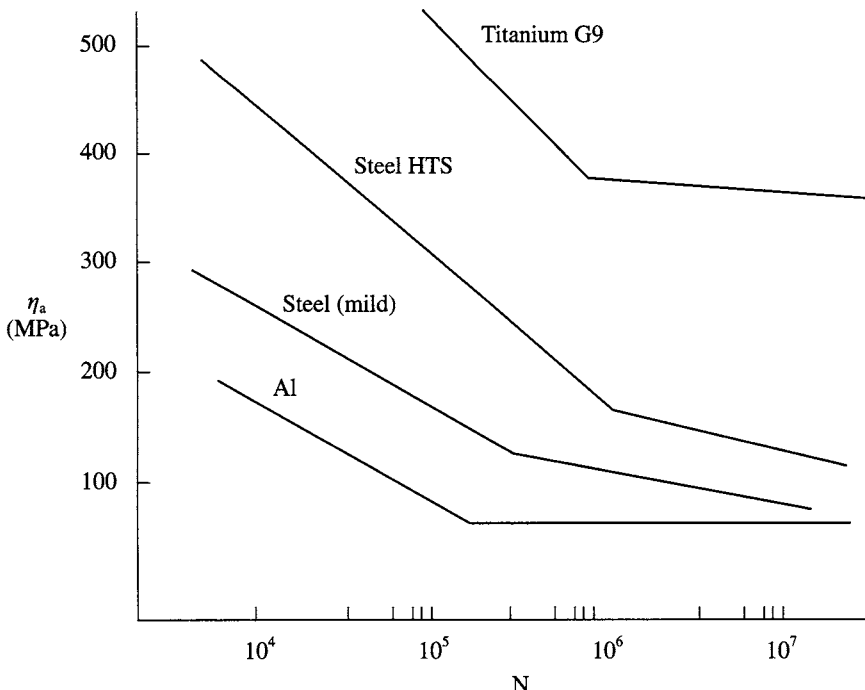


Fig. 15.48 $S-N$ curves for fatigue analysis of transmission shafts.

service, a 'corrosion allowance' should be added, in the same way as structural member scantlings are increased. Corrosion protection coatings can be an effective alternative, so long as regular inspection allows coating damage to be repaired. A combination of corrosion allowance and coating can be used to increase the inspection intervals by allowing some degradation before repair. Shafts which are not inspectable need to incorporate a corrosion allowance consistent with the craft design life and operational environment.

Craft design life is a key issue for designers, as it can add significant cost. An operator would typically expect that an ACV or SES would have a useful operating life before replacement of at least 20 years and perhaps in excess of 30 years with some repair work to the main structure. It is suggested therefore that transmission shafts should have a design fatigue life exceeding 75 years from analysis.

Couplings, bearings and supports

There are a wide variety of design options available to the ACV and SES designer for shaft bearings and couplings. Smaller craft can use systems adapted from automobile practice, while larger craft, particularly SES, use lightweight marine transmission components.

To reduce vibration, main engines are often flexibly mounted, so that a flexible coupling is also needed between it and the reduction or vee drive gearbox. Such couplings are often also used between sections of shafting to accommodate flexure of the craft structure in operation. Axial movement can be accommodated using splined shaft couplings.

Shaft sections may have bolted flanges for connection, or if the shaft end is solid, mechanical tapered locking sleeves or hydraulic locking can be employed for connecting devices, gearbelt pulley mounting, or direct mounting of propellers or impellers.

Shaft connections have to comply with the same design requirements as the shafts themselves. Having determined the design torque and fatigue loadings for a shaft these data can be used to select a suitable coupling based on performance data given by the manufacturer. Where bolting is used to secure couplings, vibration resistant locking devices will need to be installed. Flail guards are also necessary to protect against failure of universal joints on smaller craft.

Shaft bearings may be of ball or roller type. Roller bearings are more suitable for higher torque loadings as the surface pressure is lower on the race, leading to longer service life. A roller bearing, particularly the taper roller type, provides bending moment capacity and so is suited to support cantilevered propeller or water-jet pump shafts. Taper roller bearings are also able to resist the thrust loading from a propeller.

Selection of bearings is carried out initially from manufacturers' standard data, followed by direct advice. The service life rating of most bearings is based upon industrial or automotive applications and may not be conservative compared with ACV or SES use which involves frequent power level changes and start/stop cycles. The operational life of bearings in SES and ACVs before replacement is likely to be 5–10 years rather than the full craft life. Unplanned removal and replacement would cause unnecessary downtime for a craft, so such components are best selected with care.

Reduction drives and gearboxes

Utility ACVs driven by diesel engines in the power range to around 600 kW are able to use toothed non-metallic belt drive rather than gearboxes. Toothed belt drives generate very little noise and require no lubrication. Protection from foreign objects and airborne sand/grit is advisable to prevent unnecessary wear of the belt and toothed pulley surfaces. Pulleys are fabricated in aluminium alloy for minimum weight and coupled to the transmission shafts by bolted flange or taper locking interference friction couplings. Selection of pulley diameters and belt width is based on power to be transmitted, the design torque and the reduction ratio.

The principal market for this type of drive is industrial machinery such as heating and ventilating fans. Suppliers (Goodyear, Uniroyal and Fenner are examples in UK/Europe) are therefore familiar with power transmission from electrical motors, but less so for diesel engine transmission applications. The recommendations for selection are likely to be conservative and need some discussion and interpretation by the ACV designer. Larger craft such as the BHC SR.N series in the 1970s have used gearboxes specially designed and built for the application. More recently, standard lightweight industrial gearboxes have been used on some utility ACVs as an alternative to toothed belts.

SES use lightweight marine gearboxes which are manufactured in standard ranges by a number of suppliers. Manufacturers of marine gearboxes now supply ranges which allow matching of propellers, water jets and other equipment such as lift fans to the main engine types available.

A gearbox consists of a cast steel or aluminium housing containing a series of gearwheels which change the direction (parallel, right angle, vee or U drive) and/or speed of the output shaft relative to the engine input. The gearwheel shafts rotate on bearings locked into the housing. Shaft direction of rotation is reversed (e.g. clockwise to anticlockwise) unless an intermediate gearwheel is included. Support on both sides of gearwheels reduces moments applied to the bearings reducing loading and wear. References 115, 116 and 117 give guidance on gearbox design.

Bearings have to absorb any axial forces developed by gearwheels, which can be significant in the case of bevel gears and spiral cut parallel gears. In addition the gearbox may be designed to react to the propeller thrust rather than have a separate thrust bearing. This favours the use of taper roller bearings.

Gearwheels transmit torque across a line contact between the intermeshing tooth profiles. The geometry is designed to give rolling contact on the pitch line at which maximum load is transmitted, and sliding on entry and exit which is limited so as to minimize surface wear. Gearwheel service life is therefore dependent on efficient lubrication.

In a similar way to shafting, gearbox design varies according to the type of driver. Reference 116 suggests application factors for gear teeth as follows:

Driver	Coupling	Application factor K_A
Gas turbine		1.15
Diesel engine	Hydraulic	1.10
	Elastic (flexible)	1.30
	Other (e.g. bolted flange)	1.50

Higher factors apply where increased unsteady loadings will occur at the gearwheels. Further design issues for gears are provision of sufficient line contact to transmit the torque, which controls diameter and gearbox width. The tooth profile has then to withstand the bending moment generated at the contact line and transmit this back into the body of the wheel. Since teeth are cyclically loaded each revolution, the highest stresses in the tooth must be kept below the endurance limit of the material for fatigue based on normal service conditions. Craft operations above normal service limits which are infrequent must be checked to ensure fatigue degradation is acceptable and that surface contact pressures are still within the required limits.

The torque which can be transmitted and the rate of wear is also a function of the material surface hardness. The higher the strength/hardness, the more compact a gearbox can be for a given power rating. Gearwheels are surface hardened by carburizing. The wheel is heated to 900–950 °C in a furnace in the presence of hydrocarbon gasses so that carbon is absorbed into the steel. The depth of the hard case formed, normally between 0.5 (light) and 1.5 mm (heavy), is dependent on the exposure temperature and time. Gearwheels are normally hardened to a heavy specification for maximum resistance to wear.

Gearwheels are first machined to design geometry and either ground or honed to final surface finish after case hardening. Manufacturers of standard-range gearboxes design according to rules such as [116] and provide certification to that effect on request by a client. Gearboxes which are designed as one-off special units may also be designed to Classification Society rules, though costs would be higher due to the verification analysis for the unit.

Larger gearwheels are manufactured in the form of a ring carrying the teeth which is bolted to a separate boss/shaft. Heat treatment of the ring is then easier, with less tendency to distortion during treatment and quenching.

Typical power losses in a gearbox are 0.5–1.0% of transmitted power (for SES and ACV applications). This is transformed into heat at the gear teeth. Lubricating oil is usually transferred through holes in the casing walls from a suction at the bottom of the gearbox so as to spray the gear teeth on entry and exit from meshing. This assists heat dispersion and also minimizes noise generated. Spur or straight cut gear teeth produce greater noise than spiral cut teeth. High-speed marine gearboxes are therefore spiral cut. Many gearboxes include integral power offtake and hydraulic pump for circulation of lubricating oil and clutch operation if this is needed.

Monitoring of gearbox condition is normally by continuous measurement of lubricating oil temperature and pressure and inspection of lubricating oil filters or gearbox magnetic plugs at preset intervals for metallic particles which are evidence of wear. Oil temperature is a key variable since it represents the heat being dissipated. If the gears are badly worn this will increase.

Figure 15.49 shows a sample gearbox power flow diagram for a permanently meshed reversing marine box with integral hydraulic clutches. The unit itself is depicted in Fig. 15.50.

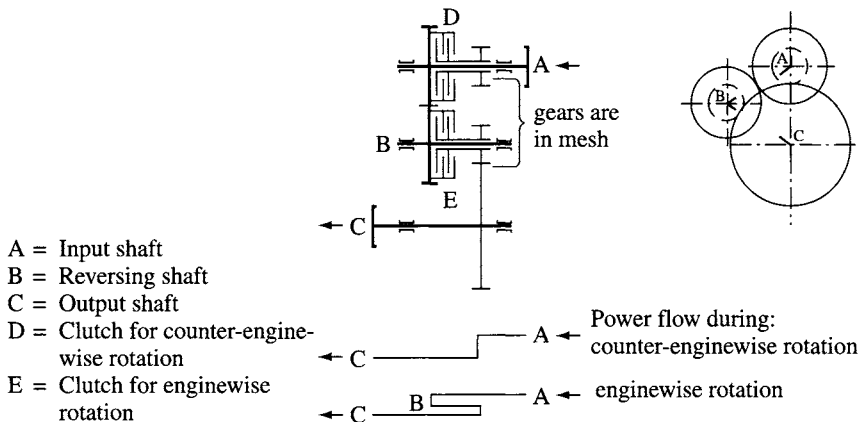


Fig. 15.49 Gearbox power-flow diagram.

15.7 Surface contact propulsion

Design considerations

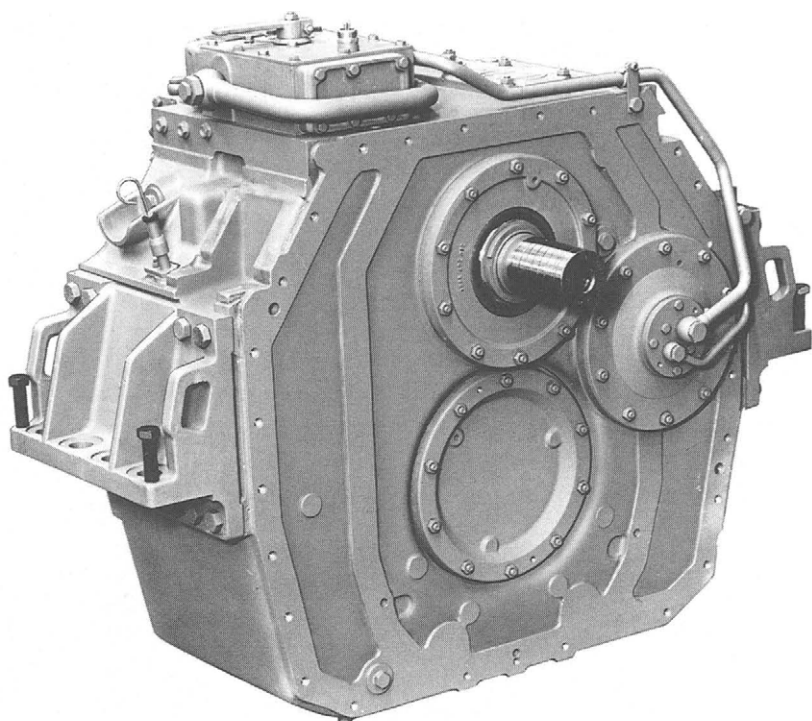
The use of surface contact propulsion is normally to push or tow an air cushion platform across sensitive terrain to deliver heavy or bulky equipment to a remote site. Examples are hoverplatforms which are towed across ice from supply ships to deliver provisions along the north coast of Russia, platforms used to deliver construction equipment across tundra in the north of Canada and north-east China, and platforms used as river ferries across rivers which ice over in the winter. Fig. 15.4 illustrates some of these.

The platform speed is governed by the chosen propulsion means, either towage by tractor, winching for river ferries, or hydraulically driven balloon wheels from power on board. In special cases Schottel units have been used to propel platforms over water and air jets have been used for propulsion or control assistance.

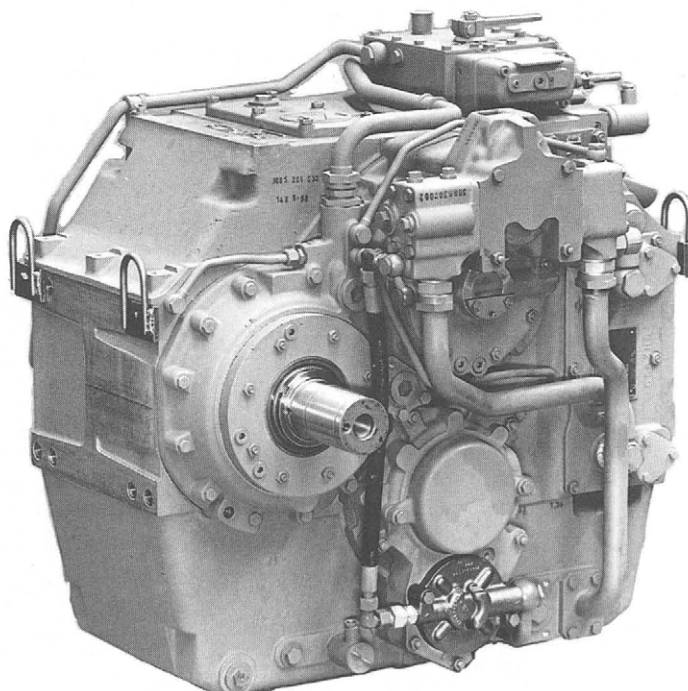
Brief guidelines

The main design considerations are the craft drag, mainly skirt contact drag over the appropriate terrain (see Chapter 3), which determines the pulling force, wind forces on the platform and gravitational forces when climbing or traversing slopes over land.

Towing a platform into wind on flat terrain or pulling directly up a slope is straightforward to analyse. If a platform meets a side wind, or cross slope, the situation becomes more complex. If the propulsion system is to be directly mounted on the platform and slopes to be traversed are significant, then contact wheels at both ends will help control the unit. The ground contact force of the propulsion unit should be sufficient to resist side wind forces and gravity forces on a side slope. A starting assumption may be a slope of 1 : 10 or approximately 6°.



(a)



(b)

Fig. 15.50 ZF gearbox type BW 450.

576 Propulsion system design

If the platform is to be towed, if the terrain is very open, for example over an ice field, then it may be acceptable for the platform to be towed skewed downwind, though the addition of a smaller vehicle with a control line at the stern will improve manœuvrability significantly.